Year : 2014

FUNCTIONAL MRI MAPPING OF THE HUMAN AUDITORY CORTEX

Da Costa Sandra Elisabeth

UNIL | Université de Lausanne

FACULTÉ DE BIOLOGIE ET DE MEDECINE

DEPARTEMENT DES NEUROSCIENCES CLINIQUES

FUNCTIONAL MRI MAPPING OF THE HUMAN AUDITORY CORTEX

THÈSE DE DOCTORAT

présentée à la

Faculté de Biologie et de Médecine
de l'Université de Lausanne

pour l'obtention du grade de

Docteur en Neurosciences

par

Sandra Elisabete Da Costa

Directeur de thèse
Prof. Stephanie Clarke

Co-directeur de thèse
Dr. Melissa Saenz

Jury

Prof. Brigitta Danuser, Présidente
Prof. Didier Grandjean, Expert
Dr. Marcus Herdener, Expert

LAUSANNE
2014

Centre Informatique La Repro, UNIL
Lausanne
2014

Département des Neurosciences Cliniques

FUNCTIONAL MRI MAPPING OF THE HUMAN AUDITORY CORTEX

Thèse de doctorat en Neurosciences

présenté à la
Faculté de Biologie et de Médecine
de l'Université de Lausanne
par

Sandra Elisabete Da Costa

Ingénieure en Sciences et Technologies du Vivant de l'Ecole Polytechnique Fédérale de Lausanne, Suisse

Jury

Prof. Brigitta Danuser, Président
Prof. Stephanie Clarke, Co-directeur
Dr. Melissa Saenz, Co-directeur
Prof. Didier Grandjean, Expert
Dr. Marcus Herdener, Expert

Thèse n° 121

LAUSANNE 2014

Programme doctoral interuniversitaire en Neurosciences des Universités de Lausanne et Genève

UNIL | Université de Lausanne
Faculté de biologie et de médecine

LEMANIC NEURO SCIENCE DOCTORAL SCHOOL

Programme doctoral interuniversitaire en Neurosciences des Universités de Lausanne et Genève

Imprimatur

Vu le rapport présenté par le jury d'examen, composé de

Président	Madame Prof. Brigitta **Danuser**
Directeur de thèse	Madame Dr Melissa **Saenz**
Co-directeur de thèse	Madame Prof. Stephanie **Clarke**
Experts	Monsieur Prof. Didier **Grandjean**
	Monsieur Dr Marcus **Herdener**

le Conseil de Faculté autorise l'impression de la thèse de

Madame Sandra Elisabete Da Costa

Master ès sciences de la vie Ecole Polytechnique de Lausanne

intitulée
FUNCTIONAL MRI MAPPING OF THE HUMAN AUDITORY CORTEX

Lausanne, le 2 avril 2014

pour Le Doyen
de la Faculté de Biologie et de Médecine

Prof. Brigitta Danuser

Acknowledgements

My thesis appeared to me as a rite of passage to get into the huge neuroscience community. As a ritual, it was also made of three different stages. At first, I moved from the EPFL to the CHUV, leaving behind the engineer sphere to a medical one. This separation phase was quite short and soft, because at that moment my office was at the CHUV-core of the CIBM where almost half of the members are engineers. Then, I moved to a transition office and finally to an office directly near the patients. This stood out my transition phase where I was in-between the two institutions, scanning at the EPFL but processing the data at the CHUV, in-between healthy young subjects and old patients. This was the longest phase, almost three years, and maybe the most challenging and demanding one. Finally, came the reintegration phase where I started to write my thesis. This one is still in progress and will be over only after the final ceremony – the public defence – and the final reward – the diploma. Several individuals played a key role all the way of this ritual.

First, I would like to acknowledge all the participants who kindly gave some of their precious time, without them I would never be able to conclude this thesis. Second, I would like to thanks my thesis co-directors, Melissa Saenz and Stephanie Clarke, but also Wietske Van der Zwaag who provided a precious help almost as an unofficial third co-director. Third, I would like to thank all my colleagues of all the different labs such as the Laboratoire de Sciences Cognitives (LCS), Laboratoire de Recherche en Neuroimagerie (LREN), Laboratoire d'Investigation en Neurophysiologie (LINE) and the Centre dImagerie BioMdicale (CIBM, from both the EPFL and CHUV platforms), with whom I could exchange advices, problems and solutions – especially during our brainstorming coffee breaks. Finally, I am extremely grateful to all my relatives – my family, my boyfriend and my friends. They always supported me during all the moments of despair and frustration, but also during all the very good moments I had during these last three years.

Abstract

Mapping the human auditory cortex with standard functional imaging techniques is difficult because of its small size and angular position along the Sylvian fissure. As a result, the exact number and location of auditory cortex areas in the human remains unknown. In a first experiment, we measured the two largest tonotopic areas of primary auditory cortex (PAC, A1 and R) using high-resolution functional MRI at 7 Tesla relative to the underlying anatomy of Heschl's gyrus (HG). The data reveals a clear anatomical–functional relationship that indicates the location of PAC across the range of common morphological variants of HG (single gyri, partial duplication and complete duplication). Human PAC tonotopic areas are oriented along an oblique posterior-to-anterior axis with mirror-symmetric frequency gradients perpendicular to HG, as in the macaque. In a second experiment, we tested whether these primary frequency-tuned units were modulated by selective attention to preferred vs. non-preferred sound frequencies in the dynamic manner needed to account for human listening abilities in noisy environments, such as cocktail parties or busy streets. We used a dual-stream selective attention experiment where subjects attended to one of two competing tonal streams presented simultaneously to different ears. Attention to low-frequency tones (250 Hz) enhanced neural responses within low-frequency-tuned voxels relative to high (4000 Hz), and vice versa when attention switched from high to low. Human PAC is able to tune into attended frequency channels and can switch frequencies on demand, like a radio. In a third experiment, we investigated repetition suppression effects to environmental sounds within primary and non-primary early-stage auditory areas, identified with the tonotopic mapping design. Repeated presentations of sounds from the same sources, as compared to different sources, gave repetition suppression effects within posterior and medial non-primary areas of the right hemisphere, reflecting their potential involvement in semantic representations.

These three studies were conducted at 7 Tesla with high-resolution imaging. However, 7 Tesla scanners are, for the moment, not yet used for clinical diagnosis and mostly reside in institutions external to hospitals. Thus, hospital-based clinical functional and structural studies are mainly performed using lower field systems (1.5 or 3 Tesla). In a fourth experiment, we acquired tonotopic maps at 3 and 7 Tesla and evaluated the consistency of a tonotopic mapping paradigm between scanners. Mirror-symmetric gradients within PAC were highly similar at 7 and 3 Tesla across renderings at different spatial resolutions. We concluded that the tonotopic mapping paradigm is robust and suitable for definition of primary tonotopic areas, also at 3 Tesla. Finally, in a fifth study, we considered whether focal brain lesions alter tonotopic representations in the intact ipsi- and contralesional primary auditory cortex in three patients with hemispheric or cerebellar lesions, without and with auditory complaints. We found evidence for tonotopic reorganisation at the level of the primary auditory cortex in cases of brain lesions independently of auditory complaints. Overall, these results reflect a certain degree of plasticity within primary auditory cortex in different populations of subjects, assessed at different field strengths.

Keywords: auditory cortex imaging; tonotopy; ultra-high field; fMRI.

Résumé

La cartographie du cortex auditif chez l'humain est difficile à réaliser avec des techniques d'imagerie fonctionnelle standard, étant donné sa petite taille et position angulaire le long de la fissure sylvienne. En conséquence, le nombre et l'emplacement exacts des différentes aires du cortex auditif restent inconnus chez l'homme. Lors d'une première expérience, nous avons mesuré, avec de l'imagerie par résonance magnétique à haute intensité (IRMf à 7 Tesla) chez des sujets humains sains, deux larges aires au sein du cortex auditif primaire (PAC; A1 et R) avec une représentation spécifique des fréquences pures préférées – ou tonotopie. Nos résultats ont démontré une relation anatomico–fonctionnelle qui définit clairement la position du PAC à travers toutes les variantes du gyrus d'Heschl's (HG). Les aires tonotopiques du PAC humain sont orientées le long d'un axe postéro-antérieur oblique avec des gradients de fréquences spécifiques perpendiculaires à HG, d'une manière similaire à celles mesurées chez le singe. Dans une deuxième expérience, nous avons testé si ces aires primaires pouvaient être modulées, de façon dynamique, par une attention sélective pour des fréquences préférées par rapport à celles non-préférées. Cette modulation est primordiale lors d'interactions sociales chez l'humain en présence de bruits distracteurs tels que d'autres discussions ou un environnement sonore nuisible (comme par exemple, dans la circulation routière). Dans cette étude, nous avons utilisé une expérience d'attention sélective où le sujet devait être attentif à une des deux voies sonores présentées simultanément à chaque oreille. Lorsque le sujet portait était attentif aux sons de basses fréquences (250 Hz), la réponse neuronale relative à ces fréquences augmentait par rapport à celle des hautes fréquences (4000 Hz), et vice versa lorsque l'attention passait des hautes aux basses fréquences. De ce fait, nous pouvons dire que PAC est capable de focaliser sur la fréquence attendue et de changer de canal selon la demande, comme une radio. Lors d'une troisième expérience, nous avons étudié les effets de suppression due à la répétition de sons environnementaux dans les aires auditives primaires et non-primaires, d'abord identifiées via le protocole de la première

étude. La présentation répétée de sons provenant de la même source sonore, par rapport à de sons de différentes sources sonores, a induit un effet de suppression dans les aires postérieures et médiales auditives non-primaires de l'hémisphère droite, reflétant une implication de ces aires dans la représentation de la catégorie sémantique.

Ces trois études ont été réalisées avec de l'imagerie à haute résolution à 7 Tesla. Cependant, les scanners 7 Tesla ne sont pour le moment utilisés que pour de la recherche fondamentale, principalement dans des institutions externes, parfois proches du patient mais pas directement à son chevet. L'imagerie fonctionnelle et structurelle clinique se fait actuellement principalement avec des infrastructures cliniques à 1.5 ou 3 Tesla. Dans le cadre dune quatrième expérience, nous avons avons évalués la cohérence du paradigme de cartographie tonotopique à travers différents scanners (3 et 7 Tesla) chez les mêmes sujets. Nos résultats démontrent des gradients de fréquences définissant PAC très similaires à 3 et 7 Tesla. De ce fait, notre paradigme de définition des aires primaires auditives est robuste et applicable cliniquement. Finalement, nous avons évalués l'impact de lésions focales sur les représentations tonotopiques des aires auditives primaires des hémisphères intactes contralésionales et ipsilésionales chez trois patients avec des lésions hémisphèriques ou cérébélleuses avec ou sans plaintes auditives. Nous avons trouvé l'évidence d'une certaine réorganisation des représentations topographiques au niveau de PAC dans le cas de lésions cérébrales indépendamment des plaintes auditives. En conclusion, nos résultats démontrent une certaine plasticité du cortex auditif primaire avec différentes populations de sujets et différents champs magnétiques.

Mots-clé: imagerie du cortex auditif humain; tonotopie; haute résolution; IRMf.

Contents

List of Figures

List of Tables

List of Abbreviations

2-IFC . . . . . 2-interval forced choice
3T . . . . . 3 Tesla
7T . . . . . 7 Tesla
A1 (hA1) . . . . . primary auditory area
AA . . . . . anterio auditory area
AC . . . . . anterior commissure
AL . . . . . anterolateral
ALA . . . . . anterolateral auditory area
AM . . . . . anteromedial
ANOVA . . . . . analysis of variance
BOLD . . . . . blood oxygenation level dependent
CD . . . . . complete duplication
CF . . . . . characteristic frequency
CN . . . . . cochlear nucleus
CT . . . . . computed tomography
CTRL . . . . . control
DCM . . . . . dynamic causal modelling
DSI . . . . . diffusion spectrum imaging
DTI . . . . . diffusion tensor imaging
EEG . . . . . electroencephalogram
EPI . . . . . echo planar imaging
FDR . . . . . false discovery rate
fMRI (IRMf) . . . . . functional magnetic resonance imaging

FTS ..... first transverse gyrus
FWHM ..... full width at hall maximum
$GABA_A$ ..... gamma-aminobutyric acid alpha
GLM ..... general linear model
HG ..... Heschl's gyrus
HRF ..... hemodynamic response function
HS (HS1) ..... Heschl's sulcus
HS2 ..... second Heschl's sulcus
IC ..... inferior colliculus
IPL ..... inferior parietal lobule
KAlt ..... primary auditory area
KAm ..... primary auditory area
LA ..... lateral auditory area
LH ..... left hemisphere
MA ..... medial auditory area
mD ..... mild deficits
MEG ..... magnetic encephalogram
MGN (MGB) ..... medial geniculate nucleus (body) of the thalamus
MP2RAGE ..... magnetic prepared 2 rapid acquisition gradient echoes
MRI ..... magnetic resonance imaging
MTG ..... medial temporal gyrus
N ..... none
NMDA ..... n-methyl-D-aspartic acid
P1 ..... patient 1
P2 ..... patient 2
P3 ..... patient 3
PA ..... posterior area

PAC . . . . . primary auditory cortex
PC . . . . . posterior commissure
PD . . . . . partial duplication
PET . . . . . positron emission tomography
PM . . . . . posteromedial
PP . . . . . planum polare
PSC . . . . . percent signal change
PT . . . . . planum temporale
R (hR) . . . . . primary auditory area
REP . . . . . repetition
RH . . . . . right hemisphere
ROI . . . . . region of interest
RT . . . . . primary auditory area
SAC . . . . . secondary auditory cortex
sD . . . . . severe deficits
SI . . . . . sulcus intermedius
sMRI . . . . . structural magnetic resonance imaging
SNR . . . . . signal-to-noise ratio
SOC . . . . . superior olive complex
STG . . . . . superior temporal gyrus
STS . . . . . superior temporal sulcus
TBI . . . . . traumatic brain injury
TE . . . . . echo time
Te1.0 . . . . . primary auditory area
TI . . . . . inversion time
TR . . . . . repetition time

Chapter 1

Introduction

1.1 General introduction

All along our life, auditory information is constantly flowing around us and processed by the auditory cortex. Even before birth, our auditory system is already stimulated by environment sounds from our relatives (our mothers voice) or their actions (her preferred music). Thus, until our last breath, auditory information is vital for social interactions, everyday life events, knowledge transmission, and human wellbeing. The auditory cortex is crucial for sounds localization and discrimination, species-specific vocalization recognition, scene analysis, and auditory memory and learning. However, little is known about auditory processing networks. First, the auditory cortex is niched inside the superior temporal plane which makes it difficult to access. In the last century, Kleist (1934) was the first to compare cortical lesions related to auditory deficits with cytoarchitectonic areas defined by Brodmann thirty years earlier. He found that Brodmanns areas 22, 41, 42, and 52 were important for auditory processing. But the results were obtained with post-mortem brains, which is difficult to extrapolate to normal functions. Second, during evolution, speech development and gyrification constrained the auditory cortex into a relatively confined region in the human brain, with several distinct functions relatively close to or overlapping each other. Much auditory literature focuses the cortical organisation in on monkey and shows evidence for a hierarchical auditory organisation (Kaas and Hackett, 2000) with clear frequency gradients in the primary core (A1, R and possibly RT),

and preferential responses to more complex sounds in the secondary belt and parabelt regions. Only recently, due to technical advances in neuroimaging and cytoarchitectonic techniques, have researchers been able to corroborate animal findings in humans.

In this introduction, I will briefly introduce some basis of the auditory system such as the auditory pathway, auditory anatomy and tonotopic mapping. But also, a general view on selective modulation of auditory responses by attention and stimulus repetition, and some fMRI principles.

1.2 Auditory principles

Auditory pathways in healthy humans

Auditory information is initially decomposed by the basilar membrane of the cochlea into a frequency-specific organization – named cochleotopy (or tonotopy). This decomposition is transferred by the auditory nerve to the cochlear nucleus (CN) in the brainstem. Auditory fibres cross majorly the brainstem to the contralateral superior olive complex (SOC), but some of them also go to the ipsilateral SOC. From there, they project to the central nucleus of the inferior colliculus (IC) in the midbrain and then to the medial geniculate nucleus (MGN) of the thalamus. The ventral MGN receives inputs from central IC nucleus and is part of the tonotopic ascending pathway, whereas medial and dorsal MGN (in gray in Figure 1.1) receive inputs from tonotopic and non-tonotopic portions of the IC (rainbow and gray regions in Figure 1.1). Finally, auditory fibres reach auditory cortices in the superior temporal gyrus where they go either to the primary auditory cortex (PAC or the core, mainly A1 and R, plus a possible third region RT; rainbow gradients in Figure 1.1) or to the secondary auditory cortex (SAC or the belt with several subfields; dark gray regions in Figure 1.1) or higher order regions such as the parabelt (light gray in Figure

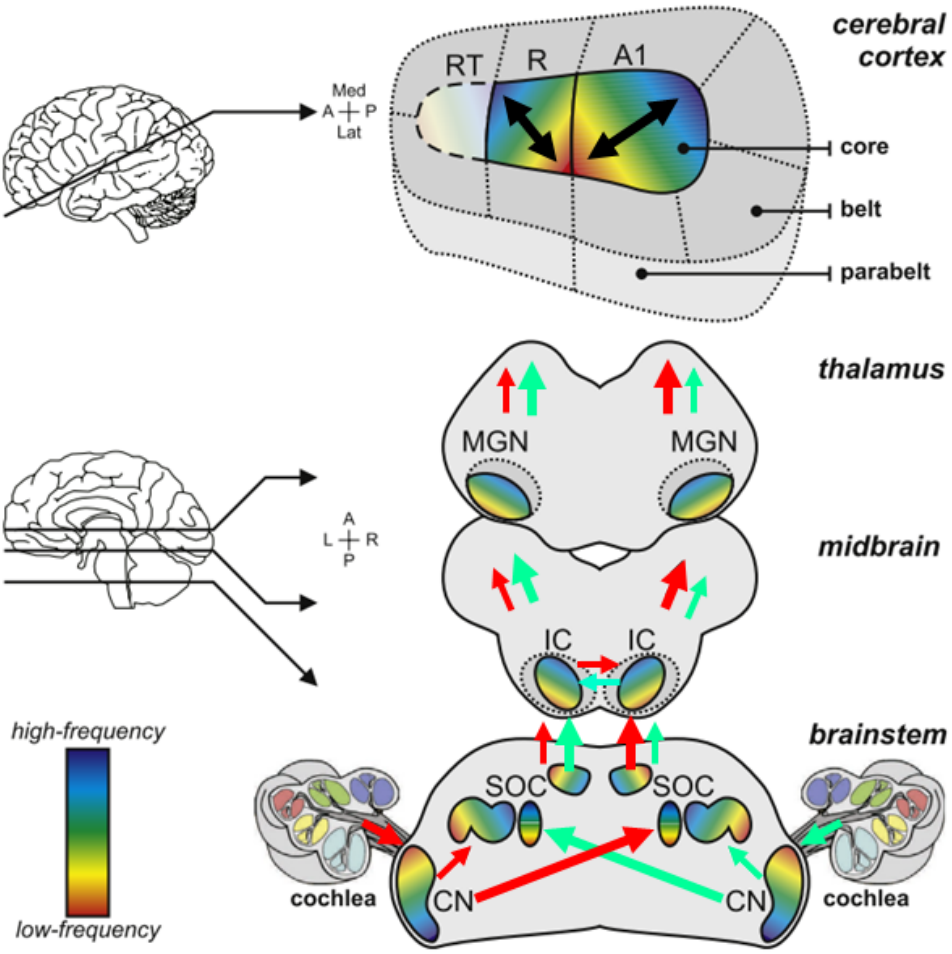

Figure 1.1: Auditory pathway with frequency-specific topographic organization. Rainbow bar: frequency gradients; CN: cochlear nucleus; SOC: superior olive complex; IC: inferior colliculus; MGN: medial geniculate nucleus; L: left; R: right; P: posterior; A: anterior; Med: medial; Lat: lateral. Red arrows: inputs from left ear; green arrows: input from the right ear. Figure modified from Saenz and Langers, 2013.

1.1) and others regions from the superior temporal plane (see next session). PAC and SAC get fibres in parallel from ventral and dorsomedial MGN nucleus, respectively. Auditory cortices process information primarily from the contralateral ear (thick arrows in Figure

1.1), however they also have significant input from the ipsilateral ear (thin arrows) coming from crossing fibres in the IC or in the corpus callosum (for review see Brugge, 2013; Di Salle et al., 2003; Saenz and Langers, 2013). Auditory information is transferred along the different auditory pathways by highly conservative and hierarchical processes before reaching several subregions of the superior temporal plane.

Auditory cortex anatomy

The superior temporal gyrus (STG) can be divided into three parts: the planum temporale (PT), Heschl's gyrus (HG) and planum polare (PP, from posterior to anterior). Pioneering post-mortem architectonic studies identified PAC in the STG based on its dense myelination, thalamic connectivity and koniocortex (well-developed layer 4; Beck, 1928; Brodmann, 1909; Campbell, 1905; Fleschig, 1908; Galaburda and Sanides, 1980; Morosan et al., 2001, 2004; Rivier and Clarke, 1997; von Economo and Horn, 1930; von Economo and Koskinas, 1925; Wallace et al., 2002). PAC colocalises with the medial two-thirds of the crest of HG with an elongated shape analogous to the core in monkey (Hackett et al., 2001). However, the exact extent, size and gyral borders are not consistent throughout the literature. In some studies, PAC expands until the PP and PT (Brodmann, 1909; von Economo and Horn, 1930; von Economo and Koskinas, 1925), whereas in others it is confined to HG borders (Beck, 1928; Galaburda and Sanides, 1980; Morosan et al., 2001, 2004) or encompassed inside HG (Rivier and Clarke, 1997; Wallace et al., 2002; see Figure 1.2 and Baumann et al, 2013 for review). This variability in PAC definition and localization is mainly due to technical differences, recent studies using more elaborated architectonic and histochemical staining compared to early work from Brodmann. These more recent techniques allowed more detailed parcellation of the STG with PAC being one (Te1.0 or A1) or two (KAlt, KAm) regions surrounded by different number of SAC subfields (Galaburda and Sanides, 1980; Morosan et al., 2001, 2004; Rivier and Clarke,

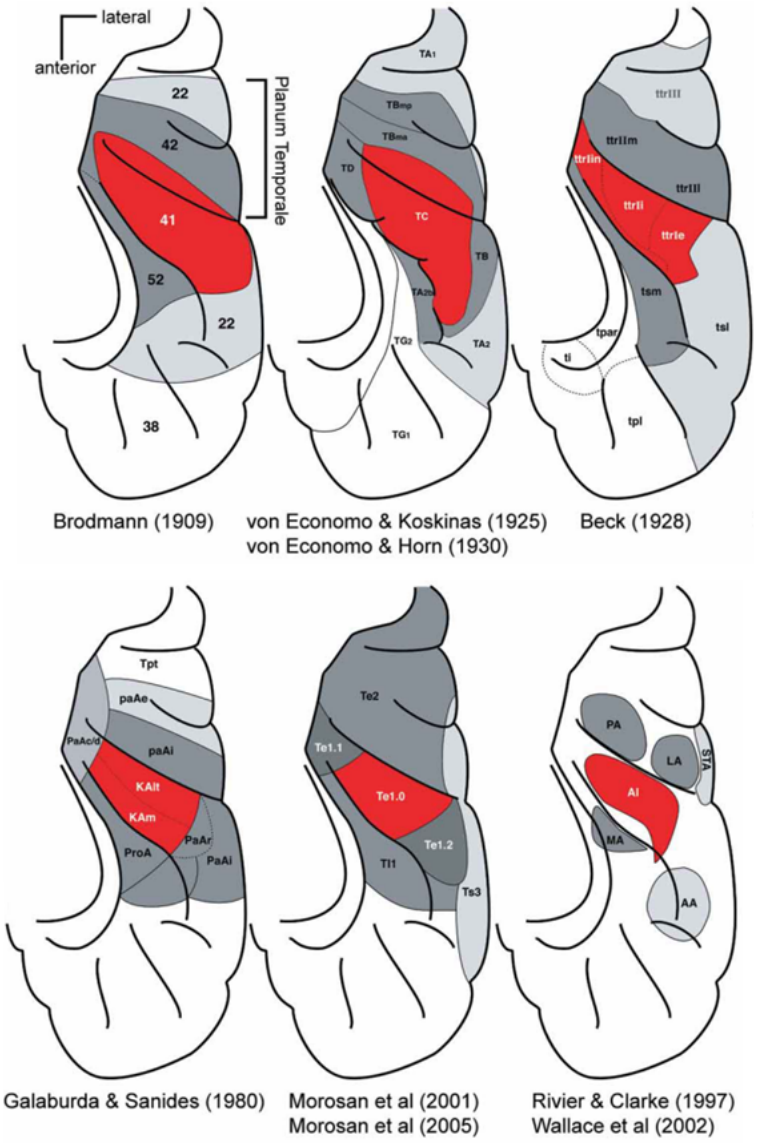

Figure 1.2: Parcelation of the superior temporal cortex. Red: PAC; dark gray: SAC; light gray: parabelt and high order regions. Figure adapted from Baumann et al., 2013.

1997; Wallace et al., 2002). However, despite the inconsistency in architectonic definition of PAC, HG remains the major landmark for PAC localisation even though intersubject and interhemisphere HG variability increases uncertainty in PAC delimitation. HG can be either a single gyrus, either partially or completely duplicated by an intermediate sulcus

(SI, Rademacher et al., 1993). In case of duplication, the posterior border of HG, the Heschl's sulcus (HS or HS1 for complete duplications), has been considered as part of PAC whereas the second sulcus (HS2) was included in the PT (Penhune et al., 2003). As part of the work done in this thesis, I have recently shown, with functional tonotopic mapping, that PAC spanned both HS, and thus both HS are part of a continuum (Da Costa et al., 2011).

Primary tonotopic representations

PAC can also been defined functionally by two tonotopic mirror-symmetric "high-low-low-high" gradients of preferred frequency responses (upper panel, black arrows in Figure 1.1). This tonotopic mapping has been widely explored in the animal literature (Brugge and Merzenich, 1973; Kaas and Hackett, 2000; Morel and Kaas, 1992; Petkov et al., 2006). In the monkey, the core (A1, R and RT) is oriented along a posterior-to-anterior axis and is organized in three frequency gradients: a first high-to-low gradient (A1) followed by reversal low-to-high (R), and then a third smaller and less distinct high-to-low (RT). In the human, functional imaging studies revealed frequency gradients in the STG (Da Costa et al., 2011; Formisano et al., 2003; Humphries et al., 2010; Langers and Dijk, 2012; Moerel et al., 2012; Schönwiesner et al., 2002; Striem-Amit et al., 2011; Talavage et al., 2000; Woods and Alain, 2009; Woods et al., 2011). As in architectonic studies, there is still inconsistency in gradient definitions. These studies did not consistently describe mirror-symmetric gradients along or across HG. Fortunately, a recent review from Baumann et al. (2013) reconciled all these findings using comparison between seminal results of monkey and human literature. Baumann and colleagues highlighted the fact that posterior and anterior high frequency subfields are closer in the medial side compared to the lateral side of HG, and conclude that the orientation of the tonotopic gradient is oblique, going from the posteromedial to the anteriolateral bulck of the STG, and not

parallel or perpendicular to HG (for more details, see Baumann et al., 2013). The border between A1 and R colocalise with the central low frequency subfield and the koniocortex of architectonic studies. Moreover, this low frequency subfield colocalised with the crown of single HG or the SI of duplicated HG (Da Costa et al., 2011). RT high-to-low gradient and other nonprimary subfields (from belt areas) are less reliable in human studies, mainly because these fields are less tonotopic and/or prefer more complex sounds. PAC areas receive bottom-up inputs from lower auditory nuclei (as explained earlier in this introduction), but can also be modulated by top-down inputs from auditory-related areas during complex processes such as attention or semantic categorization.

In the section 3.1 of this thesis, I describe the high-resolution tonotopic mapping experiments that have contributed to this improved understanding of auditory cortical organisation in the human (Da Costa et al., 2011). Importantly, our study clearly demonstrated that the primary tonotopic gradients consistently run across Heschl's gyrus in the human brain, and are thus consistent with the anterior-to-posterior orientation of the same gradients in the monkey. Further, our study demonstrated an unexpected anatomical–functional relationship that indicated the location of PAC across the common morphological variants of HG, which appeared to be part of a continuum rather than distinct subtypes.

In the section 3.4 of this thesis, I prove the reproducibility of these results at lower field strength. Our comparison between the tonotopic mapping paradigm at 3T and 7T revealed highly similar mirror-symmetric gradients within the primary auditory cortex across renderings at different spatial resolutions. Therefore, the tonotopic paradigm is robust and suitable for tonotopic studies, also at 3T, allowing a reliable identication of the primary auditory cortex in healthy subjects, but also in patients as illustrated in the section 3.5 of this thesis. Our preliminary study reported some tonotopic reorganisation at the level of the primary auditory cortex in cases of brain lesions independently of auditory complaints.

Selective attention modulation

In the beginning of the fifties, Cherry (1953) defined the "cocktail party problem" with a simple question: "how do we recognize what one person is saying when others are speaking at the same time?" During a conversation with distractive noise around, we need top-down and bottom-up interactions to selectively focus our attention on a particular voice. An object of interest is selected based on its features (e.g. female or male voice, low or high pitches) and then attention is switched between the object and the background environment (for review, see Lee et al., 2013). In the auditory field, few studies investigated object-based attention (for review: Shinn-Cunningham, 2008), but functional studies showed attention modulation in primary auditory regions (Bidet-Caulet et al., 2007; Fujiwara et al., 1998; Hillyard et al., 1973; Jäncke et al., 1999; Oh et al., 2012; Paltoglou et al., 2009, 2011; Rinne et al., 2008; Woldorff et al., 1993; Woods et al., 1984) and secondary auditory regions (Ahveninen et al., 2011; Petkov et al., 2004; Woods et al., 2009, 2010). Attention increases the contrast between target object and background noise (Fritz et al., 2003, 2007) in an object-specific attention-modulated gain control manner. Beyond the auditory cortex, attention activates a network amid superior temporal sulcus, middle temporal gyrus, premotor cortex, and inferior parietal cortex (Shinn-Cunningham, 2008).

In the section 3.2 of this thesis, I asked whether neurons of the primary auditory cortex, which show clear tuning to preferred frequencies, could filter sound information based on selected frequency-content. If so, spectral filtering by attention could be an important function of the primary auditory cortex, contributing to the downstream selection of complex sound stimuli such as speech. We found that neural responses within low- or high-frequency tuned regions of PAC were enhanced when subjects attention to low- or high-frequency tones, respectively (Da Costa et al., 2013).

Auditory repetition suppression

Auditory (but also other sensory modalities) repetition suppression is a response reduction measured after immediate single or several stimuli repetition (Grill-Spector et al., 2006). This effect has been largely used to categorize the functional specificity of brain areas to different types of stimuli (e.g. human voices, environmental sounds, music instruments) using different imaging techniques (Altmann et al., 2007; Andics et al., 2013; Bergerbest et al., 2004; Bourquin et al., 2012; De Lucia et al., 2010; Leaver and Rauschecker, 2010; Petkov et al., 2009). Repetition suppression is mainly due to automatic bottom-up processing such as adaptation. Auditory stimuli activate unspecific but also stimulus-specific auditory regions. If the same stimulus is presented again once or several times, neuronal activity will decrease – thus adapt – in regions categorizing this stimulus and will remain constant in unspecific regions.

In the section 3.3 of this thesis, I use a repetition suppression paradigm to assess semantic representation within early auditory cortical areas. Repetition of different environmental sounds of the same source induced repetition suppression effects in the right posterior and medial early-stage auditory areas, right posterior middle temporal gyrus, and repetition enhancement in the anterior medial temporal gyrus. Thus, parts of the planum temporale and medial Heshcl's gyrus are likely to carry semantic representations of static environmental sounds.

1.3 MRI principles

fMRI principles

Functional magnetic resonance imaging (fMRI), in combination with structural mag-

netic resonance imaging (sMRI), is widely used to investigate brain functions and organisation. fMRI measures spatially specific signal intensity changes correlated to different cognitive states at a macroscopic level (voxel) compared to the underlying neuronal population (neurons and astrocytes). These signal intensity variations are an indirect measure of brain metabolic activity, signalling changes in haemoglobin oxygenation. Haemoglobin molecules are present in the brain either in their oxygenated or reduced state. When linked to oxygen, these molecules do not alter magnetic properties of brain tissue. But once the tissue has extracted the oxygen molecule, the haemoglobin became paramagnetic and local magnetic field homogeneity is reduced, resulting in a diminution of the signal. The measured signal depends on the homeostasis between the concentration of oxygenated and reduced haemoglobin. When neurons get activated, the concentration of reduced haemoglobin decrease and signal loss is diminished, inducing a signal increase. fMRI measures the blood oxygenation level dependent (BOLD) hemodynamic response related to oxygen consumption. This response can be divided into four components: the initial dip briefly appearing in some brain regions after stimulus presentation, the rapid positive increase correlated with increased oxygen consumption, the return to baseline associated with blood flow decrease, and the post-stimulus undershoot caused by a temporal decoupling between blood flow recovery and blood volume decreases oxygen delivery (for a nice review on auditory cortex imaging, see section 3 in Talavage et al., 2013).

High and ultra-high field imaging

Usually, fMRI experiments are done at high field strength (3 Tesla), but ultrahigh field scanners (7 Tesla) are used more and more to explore specific brain regions of interest. 3 Tesla scanners allow whole brain imaging and are commonly used for global network research, in healthy subjects and patients. However, this global view (generally with 3 mm isotropic spatial resolution) does not allow the investigation of more subtle differences inside a small region of the interest, such as the auditory subfields. For that, 7 Tesla

machines allow higher resolution imaging, with the potential to a measure responses at column-specific levels (De Martino et al., 2013a, 2013b; Yacoub et al., 2007). At 7 Tesla, signal-to-noise ratio (SNR) and BOLD signal are increased and more specific to grey matter, due to a lesser amount of draining vein signals. This allows the use of smaller voxel sizes (generally 1 – 2 mm isotropic resolution) and increases BOLD signal specificity (De Martino et al., 2012; van der Zwaag et al., 2009, 2011). One caveat of ultrahigh field imaging is increased signal drop-out around the sinus and mastoid cavities. To overcome these limitations, one can either reduce the region of acquisition to areas that are not affected by gradients, reduce the slice thickness, optimise slice orientation, use spin-echo sequences, use rf-coils with larger number of coils or all together. Nevertheless, as mentioned, the use of 3 or 7 Tesla scanners depends on the question of interest. In some cases, such as experiments with patients, practical constraints will dictate the scanner choice. For example, the necessity to have medical devices in the same scanner will favour high field imaging over ultrahigh field without medical safeguarding.

Phase encoding analysis

Classically, fMRI data are processed with a standard general linear model where the measured signal corresponds to the modulation of the original data by experimental factors (plus some noise). This model fitted well conventional paradigms with stimuli presented randomly or pseudo-randomly during a session. However, at the beginning of the nineties, a group from Stanford proposed a new model called phase-encoding or "travelling wave" specific to phase-encoded paradigm. This group was trying to measure neuronal activity in the visual cortex using stimuli presented continuously in a specified order. They presented a circular checkerboard looming from a central position to the peripheral part of the visual field and measured delayed responses characterised by different phases (Engel et al., 1994; Engel, 2012). As the checkerboard slid towards the periphery, a travelling wave of activity (orange-yellow wave in Figure 1.3) spread from the anterior to

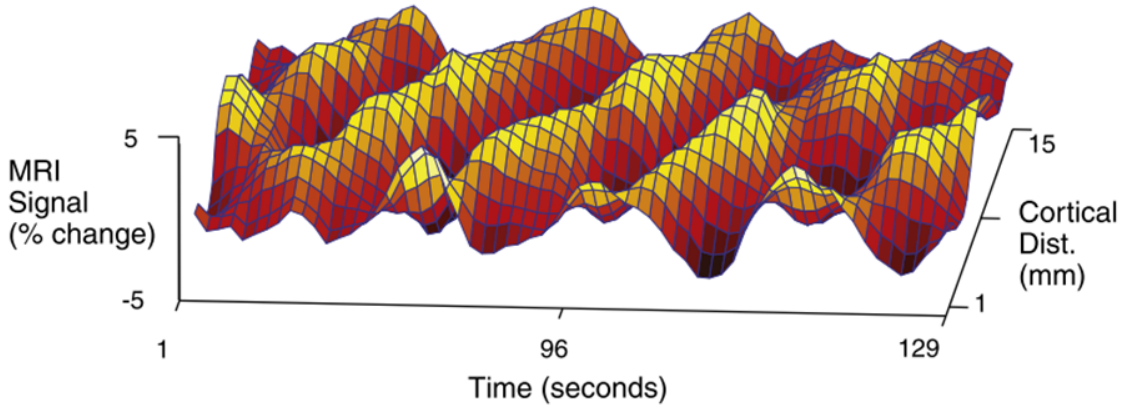

Figure 1.3: Travelling wave of activity. Voxels showing early activity preferred foveal stimuli whereas late activity voxels preferred peripheral stimuli. Yellow colors correspond to peak of activity related to stimulus presentation. Figure adapted from Engel, 2012.

posterior along the anterior calcarine sulcus. Thus voxels showing early activity preferred foveal stimuli whereas late activity voxels preferred peripheral stimuli. This was the beginning of the phase-encoding (retinotopic) history. Later on, studies on other sensory modalities used comparable designs to measure topographic organisation in distinct regions (tonotopy: Da Costa et al., 2011; Striem-Amit et al., 2011; Talavage et al., 2004; somatosentory: Sanchez-Panchuelo et al., 2010).

References

Ahveninen, J., Hämäläinen, M., Jääskeläinen, I.P., Ahlfors, S.P., Huang, S., Lin, F.-H., Raij, T., Sams, M., Vasios, C.E., Belliveau, J.W., 2011. Attention-driven auditory cortex short-term plasticity helps segregate relevant sounds from noise. Proc. Natl. Acad. Sci. 108, 4182 – 4187.

Altmann, C.F., Doehrmann, O., Kaiser, J., 2007. Selectivity for Animal Vocalizations in the Human Auditory Cortex. Cereb. Cortex 17, 2601– 2608.

Andics, A., Gál, V., Vicsi, K., Rudas, G., Vidnyánszky, Z., 2013. FMRI repetition suppression for voices is modulated by stimulus expectations. NeuroImage 69, 277 – 283.

Baumann, S., Petkov, C.I., Griffiths, T.D., 2013. A unified framework for the organization of the primate auditory cortex. Front. Syst. Neurosci. 7:11.

Beck, E., 1928. Die myeloarchitektonische Feldung des in ders Sylvischen Furche gelegenen Teiles des menschlien Schlafenlappens. J Psychol Neurol 1 – 21.

Bergerbest, D., Ghahremani, D.G., Gabrieli, J.D.E., 2004. Neural Correlates of Auditory Repetition Priming: Reduced fMRI Activation in the Auditory Cortex. J. Cogn. Neurosci. 16, 966 – 977.

Bidet-Caulet, A., Fischer, C., Besle, J., Aguera, P.-E., Giard, M.-H., Bertrand, O., 2007. Effects of selective attention on the electrophysiological representation of concurrent sounds in the human auditory cortex. J. Neurosci. Off. J. Soc. Neurosci. 27, 9252 – 9261.

Bourquin, N.M.-P., Spierer, L., Murray, M.M., Clarke, S., 2012. Neural plasticity associated with recently versus often heard objects. NeuroImage 62, 1800 – 1806.

Brodmann, K., 1909. Vergleichende Lokalisationslehre der Grosshirnrinde in ihren Prinzipien dargestellt auf Grund des Zellenbaues., Leipzig: Barth. ed.

Brugge, J.F., Merzenich, M.M., 1973. Responses of neurons in auditory cortex of the macaque monkey to monaural and binaural stimulation. J. Neurophysiol. 36, 1138 – 1158.

Brugge, J.F., 2013. Chapter 2 - Anatomy and physiology of auditory pathways and cortex, in: Gastone G. Celesia (Ed.), Handbook of Clinical Neurophysiology, Disorders of Peripheral and Central Auditory Processing. Elsevier, pp. 25 – 59.

Campbell, A.W., 1905. Histological studies on the localization of cerebral function. Cambridge: University Press.

Da Costa, S., van der Zwaag, W., Marques, J.P., Frackowiak, R.S.J., Clarke, S., Saenz, M., 2011. Human Primary Auditory Cortex Follows the Shape of Heschl's Gyrus. J. Neurosci. 31, 14067 – 14075.

De Lucia, M., Cocchi, L., Martuzzi, R., Meuli, R.A., Clarke, S., Murray, M.M., 2010. Perceptual and semantic contributions to repetition priming of environmental sounds. Cereb.

Cortex N. Y. N 1991 20, 1676 – 1684.

De Martino, F., Moerel, M., van de Moortele, P.-F., Ugurbil, K., Goebel, R., Yacoub, E., Formisano, E., 2013a. Spatial organization of frequency preference and selectivity in the human inferior colliculus. Nat. Commun. 4, 1386.

De Martino, F., Schmitter, S., Moerel, M., Tian, J., Ugurbil, K., Formisano, E., Yacoub, E., de Moortele, P.-F. van, 2012. Spin echo functional MRI in bilateral auditory cortices at 7 T: an application of B1 shimming. NeuroImage 63, 1313 – 1320.

De Martino, F., Zimmermann, J., Muckli, L., Ugurbil, K., Yacoub, E., Goebel, R., 2013b. Cortical Depth Dependent Functional Responses in Humans at 7T: Improved Specificity with 3D GRASE. PloS One 8, e60514.

Di Salle, F., Esposito, F., Scarabino, T., Formisano, E., Marciano, E., Saulino, C., Cirillo, S., Elefante, R., Scheffler, K., Seifritz, E., 2003. fMRI of the auditory system: understanding the neural basis of auditory gestalt. Magn. Reson. Imaging 21, 1213 – 1224.

Engel, S.A., 2012. The development and use of phase-encoded functional MRI designs. NeuroImage 62, 1195 – 1200.

Engel, S.A., Rumelhart, D.E., Wandell, B.A., Lee, A.T., Glover, G.H., Chichilnisky, E.J., Shadlen, M.N., 1994. fMRI of human visual cortex. Nature 369, 525.

Fleschig, P., 1908. Bemerkungen über die Hörsphäre des menschlichen Gehirns. Neurol. Zentralbl. 27.

Formisano, E., Kim, D.S., Di Salle, F., van de Moortele, P.F., Ugurbil, K., Goebel, R., 2003. Mirror-symmetric tonotopic maps in human primary auditory cortex. Neuron 40, 859 – 869.

Fritz, J., Shamma, S., Elhilali, M., Klein, D., 2003. Rapid task-related plasticity of spectrotemporal receptive fields in primary auditory cortex. Nat. Neurosci. 6, 1216 – 1223.

Fritz, J.B., Elhilali, M., David, S.V., Shamma, S.A., 2007. Auditory attention–focusing the searchlight on sound. Curr. Opin. Neurobiol. 17, 437 – 455.

Fujiwara, N., Nagamine, T., Imai, M., Tanaka, T., Shibasaki, H., 1998. Role of the primary auditory cortex in auditory selective attention studied by whole-head neuromagnetometer. Brain Res. Cogn. Brain Res. 7, 99 – 109.

Galaburda, A., Sanides, F., 1980. Cytoarchitectonic organization of the human auditory cortex. J. Comp. Neurol. 190, 597 – 610.

Grill-Spector, K., Henson, R., Martin, A., 2006. Repetition and the brain: neural models of stimulus-specific effects. Trends Cogn. Sci. 10, 14 – 23.

Hackett, T.A., Preuss, T.M., Kaas, J.H., 2001. Architectonic identification of the core region in auditory cortex of macaques, chimpanzees, and humans. J. Comp. Neurol. 441, 197 – 222.

Hillyard, S.A., Hink, R.F., Schwent, V.L., Picton, T.W., 1973. Electrical signs of selective attention in the human brain. Science 182, 177 – 180.

Humphries, C., Liebenthal, E., Binder, J.R., 2010. Tonotopic organization of human auditory cortex. NeuroImage 50, 1202 – 1211.

Jäncke, L., Mirzazade, S., Shah, N.J., 1999. Attention modulates activity in the primary and the secondary auditory cortex: a functional magnetic resonance imaging study in human subjects. Neurosci. Lett. 266, 125 – 128.

Kaas, J.H., Hackett, T.A., 2000. Subdivisions of auditory cortex and processing streams in primates. Proc. Natl. Acad. Sci. 97, 11793 – 11799.

Langers, D.R.M., Dijk, P. van, 2012. Mapping the Tonotopic Organization in Human Auditory Cortex with Minimally Salient Acoustic Stimulation. Cereb. Cortex 22, 2024 – 2038.

Leaver, A.M., Rauschecker, J.P., 2010. Cortical Representation of Natural Complex Sounds: Effects of Acoustic Features and Auditory Object Category. J. Neurosci. 30, 7604 – 7612.

Lee, A.K.C., Larson, E., Maddox, R.K., Shinn-Cunningham, B.G., 2013. Using neuroimaging to understand the cortical mechanisms of auditory selective attention. Hear. Res. Epub.

Moerel, M., De Martino, F., Formisano, E., 2012. Processing of natural sounds in human auditory cortex: tonotopy, spectral tuning, and relation to voice sensitivity. J. Neurosci. Off. J. Soc. Neurosci. 32, 14205 – 14216.

Morel, A., Kaas, J.H., 1992. Subdivisions and connections of auditory cortex in owl mon-

keys. J. Comp. Neurol. 318, 27 – 63.

Morosan, P., Rademacher, J., Palomero-Gallagher, N., Zilles, K., 2004. Anatomical organization of the human auditory cortex: Cytoarchitecture and transmitter receptors., in: The Auditory Cortex - A Synthesis of Human And Animal Research.

Morosan, P., Rademacher, J., Schleicher, A., Amunts, K., Schormann, T., Zilles, K., 2001. Human Primary Auditory Cortex: Cytoarchitectonic Subdivisions and Mapping into a Spatial Reference System. NeuroImage 13, 684 – 701.

Oh, J., Kwon, J.H., Yang, P.S., Jeong, J., 2012. Auditory Imagery Modulates Frequency-specific Areas in the Human Auditory Cortex. J. Cogn. Neurosci. 25, 175 – 187.

Paltoglou, A.E., Sumner, C.J., Hall, D.A., 2009. Examining the role of frequency specificity in the enhancement and suppression of human cortical activity by auditory selective attention. Hear. Res. 257, 106 – 118.

Paltoglou, A.E., Sumner, C.J., Hall, D.A., 2011. Mapping feature?sensitivity and attentional modulation in human auditory cortex with functional magnetic resonance imaging. Eur. J. Neurosci. 33, 1733 – 1741.

Penhune, V.B., Cismaru, R., Dorsaint-Pierre, R., Petitto, L.A., Zatorre, R.J., 2003. The morphometry of auditory cortex in the congenitally deaf measured using MRI. NeuroImage 20, 1215 – 1225.

Petkov, C.I., Kang, X., Alho, K., Bertrand, O., Yund, E.W., Woods, D.L., 2004. Attentional modulation of human auditory cortex. Nat. Neurosci. 7, 658 – 663.

Petkov, C.I., Kayser, C., Augath, M., Logothetis, N.K., 2006. Functional Imaging Reveals Numerous Fields in the Monkey Auditory Cortex. PloS Biol 4, e215.

Petkov, C.I., Logothetis, N.K., Obleser, J., 2009. Where are the human speech and voice regions, and do other animals have anything like them? Neurosci. Rev. J. Bringing Neurobiol. Neurol. Psychiatry 15, 419 – 429.

Rademacher, J., Caviness, V.S., Steinmetz, H., Galaburda, A.M., 1993. Topographical Variation of the Human Primary Cortices: Implications for Neuroimaging, Brain Mapping, and Neurobiology. Cereb. Cortex 3, 313 – 329.

Rinne, T., Balk, M.H., Koistinen, S., Autti, T., Alho, K., Sams, M., 2008. Auditory se-

lective attention modulates activation of human inferior colliculus. J. Neurophysiol. 100, 3323 – 3327.

Rivier, F., Clarke, S., 1997. Cytochrome oxidase, acetylcholinesterase, and NADPH-diaphorase staining in human supratemporal and insular cortex: evidence for multiple auditory areas. NeuroImage 6, 288 – 304.

Saenz, M., Langers, D.R.M., 2013. Tonotopic mapping of human auditory cortex. Hear. Res. Epub.

Sanchez-Panchuelo, R.M., Francis, S., Bowtell, R., Schluppeck, D., 2010. Mapping human somatosensory cortex in individual subjects with 7T functional MRI. J. Neurophysiol. 103, 2544 – 2556.

Schönwiesner, M., von Cramon, D.Y., Rübsamen, R., 2002. Is it tonotopy after all? NeuroImage 17, 1144 – 1161.

Shinn-Cunningham, B.G., 2008. Object-based auditory and visual attention. Trends Cogn. Sci. 12, 182 – 186.

Striem-Amit, E., Hertz, U., Amedi, A., 2011. Extensive cochleotopic mapping of human auditory cortical fields obtained with phase-encoding FMRI. PloS One 6, e17832.

Talavage, T.M., Gonzalez-Castillo, J., Scott, S.K., 2013. Auditory neuroimaging with fMRI and PET. Hear. Res. Epub.

Talavage, T.M., Ledden, P.J., Benson, R.R., Rosen, B.R., Melcher, J.R., 2000. Frequency-dependent responses exhibited by multiple regions in human auditory cortex. Hear. Res. 150, 225 – 244.

Talavage, T.M., Sereno, M.I., Melcher, J.R., Ledden, P.J., Rosen, B.R., Dale, A.M., 2004. Tonotopic organization in human auditory cortex revealed by progressions of frequency sensitivity. J. Neurophysiol. 91, 1282 – 1296.

Van der Zwaag, W., Gentile, G., Gruetter, R., Spierer, L., Clarke, S., 2011. Where sound position influences sound object representations: a 7-T fMRI study. NeuroImage 54, 1803 – 1811.

Van der Zwaag, W., Marques, J.P., Lei, H., Just, N., Kober, T., Gruetter, R., 2009. Minimization of Nyquist ghosting for echo-planar imaging at ultra-high fields based on a

"negative readout gradient" strategy. J. Magn. Reson. Imaging JMRI 30, 1171 – 1178.

Von Economo, C., Horn, L., 1930. Über Winddungsrelief, Masse und Rindenarchitektonik der Supratemporalfläche, ihre individuellen und ihre Seitenunterschiede. Z. Ges. Neurol. Psychiatr. 130, 678 – 757.

Von Economo, C., Koskinas, G.N., 1925. Die Cytoarchitektonik der Grosshirnrinde des erwachsenen Menschen., Berlin: Springer. ed.

Wallace, M.N., Johnston, P.W., Palmer, A.R., 2002. Histochemical identification of cortical areas in the auditory region of the human brain. Exp. Brain Res. Exp. Hirnforsch. Expérimentation Cérébrale 143, 499 – 508.

Woldorff, M.G., Gallen, C.C., Hampson, S.A., Hillyard, S.A., Pantev, C., Sobel, D., Bloom, F.E., 1993. Modulation of early sensory processing in human auditory cortex during auditory selective attention. Proc. Natl. Acad. Sci. 90, 8722 – 8726.

Woods, D.L., Alain, C., 2009. Functional imaging of human auditory cortex. Curr. Opin. Otolaryngol. Head Neck Surg. 17, 407 – 411.

Woods, D.L., Herron, T.J., Cate, A.D., Kang, X., Yund, E.W., 2011. Phonological processing in human auditory cortical fields. Front. Hum. Neurosci. 5, 42.

Woods, D.L., Herron, T.J., Cate, A.D., Yund, E.W., Stecker, G.C., Rinne, T., Kang, X., 2010. Functional properties of human auditory cortical fields. Front. Syst. Neurosci. 4, 155.

Woods, D.L., Hillyard, S.A., Hansen, J.C., 1984. Event-related brain potentials reveal similar attentional mechanisms during selective listening and shadowing. J. Exp. Psychol. Hum. Percept. Perform. 10, 761 – 777.

Woods, D.L., Stecker, G.C., Rinne, T., Herron, T.J., Cate, A.D., Yund, E.W., Liao, I., Kang, X., 2009. Functional Maps of Human Auditory Cortex: Effects of Acoustic Features and Attention. PloS One 4, e5183.

Yacoub, E., Shmuel, A., Logothetis, N., Ugurbil, K., 2007. Robust detection of ocular dominance columns in humans using Hahn Spin Echo BOLD functional MRI at 7 Tesla. NeuroImage 37, 1161 – 1177.

Chapter 2

Main research axes

In this thesis, I looked at the auditory cortex modulation, especially the plasticity of the primary auditory areas with three major questions:

1. Can we define a clear tonotopic map of the primary auditory cortex using high resolution imaging ?

2. Is the primary auditory cortex modulated by top-down mechanisms such as attention ?

3. Does repetition suppression modulate responses from primary and non-primary early-stage auditory and auditory-related areas responses ?

In the following pages, I will show results answering to these questions and also present some examples of how tonotopic maps are altered by brain injuries.

Chapter 3

Results

In this chapter, I will present the results from my thesis in paper format as they have been published or would be submitted. Each section is dedicated to one of the five projects discussed here.

All the data presented here was acquired by myself alone or with Wietske van der Zwaag or Melissa Saenz on two different MR scanners from the Centre d'Imagerie BioMédicale of the Université de Lausanne, Université de Genève, Hôpitaux Universitaires de Genève et de Lausanne, Ecole Polytechnique Fédérale de Lausanne at the Ecole Polytechnique Fédérale de Lausanne (7 Tesla) or at the Centre Hospitalier Universitaire Vaudois, Lausanne (3 Telsa). Data had been analysed by Melissa Saenz and I. The design were discussed and built by Melissa Saenz, Wietske van der Zwaag, Stephanie Clarke and myself. The manuscripts were written by the same people with the respective collaborators.

In all studies, no healthy subjects were discarded due to neurological or psychological diseases. They were all paid for their participation by a Swiss National Science Foundation Grant 3200030-124897 from Stephanie Clarke. Patients were from the Service of Neuropsychology and Neurorehabilitation of the Centre Hospitalier Universitaire Vaudois, Lausanne.

3.1 Human Primary Auditory Cortex Follows the Shape of Heschl's Gyrus

Sandra Da Costa, Wietske van der Zwaag, Jose P. Marques, Richard S. J. Frackowiak, Stephanie Clarke, and Melissa Saenz

This article has been published in Journal of Neuroscience in October 2011 (Da Costa et al., 2011).

Ackowledgements

This work was supported by a Swiss National Science Foundation Grant 3200030-124897 to S.C. and done in collaboration with the Centre d'Imagerie BioMédicale of the Université de Lausanne, Université de Genève, Hôpitaux Universitaires de Genève et de Lausanne, Ecole Polytechnique Fédérale de Lausanne, and the Leenaards and Louis-Jeantet Foundations. We thank Artur Marchewka for assistance with pilot data collection.

Abstract

The primary auditory cortex (PAC) is central to human auditory abilities, yet its location in the brain remains unclear. We measured the two largest tonotopic subfields of PAC (hA1 and hR) using high-resolution functional MRI at 7 T relative to the underlying anatomy of Heschl's gyrus (HG) in 10 individual human subjects. The data reveals a clear anatomicalfunctional relationship that, for the first time, indicates the location of PAC across the range of common morphological variants of HG (single gyri, partial duplications, and complete duplications). In 20/20 individual hemispheres, two primary mirror-symmetric tonotopic maps were clearly observed with gradients perpendicular to HG. PAC spanned both divisions of HG in cases of partial and complete duplications (11/20 hemispheres), not only the anterior division as commonly assumed. Specifically,

the central union of the two primary maps (the hA1 – R border) was consistently centered on the full Heschl's structure: on the gyral crown of single HGs and within the sulcal divide of duplicated HGs. The anatomical-functional variants of PAC appear to be part of a continuum, rather than distinct subtypes. These findings significantly revise HG as a marker for human PAC and suggest that tonotopic maps may have shaped HG during human evolution. Tonotopic mappings were based on only 16min of fMRI data acquisition, so these methods can be used as an initial mapping step in future experiments designed to probe the function of specific auditory fields.

Introduction

Over 100 years ago human primary auditory cortex (PAC, Brodmanns Area 41) was first identified based on its dense cellular structure (koniocortex) and myelination in post-mortem tissue (Brodmann, 1909; Campbell, 1905; Fleschig, 1908; von Economo and Koskinas, 1925). Today PAC is still not routinely identifiable in the living human brain. The transverse gyrus of Hesch's (HG, approximately medial two-thirds) located bilaterally on the temporal plane is an important but rough marker for PAC, not indicating exact architectonic borders (Rademacher et al., 2001). Complicating the matter, HG has high morphological variability across individuals and brain hemispheres. Duplications of HG, ranging from partial to complete, are common (estimated occurrence 41%, Rademacher et al., 1993), and architectonic evidence has never been clear about whether PAC occupies one or both divisions of duplicated Heschl's gyri. However, it is commonly assumed that PAC occupies only the first (more anterior) division of HG duplications (Penhune et al., 1996; Rademacher et al., 1993).

In the monkey, the primary auditory cortex is subdivided into three fields, A1, R and RT, which together correspond to the architectonic core and each have primary-like features, including direct thalamic input (ventral medial geniculate nucleus, Rauschecker et al., 1997). The neurons of each field respond to tones over a limited frequency range and are spatially arranged according to preferred frequencies – tonotopy (Brugge and Merzenich, 1973; Kaas and Hackett, 2000; Morel and Kaas, 1992). Along a posterior-to-anterior axis, there is a continuous mapping of preferred frequencies from high to low (A1), followed

by a reversed mapping of low back to high (R), followed by a third smaller mapping of high back to low (RT). The borders between the individual fields are marked by reversals in the frequency gradients. These tonotopic maps have been imaged in the macaque with high-resolution functional MRI in good agreement with previous maps derived from single-neuron recordings (Petkov et al., 2006). Unlike the human, the monkey temporal plane is relatively flat (no HG, Hackett et al., 2001); thus, the monkey model does not allow direct prediction of human PAC location relative to HG.

Human tonotopic maps have been challenging to obtain thus far because of their small size relative to the spatial resolution of standard non-invasive neuroimaging techniques. Using fMRI, Formisano et al. (Formisano et al., 2003) and others (Talavage et al. 2004; Woods and Alain 2009; Humphries et al. 2010) confirmed the presence in humans of at least two tonotopic maps with a mirror-symmetric "high-low-low-high" progression, likely homologues of areas A1 and R. The human data so far have not been clear about the spatial layout of tonotopic fields relative to HG, and no study has addressed the issue of PAC location across the common anatomical variants of HG. Here, we measured tonotopic maps individually in 10 human subjects using high-resolution fMRI (7T) and found a striking and highly consistent relationship between the functional tonotopic maps of PAC and the underlying anatomical shape of HG.

Materials and Methods

Subjects

Ten subjects (5 male, 5 female, ages 20 – 35) participated after giving written, informed consent. No subject had a known hearing deficit or history of neurological or psychiatric illness. Experimental procedures were approved by the Ethics Committee of the Faculty of Biology and Medicine of the University of Lausanne.

MRI data acquisition

Blood oxygenation-level dependent (BOLD) functional imaging was performed with an actively shielded 7 Tesla Siemens MAGNETOM scanner (Siemens Medical Solutions)

located at the Centre d'Imagerie BioMédicale (CIBM) in Lausanne, Switzerland.

The increased signal-to-noise ratio (SNR) and available BOLD signal arising from the use of ultra-high magnetic field systems ($>$ 3T) allow the use of smaller voxel sizes in fMRI. Also, the signal strength of venous blood is reduced due to a shortened relaxation time, restricting activation signals to the cortical gray matter and thus improving the spatial specificity of the BOLD signal (van der Zwaag et al., 2009, 2011). fMRI data were acquired using an eight-channel head volume rf-coil (RAPID Biomedical) and an EPI pulse sequence with sinusoidal read-out (Speck et al., 2008; 1.5 x 1.5 mm in-plane resolution, slice thickness = 1.5 mm, TR = 2000 ms, TE = 25 ms, flip angle = 47°, slice gap = 1.57 mm, matrix size = 148 x 148, field of view 222 x 222, 30 oblique slices covering the superior temporal plane, first three EPI images discarded). The sinusoidal shape of the readout gradients reduces the acoustic noise produced by the scanner. A T1-weighted high-resolution 3D anatomical image (resolution = 1 x 1 x 1 mm, TR = 5500 ms, TE = 2.84 ms, slice gap = 1 mm, matrix size = 256 x 240, field of view = 256 x 240) was acquired for each subject using the MP2RAGE pulse sequence optimized for 7T MRI (Marques et al., 2010). Anatomical images were used to co-register functional scans and to generate of cortical surface representations.

Auditory stimuli

Sound stimuli were generated using MATLAB and the Psychophysics Toolbox (www.psychtoolbox.org) with a sampling rate of 44.1 kHz. Stimuli were delivered via MRI-compatible headphones (AudioSystem, NordicNeuroLab) featuring flat frequency transmission from 8 Hz to 35 kHz. Subjects were instructed to keep their eyes closed during all scans.

To measure tonotopy (Figure 3.1), pure tone stimuli were presented to subjects in ordered progressions from low frequencies to high: 88, 125, 177, 250, 354, 500, 707, 1000, 1414, 2000, 2828, 4000, 5657, and 8000 Hz (half-octave steps). Starting with the lowest frequency, pure tone bursts of that frequency were presented for a 2 s block before stepping to the next higher frequency until all 14 frequencies had been presented. This 28 s low-to-high progression was followed by a 4 s silent pause, and this 32 s cycle was repeated

15 times per 8 minute scan run. Each subjects participated in two 8 minute scan runs, resulting in 30 frequency progressions per subject. Frequency progressions were designed to induce a travelling wave of response across cortical tonotopic maps: responses should peak first in regions preferring low frequencies and sequentially later in regions preferring higher frequencies. As described further below, cross-correlation was used to determine the time to peak of the response on a per-voxel basis. This procedure is equivalent to the phase-encoded mapping techniques shown to be highly efficient in visual retinotopic mapping (Engel et al. 1994; Sereno et al. 1995).

During each 2 s frequency block, eight tone bursts of the same frequency were presented. Tone bursts were either 50 ms or 200 ms in duration (interstimulus interval = 50 ms) and were alternated in pseudo-randomized order during the 2 s block, resulting in a rhythmic pattern of tone onsets. This rhythmic pattern served to increase the perceptual salience of the stimuli over the regular pattern of background scanner noise.

Perceived volume (a perceptual rather than physical quality of sound) varies widely as a function of frequency, mostly due to peripheral sensitivities in the cochlea. After sound system calibration, sound intensities were adjusted according to standard equal-loudness curves (ISO 226, phon 65) to approximate equal perceived volume across all frequencies. Actual sound intensities (62-84dB) matched the perceived volume of a 1000Hz tone (reference frequency) at 65 dB. Sound levels were further attenuated ($\sim$ 24 dB) by the required use of protective ear plugs. Background EPI scan noise was $<$ 104 dB as measured with an MR-compatible optical microphone (Sennheiser, MO 2000) and acoustic calibrator (Cesva Acoustic Instruments). Scan noise was attenuated +30 dB by the headphone ear cups and dense foam padding around the head used to stabilize position. Despite the moderate sound intensities used, subjects reported hearing all tones over the background noise at a clear and comfortable level.

Five of the 10 subjects also participated in two additional scan runs (30 frequency progressions) in which tone frequencies progressed in reversed order from high-to-low in order to verify that the order of stimulus presentation did not alter the observed layout of the tonotopic maps. Data from one reversed-order scan run was discarded due to head motion (second run of subject no. 10).

Analysis

Brain Voyager QX software v2.3 (Brain Innovation) and MATLAB (R2008b) were used for data analysis and display. Standard fMRI data preprocessing steps included linear tread removal, temporal high-pass filtering, and motion correction. Spatial smoothing was not applied. Functional time-series were interpolated into 1 x 1 x 1 mm^3 volumetric space in registration with each subjects 3D Talairach-normalized anatomical data set. Functional-to-anatomical registrations were all visually inspected for verification. Cortical surface meshes were generated from the anatomical images using automated segmentation tools in BrainVoyager QX. The resulting surface meshes were minimally inflated (100 steps), just enough to allow viewing of the temporal plane while incurring the least amount of spatial distortion.

Statistical analyses (using linear cross-correlation) were performed in volumetric space (Figure 3.1.B) for each subject individually. A hemodynamic time-course was predicted in response to the first 2-sec sound block of each stimulus cycle. This cyclical model function was shifted successively in time in 2 s increments (corresponding to the TR) to generate 14 time-lagged functions. Linear cross-correlation was applied (between all 14 model functions and the measured fMRI time course) on a per-voxel basis. The time course was averaged from the two scan runs per experiment (240 volumes). Each voxel was then color-coded according to the lag function resulting in the highest correlation value with its time course (winner-take-all). Correlation maps were projected onto partially-inflated cortical surface meshes to facilitate viewing (Figure 3.1.C) and spatial smoothing of the maps was not applied. Individual subject correlation maps are displayed in Figure 3.1 with a statistical threshold of $p < 0.05$ corrected for multiple comparisons using the false discovery rate (FDR) method. Correlation values at this significance level were $r > 0.17$. 0.16 and 0.15 for the three data displays of Figure 3.1.C.

Group-averaged tonotopic maps (Figure 3.1.E) were generated using cortex-based alignment (Fischl et al., 2004) as implemented in BrainVoyager QX. This is a non-rigid alignment of cortical surface meshes across individuals based on the gyral and sulcal folding patterns. Each subjects cortical surface meshes were aligned to a target mesh (separately for left and right hemispheres) and the target meshes were chosen from a subject with

intermediate HG anatomy (subject 2, partial HG duplication in each hemisphere). All alignment were visually inspected. In all cases, the FTS (first tranverse sulcus, anterior border of HG) aligned to the target FTS. In all cases when a single or partially duplicated HG was present, the HS (Heschl's sulcus, posterior border of HG) aligned to the target HS. In the three cases of complete duplications, it was HS2 (the more posterior of the two Heschl's sulci) that aligned with the target HS. Thus, in all cases, the sulci bordering the full Heschl's structure aligned. Following cortex-based alignments, individual-subject tonotopic maps were projected onto the target surface mesh so that all subjects maps were in a common, aligned coordinate space where tonotopic maps were subsequently averaged. The maps in Figure 3.1.E are the result of a direct averaging the lag and correlation values across the 10 subjects at each surface coordinate. Maps are displayed with a correlation threshold of $r > 0.15$, the average correlation value corresponding to $p < 0.05$ (FRD corrected) in the individual subject analysis.

Plots of primary auditory cortex (surface patches of figures 3.2 and 3.3)

Two tonotopic gradients with mirror-symmetry ("high-low-low-high") were clearly observed in all hemispheres. Our goal was to evaluate the spatial layout of these two primary tonotopic fields relative to the underlying anatomy of HG in each subject. To this end, we manually selected contiguous patches of cortical surface containing the two primary gradients in each hemisphere (n = 20), and then plotted those surface patches with gyral borders overlaid (Figures 3.2 and 3.3) as described next.

How were the regions plotted ?

All vertices within the contiguous selected regions were exported and plotted. Specifically, five values were exported for each vertex: x, y, and z coordinates, a best-fitting lag value (1-14), and a curvature value. The coordinates were plotted in the x-y plane and collapsed across z-coordinates. Open circles show overlapping points in the collapsed z-dimension. A color scale indicates the best-fitting lag value of each point.

This 2D collapsed presentation (of partially inflated surface coordinates) was chosen, rather than standard flat maps, to minimize anatomical distortion due to continued inflation or complete flattening. In particular, we chose to collapse across the z-direction to preserve as well as possible x-y spatial relationships since there has been much interest in the particular orientation of the tonotopic gradients within the x-y plane (see Discussion). We find that previous human fMRI tonotopy studies have made this orientation difficult to interpret by display of data on highly inflated or fully flattened surfaces that had significant x-y spatial distortions. A disadvantage of our collapsed presentation is that the gradients are somewhat squeezed in the direction orthogonal to HG, however as noted above data points are plotted with open circles so that overlapping data points remain visible.

What statistical threshold was used ?

Within the plotted surface patches (Figures 3.2 and 3.3), no statistical threshold was applied. This is because of the arbitrariness of selecting a voxel-wise correlation threshold when the goal is to observe the pattern of data across all voxels within an area of interest. Thus, the plots of Figures 3.2 and 3.3 show data from all vertices within the contiguous selected regions, with no points excluded due to thresholding.

How were gyral borders drawn ?

Curvature values were calculated as implemented in BrainVoyager QX and correspond to what is geometrically defined as mean curvature. Normal curvature is measured as 1/r where r is the radius of an inscribed circle. A vertex on a 3D surface has an infinite number of normal curvatures, and the mean curvature is the average of the principal (max and min) curvatures. The units are in 1/mm. Extracted curvature values identified each vertex as convex (gyral) or concave (sulcal) on a continuous negative-to-positive scale and are based on the original geometry of the surface mesh before inflation. To estimate gyral/sulcal borders, we plotted binarized curvature values and drew edges at the transitions from convexity to concavity. Edges were overlaid on the correlation maps, as demonstrated in the lower left inset of Figure 3.2.

Results

Anatomical variants of Heschl's gyrus (HG) have been previously classified into three subtypes (Abdul-Kareem and Sluming, 2008; Leonard et al., 1998). In the first subtype, HG is single and has a smooth crown (single HG). It is bordered by the first transverse sulcus (FTS) on the anterior side and Heschl's sulcus (HS) on the posterior side. In the second subtype, HG is partially divided along its length by a sulcus intermedius (SI). The length of the SI can be short or long and its depth can vary, but the division is considered partial if the SI does not extend down to the medial base of HG, leaving the two divisions of HG connected by a common stem (partial duplication or common stem duplication). In the third subtype, HG is fully divided by a sulcus extending all the way down to its medial base, dividing the structure into two parallel gyri without a common medial stem (complete duplication). In case of complete duplications the standard nomenclature of the sulci differs and there are considered to be two Heschl's sulci (HS1 and HS2): the dividing sulcus is called HS1 and the sulcus behind the posterior division is HS2. The 20 hemispheres in our study (which were not preselected for anatomy) had the following distribution of the three HG subtypes: 9 single gyri, 8 partial duplications, and 3 complete duplications.

In 20/20 individual hemispheres, we clearly observed two mirror-symmetric frequency progressions (high-low-low-high) in the region of HG. Figure 3.1.D shows maps in three sample hemispheres (voxelwise statistical threshold $p < 0.05$, after FDR correction for multiple comparisons). The two mirror-symmetric maps correspond with those first identified by Formisano et al. (2003) and are likely homologues of macaque areas A1 and R. The more posterior of the two maps (high-to-low) corresponds to A1 and the anterior map (low-to-high) corresponds to R. Here, we refer to these regions as human A1 (hA1) and hR. Additional smaller frequency progressions were in some cases observed posterior and anterior to the main two maps and these may correspond to non-primary auditory fields (Rivier and Clarke, 1997); however these maps were less consistent and are not further addressed here. The spatial layouts of the two primary tonotopic maps relative to HG were consistent enough across subjects to be evident on group-averaged maps (n = 10) that were combined using a cortex-based alignment (Figure 3.1.E).

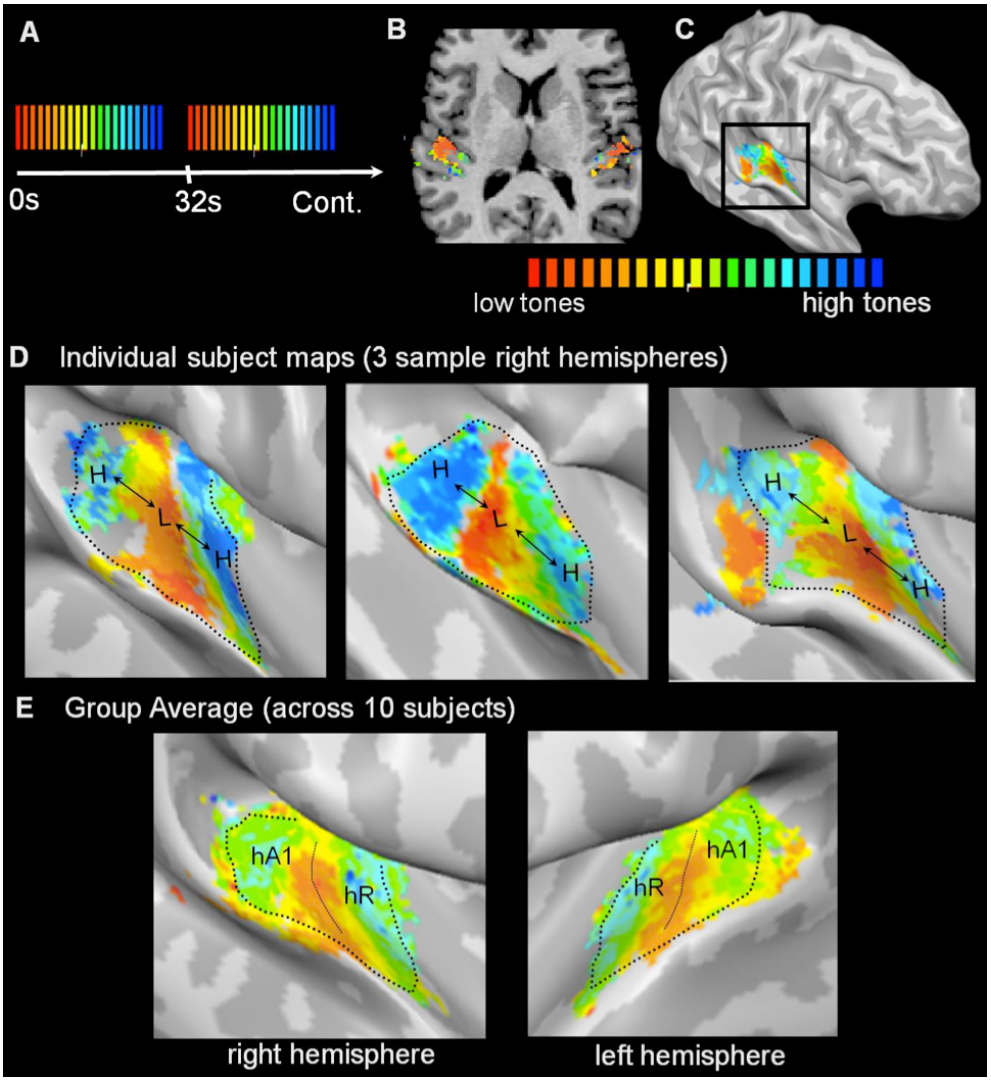

Figure 3.1: Tonotopic maps in auditory cortex. **(A)** Sound stimuli were pure tone bursts presented in cycled progressions from low frequencies to high: 88 to 8000Hz in half-octave steps. Each 28s progression from low to high (red-to-blue color scale) was followed by a 4 sec stimulus pause. Sound stimuli were designed to induce a traveling wave of response across cortical tonotopic maps: fMRI responses peak sooner in map regions preferring low frequencies and progressively later in regions preferring higher frequencies. Linear cross-correlation analysis was used to determine the temporal delay which best fit the observed fMRI response time-course od each voxel and to assign a corresponding best frequency. **(B)** Analyses were performed in each individual subjects (n = 10) volumetric space. **(C)** Resulting color-coded maps were projected onto each subjects cortical surface meshes. Surfaces were minimally inflated to expose the auditory cortex on the temporal plane **(D, E)**. In 20/20 hemispheres, two primary mirror-symmetric tonotopic maps (high-to-low-low-to-high) were observed and 3 sample right hemispheres are shown. The posterior (high-to-low) and anterior (low-to-high) maps contain the subregions human A1 and R, respectively, and the low frequency union between the two maps is the hA1-R border (dotted line). Group averaged tonotopic maps across all 10 subjects after cortex-based alignment indicates the consistency of tonotopic map location relative to HG. Linear correlation threshold for all subfigures $r > 0.15$.

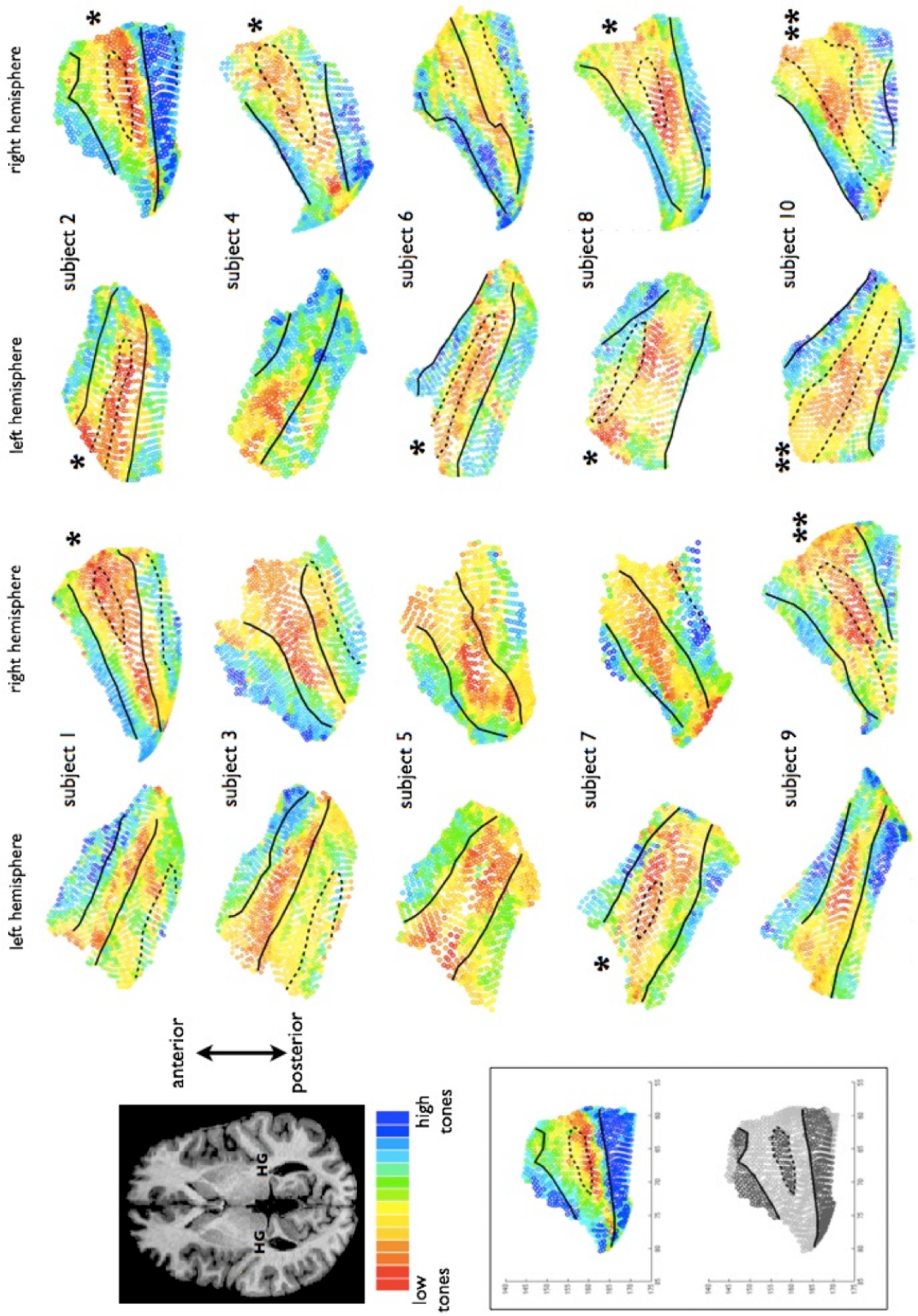
left hemisphere
right hemisphere
subject 1
subject 2
subject 3
subject 4
subject 5
subject 6
subject 7
subject 8
subject 9
subject 10
anterior
posterior
HG
HG
low tones
high tones

Figure 3.2: Spatial layout of PAC relative to HG. The two primary mirror-symmetric tonotopic maps ("high-low-low-high") containing hA1 and hR were identified and extracted from the cortical surface meshes (n = 20 hemispheres) and are plotted here with the borders of HG indicated (solid lines: anterior border = FTS, first transverse sulcus; posterior border = HS, Heschl's sulcus). In 9/20 hemispheres, HG was a single gyrus with a smooth crown. In 8/20 hemispheres (partial duplications, *) a sulcus intermedius (SI) was present on the gyral crown (dotted lines) splitting HG into two divisions that remained connected by a common medial stem. In 3/20 hemispheres (complete duplications, **) a dividing sulcus was present that reached all the way down to the medial base of HG so that the two divisions did not remain connected by a common medial stem (also indicated with dotted lines). Note that in the case of complete duplications there is a difference in the standard nomenclature and there are considered to be two Heschl's sulci (HS1 and HS2): the dividing sulcus (dotted line) is HS1 and the posterior border (solid line) is HS2. In some cases the posterior end of the functional maps extended onto less prominent gyri of the planum temporale, which are also indicated by dotted lines (outside the posterior border of HG) when present. These plots reveal a continuous anatomical-functional relationship across the anatomical variants of HG, as described in Results. As shown in the lower left inset, gyral/sulcal borders were drawn corresponding to cortical surface transitions between convexity and concavity, as described in Material and Methods.

Our goal was to evaluate the spatial layout of PAC relative to the underlying anatomy of HG in each subject individually. To this end, we outlined the "high-low-low-high" maps observed on each surface mesh (n = 20, see outlines on Figure 3.1.D) and plotted those contiguous surface patches with gyral borders overlaid (Figure 3.2). Every surface voxel within each patch is displayed and color coded according to preferred frequency, with no points excluded due to thresholding. Cases of single gyri, partial duplications, and complete duplications are indicated. The plots in Figure 3.2 show several patterns of interest. First, it was evident in 20/20 hemispheres that tonotopic gradients ran perpendicular to the long-axis of HG (correspondingly, map iso-frequency lines ran parallel to HG). Second, in cases of partial or complete duplications, PAC (the combined maps of hA1+ hR) clearly spanned both anterior and posterior divisions of HG, not only the anterior division as commonly assumed. Third, consistent with previous architectonic reports, PAC was not always limited by the outer borders of HG. In some cases (subjects 1, 2, 3, 6, and 7), the posterior map (hA1) continued a variable extent beyond Heschl's sulcus (HS) onto less pronounced gyri of the planum temporale.

Finally, and most surprisingly, there was a highly consistent relationship between the

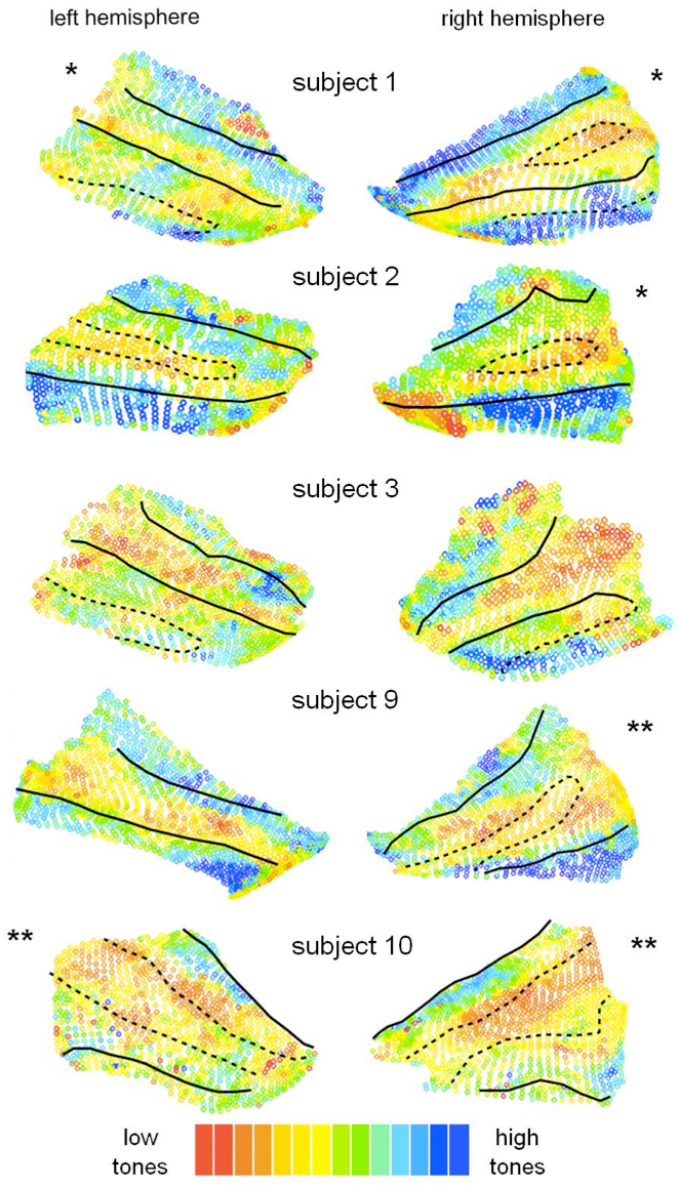

Figure 3.3: Results of reversed-order. Results of separate scans run in five of the same subjects in which the tonotopic mapping stimuli were presented in reversed order (high frequencies-to-low, rather than low-to-high). A consistent anatomical-functional relationship is observed.

spatial layout of the maps and the underlying shape of HG. On all single HGs (9/20 hemispheres, subtype 1), the low frequency union between the two maps (the hA1 – R border) occurred on the crown of the gyrus. In all cases of partial duplication (8/20 hemispheres,

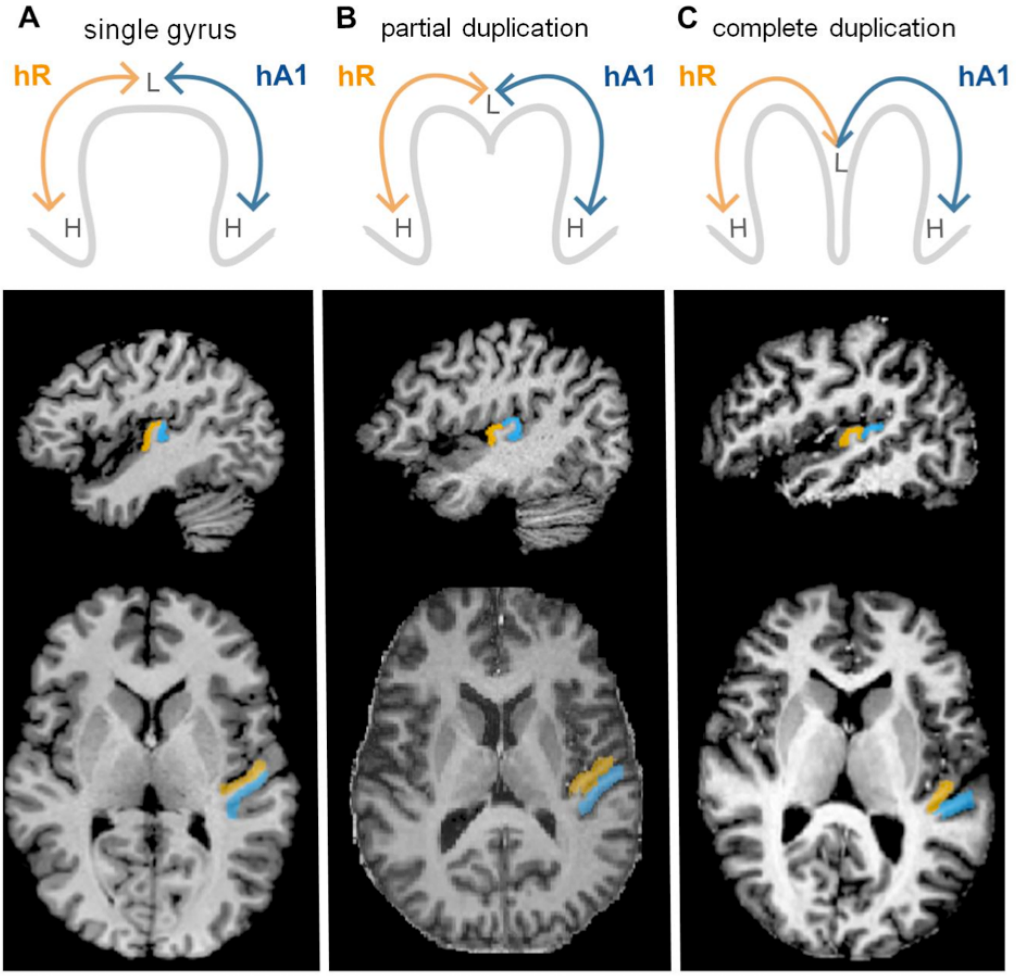

Figure 3.4: Heschl's gyrus variants are part of a continuum, rather than distinct subtypes. top row: Diagrams of hA1 (blue) and hR (orange) locations on cross-sections of Heschl's gyrus. hA1 is located on the posterior side or division of HG on single and duplicated gyri, respectively. hR is likewise on the anterior side or division of HG. L and H depict the location of low and high frequencies on the tonotopic maps - **middle and bottom rows:** Actual hA1 and hR locations in axial and sagittal anatomical views from three sample subjects, as identified based on the functional tonotopy data. The regions were selected on the cortical surface meshes and projected into volumetric anatomical space. The border between hA1 and hR was defined along the elongated low frequency representation between the two frequency gradients (i.e. at the gradient reversal).

subtype 2) the hA1 – R border occurred either in or very near the SI. In all cases of complete duplication (3/20 hemispheres, subtype 3), the hA1 – R border also occurred within the dividing sulcus (HS1) which thus appears to be a continuation of the pattern seen on

partial duplications. As shown in Figure 3.3, reversing the order of stimulus presentation during mapping (tones presented from high frequencies to low) did not influence the spatial layout of the observed maps with respect these observed patterns.

This precise structural-functional relationship reveals that the anatomical variants of HG are part of a continuum, rather than distinct subtypes as summarized in Figure 3.4. hA1 (the posterior high-to-low map) is located on the posterior side of HG when the gyrus is single (Figure 3.4.A) and on the posterior division of HG when the gyrus is duplicated (Figures 3.4.B and 3.4.C). hR (the anterior low-to-high map) is likewise located on the anterior side or division of HG. The lower panels of Figure 3.4 show the actual locations of hA1 and hR in three sample subjects, as identified by their own functional tonotopic mappings. The regions correspond to the coordinates of the subjects "high-low-low-high" contiguous surface patches projected into each subjects own native anatomical space. The border between hA1 and hR was defined along the reversal between the two primary frequency gradients (as demonstrated on the group-average map in Figure 3.1.E).

Figure 3.5.A shows the relationship between frequency representation and cortical curvature values across all PAC surface voxels of all single HG hemispheres (means and SE bars computed over all voxels of all 9 hemispheres combined, number of voxels = 10,400). The curvature value of each voxel is a measure of the voxels local concavity versus convexity on the cortical surface mesh before inflation. Negative values are convex (gyral) and positive values are concave (sulcal). There was a significant correlation between frequency and curvature values: correlation values, R, were computed over all voxels of each of the nine hemispheres separately (hence n = 9) and were significantly different from zero (mean positive correlation value r = 0.34; $p < 0.0005$, t-test). Thus, we found a systematic relationship in that frequencies near the union of the mirror-symmetric maps (i.e. low frequencies) tend to occur on a gyrus (HG) and those frequencies farthest from the union (i.e. high frequencies) tend to occur in sulci. A similar relationship (Figure 3.5.B, number of voxels = 9763) was also observed in cases of partial duplication (n = 8, mean r = 0.34, $p < 0.005$, t-test); however, the pattern was fully disrupted (Figure 3.5.C, number of voxels = 3932) in cases of complete duplications (n = 3, mean r = -0.15, t-test). Interestingly, the union of mirror symmetric retinotopic maps on a gyrus also occurs in the visual system at the V1/V2 border (Van Essen 1997; Rajimehr and Tootell 2009, see

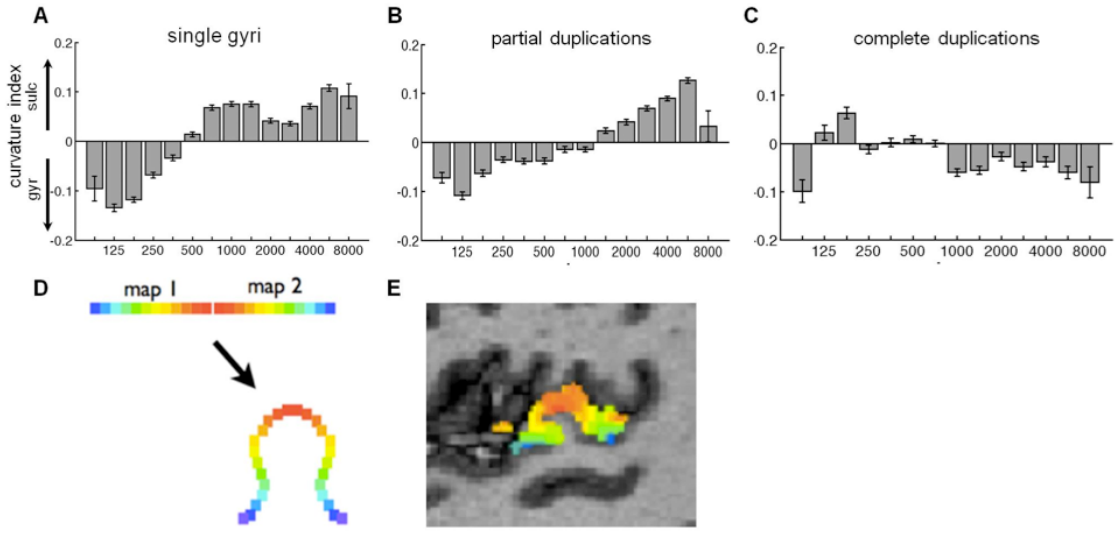

Figure 3.5: Tonotopy relative to curvature of HG. Curvature index vs. preferred frequency values of all surface voxels within the two primary tonotopic maps, across all subjects hemispheres with a **(A)** single HG **(B)** partial duplication, and **(C)** complete duplication. Positive curvature values indicate concavity (sulcal), and negative values indicate convexity (gyral). Systematically, low frequencies tend to be represented on a gyrus (HG) and high frequencies within adjacent sulci. Error bars indicate S.E.M. **(D)** Diagram showing how a fold between mirror symmetric maps brings equivalent topographic points on the two maps closer together in space (in the case of a single gyrus). **(E)** Actual tonotopy data on HG from a sample subject for comparison, sagittal slice view.

Discussion). The analysis here of map value versus curvature value is similar to that of Rajimehr and Tootells (2009) quantification of this structure-function relationship in the visual cortex.

Discussion

These data reveal a striking and highly consistent relationship between the tonotopic maps of hA1 and hR and the underlying anatomy of Heschl's gyrus. These findings significantly revise HG as a marker for human PAC and suggest that tonotopic maps may have shaped HG during human evolution, as discussed below.

It is important to note that the mapping of human auditory cortex is not yet complete. Based on the monkey model, a third smaller primary field (RT) is expected anterior to R, as well as additional gradients outside the primary core (non-primary belt fields). These additional fields have been imaged with fMRI in the macaque in good agreement with previous single-unit recordings (Petkov et al., 2006). Additional tonotopic fields have been imaged in the human as well, but they are seen less reliably than the main two gradients (Humphries et al., 2010; Striem-Amit et al., 2011; Talavage et al., 2004; Woods et al., 2009). We also observed, in some cases, additional frequency reversals anterior to hR (see Figure 3.1.D, example 1) and posterior to hA1 (Figure 3.1.D, example 3). Potential reasons that these fields are imaged less reliably in the human could be that these fields are small, less strictly tonotopic, not optimally driven by pure tones, and/or different from monkeys.

It is also important to note that the lateral and medial boundaries of PAC are still unclear. Human PAC is expected on the medial two-thirds (approximately) of HG, with nonprimary architectonic regions occupying the lateral end of HG (Rivier and Clarke, 1997). In the macaque, iso-frequency bands of the core gradients continue laterally and medially into the belt fields, so it is not expected to be able to discern the lateral and medial borders of the primary core based solely upon tonotopic maps. The observed tonotopic patterns extended the full lateralmedial extent of HG. Thus, it is very likely that the lateral edges of the maps include some portion of lateral belt fields, and also possible that the medial edge includes a small portion of medial belt. A functional method of determining the human corebelt boundary remains to be demonstrated. A recent study estimates the corebelt boundary at a fixed spatial extent from the centre of auditory activation (Chevillet et al., 2011), but this does not reveal exact boundaries nor take into account individual differences.

PAC spans both divitions of duplicated Heschl's gyri

We find that human PAC covers both divisions of duplicated Heschl's gyri, not only the first (more anterior) division as commonly assumed (Rademacher et al., 1993; Penhune et al., 1996). This distinction affects a broad literature that uses anatomical criteria to estimate the size of human PAC (and the adjacent planum temporale) in relation to

brain laterality, language and music abilities, and auditory-related pathologies, including dyslexia, autism, and schizophrenia (for review, see (Abdul-Kareem and Sluming, 2008). By current convention, only the anterior division of duplicated HGs is included in PAC measurements (Emmorey et al., 2003; Gage et al., 2009; Hubl et al., 2010; Leonard et al., 2001; Penhune et al., 1996; Rademacher et al., 1993; Schneider et al., 2002, 2009; Warrier et al., 2009; Wong et al., 2008) with the posterior division assigned instead to the planum temporale (Dorsaint-Pierre et al., 2006). The criteria proposed by Penhune et al. (1996) (to consider only the anterior division as part of PAC if there is an SI extending half the length of HG) would wrongly exclude the posterior division of PAC (the entire hA1 subfield) in 7 out of 20 of our cases.

It is important to note that our study does not aim to propose a new set of anatomical criteria for estimating PAC size. We corroborate previous architectonic reports (Morosan et al., 2001) that PAC is not always contained within the anatomical borders of HG. In particular, PAC in many cases extended posteriorly onto the planum temporale. We concur with previous assertions that estimating PAC size based on gross anatomical landmarks is prone to error (Abdul-Kareem and Sluming, 2008).

Tonotopic gradients run across Heschl's gyrus

A leading model has been that tonotopic gradients run parallel to HG, rather than perpendicular. This model stems from architectonic reports (Hackett et al., 2001) that claim that human primary auditory cortex forms an elongated strip (posteromedial-to-anterolateral) along HG, the shape of which appears similar to the elongated auditory core in monkeys (posterior-to-anterior), which contains the three tonotopic fields A1, R, and RT. Thus, it was expected that human tonotopic gradients were rotated compared to the macaque and would be found running along (or parallel to) HG rather than across it. This model was somewhat supported by MEG measurements (Romani et al., 1982) and chronic microelectrode recordings (Howard et al., 1996) placing high frequencies medially on HG and low frequencies laterally on HG (thus potentially accounting for the low-to-high map of A, but not R). Those recording methods were limited by poor localization accuracy and by limited sampling, respectively.

On the other hand, tonotopic gradients measured with fMRI have repeatedly appeared to run across HG, consistent with the posterior–to–anterior orientation in the macaque (Formisano et al., 2003; Humphries et al., 2010; Striem-Amit et al., 2011; Talavage et al., 2004; Woods et al., 2009). However, data have often been unclear and interpretation has been made difficult by display on highly inflated or fully flattened surfaces with distorted spatial relationships. For example, despite gradients appearing to run across HG, Formisano et al. (2003) concluded that gradient orientation was "posteromedial-to-anterolateral", thus apparently confirming the model of parallel gradients. Our mappings lead us to strongly conclude that the primary tonotopic gradients run across HG, rather than along it, and that this orientation is highly consistent across individuals (n = 20 hemispheres) and across the morphological variants of HG.

It should also be noted that the gradients do not have to be strictly perpendicular and could be tilted in a number of orientations. The maps of hA1 and hR could run along an axis across HG that is tilted posteromedial (PM)-to-anterolateral (AL), or likewise, tilted posterolateral (PL)-to-anteromedial (AM). Another intriguing possibility is that the core axis is curved (as in the macaque, Kaas and Hackett, 2000) with the map of hA1 angled PM-to-AL and the map of hR angled PL-to-AM. Such a curved orientation would help explain why the low-frequency representation often appears wider laterally and could explain the earlier interpretation of MEG data. The exact orientation depends on how one establishes the starting (high) and end (low) points of the gradients, which is not obvious since the high- and low-frequency representations are not distinct points but rather iso-frequency bands that continue into nonprimary belt areas. The exact orientations may be clarified by future mapping studies that can distinguish core from belt regions, thus giving a better estimate of gradient starting and end points.

Measuring tonotopy with BOLD fMRI

In single-neuron recordings in animals, neuronal frequency tuning is characterized at threshold volume levels (characteristic frequency, CF), and tuning tends to broaden progressively as sound volume increases (Phillips et al., 1994). This leads to the question of how frequency tuning can be measured with fMRI, which requires the use of suprathreshold stimuli to illicit robust responses. Recent high-field fMRI studies (Petkov et al., 2009,

2006; Tanji et al., 2010) using suprathreshold stimuli (70-90 dB) have imaged multiple tonotopic fields in the macaque (including A1, R, RT, and belt areas) that matched the expected location, size, and gradient orientations known from previous electrophysiological and anatomical measures. As such, the BOLD response may be measuring (1) subtle preferences at high stimulus intensities and/or (2) the tuning of some neurons that remain sharp at high intensities. Such neurons have been reported in primary auditory cortex of the awake macaque (Recanzone et al., 2000) and in more recent studies that suggest the tuning is sharper in awake compared to anesthetized animals and more invariant to stimulus intensity (Bartlett et al., 2011; Sadagopan and Wang, 2008). Intracranial recordings on HG in alert humans show sharp frequency tuning at suprathreshold stimulus levels (Bitterman et al., 2008).

In the macaque, the cortical representation in A1 is $\sim$1 octave/mm. Given that our mapping stimuli (in humans) spanned 7 octaves (88-8000 Hz), associated maps would be expected to span at least 7 mm each (14 mm total for hA1 + hR), if not more considering human cortical expansion. The topological distance across our maps of hA1 + hR (angled across HG) was 27.6 $\pm$ 3.9 mm (mean $\pm$ SD), thus indicating sufficient space across HG to accommodate the expected length of two primary frequency gradients. In terms of limitations of fMRI imaging, there still remains an unknown impact of scanner noise on the cortical response to sound. The impact can be reduced with sparse scanning techniques (Humphries et al., 2010; Petkov et al., 2009) but with a significant trade-off in scan time. Also, it is unknown whether different physiological properties at different parts of the map differentially influence the BOLD response.

Comparison to architectonic measures of human PAC

After a century of mapping cortical architecture (Campbell, 1905; Clarke and Rivier, 1998; Fullerton and Pandya, 2007; Galaburda and Sanides, 1980; Hackett et al., 2001; Morosan et al., 2001; Rademacher et al., 1993; Rivier and Clarke, 1997; Sweet et al., 2005; von Economo and Horn, 1930; von Economo and Koskinas, 1925; Wallace et al., 2002), it appears that human PAC is not uniform, and multiple subdivisions have been proposed. The central regions of PAC show the strongest primary (koniocortical) features. von Economo and Horn (1930) noted that within PAC, the densest packing of granular

cells is found on the crown of HG (referring to single gyri); and Hackett et al. (2001) found that the most prominent core region fell along the SI (referring to partial duplications). Our data suggest that this region of densest cellular structure (the crown of single gyri and the SI of duplicated gyri) may correspond to the low-frequency representation at the border between hA1 and hR.

Mirror-symmetric maps meet on a gyrus: parrallel with visual cortex

Interestingly, the data reveal a previously unknown organizational parallel with the visual cortex: the union of mirror-symmetric tonotopic maps (the hA1– R border) occurs on the crown of the gyrus in humans, just as the union between mirror-symmetric retinotopic maps (the V1/V2 border) occurs on a gyrus in humans and macaques (Rajimehr and Tootell, 2009; Van Essen, 1997). This phenomenon in the visual system has been the primary argument for the hypothesis (Van Essen, 1997) that cortical folds occur as a result of axonal tension between highly interconnected regions during development. According to this hypothesis, interconnected mirror-symmetric maps are pulled together during development (Figure 3.5.D and 3.5.E), resulting in compact cortical wiring. Indeed, monkey AI and R are highly interconnected between matching tonotopic locations (Morel and Kaas, 1992; Morel et al., 1993). While this hypothesis could explain the emergence of HG, it would not explain the variable existence of the SI. It is also possible that there are differences in cortical architecture (e.g., cell density, cortical thickness) linked to the region of low-frequency representation that make this region more likely to fold.

Heschl's gyrus is a cortical fold that is specific to human evolution: the macaque auditory cortex has mirror-symmetric tonotopy but is flat (no transverse gyri), chimpanzees may have a primitive transverse gyrus, and humans typically have 1-2 HGs per hemisphere (Hackett et al., 2001). Cats and rodents also have multiple tonotopic fields with gradient reversals (Hackett et al., 2011; Schreiner and Winer, 2007). Thus, mirror-symmetric tonotopy apparently preceded HG phylogenetically and may have guided the formation of HG during human evolution, as additional folding occurred to meet increased demand for cortical surface. It is not known whether HG duplications affect auditory processing. Interestingly, HG duplications are more common in the left hemisphere of expert phoneticians (Golestani et al., 2011) and in individuals with Williams syndrome (Wengenroth et

al., 2010).

Future directions

On a final note, the functional specializations of A1 and R remain unknown in monkey and human. Because tonotopic maps required only 16 min of fMRI data acquisition, these methods can be used as an initial mapping step in future studies of the specific auditory fields, much like the use of retinotopic mapping in visual cortex (Wandell and Winawer, 2011). Identification of these auditory fields is a necessary first step toward further study of the function, evolution, and plasticity of the human auditory cortex.

References

Abdul-Kareem, I.A., Sluming, V., 2008. Heschl gyrus and its included primary auditory cortex: structural MRI studies in healthy and diseased subjects. J. Magn. Reson. Imaging 28, 287 – 299.

Bartlett, E.L., Sadagopan, S., Wang, X., 2011. Fine frequency tuning in monkey auditory cortex and thalamus. J. Neurophysiol. 106, 849 – 859.

Bitterman, Y., Mukamel, R., Malach, R., Fried, I., Nelken, I., 2008. Ultra-fine frequency tuning revealed in single neurons of human auditory cortex. Nature 451, 197 – 201.

Brodmann, K., 1909. Vergleichende Lokalisationslehre der Grosshirnrinde in ihren Prinzipien dargestellt auf Grund des Zellenbaues., Leipzig: Barth. ed.

Brugge, J.F., Merzenich, M.M., 1973. Responses of neurons in auditory cortex of the macaque monkey to monaural and binaural stimulation. J. Neurophysiol. 36, 1138 – 1158.

Campbell, A.W., 1905. Histological studies on the localization of cerebral function. Cambridge: University Press.

Clarke, S., Rivier, F., 1998. Compartments within human primary auditory cortex: evidence from cytochrome oxidase and acetylcholinesterase staining. Eur. J. Neurosci. 10,

741 – 745.

Da Costa, S., van der Zwaag, W., Marques, J.P., Frackowiak, R.S.J., Clarke, S., Saenz, M., 2011. Human Primary Auditory Cortex Follows the Shape of Heschl's Gyrus. J. Neurosci. 31, 14067 – 14075.

Dorsaint-Pierre, R., Penhune, V.B., Watkins, K.E., Neelin, P., Lerch, J.P., Bouffard, M., Zatorre, R.J., 2006. Asymmetries of the planum temporale and Heschl's gyrus: relationship to language lateralization. Brain J. Neurol. 129, 1164 – 1176.

Emmorey, K., Allen, J.S., Bruss, J., Schenker, N., Damasio, H., 2003. A morphometric analysis of auditory brain regions in congenitally deaf adults. Proc. Natl. Acad. Sci. U. S. A. 100, 10049 – 10054.

Engel, S.A., Rumelhart, D.E., Wandell, B.A., Lee, A.T., Glover, G.H., Chichilnisky, E.J., Shadlen, M.N., 1994. fMRI of human visual cortex. Nature 369, 525.

Fischl, B., van der Kouwe, A., Destrieux, C., Halgren, E., Ségonne, F., Salat, D.H., Busa, E., Seidman, L.J., Goldstein, J., Kennedy, D., Caviness, V., Makris, N., Rosen, B., Dale, A.M., 2004. Automatically parcellating the human cerebral cortex. Cereb. Cortex 14, 11 – 22.

Fleschig, P., 1908. Bemerkungen über die Hörsphäre des menschlichen Gehirns. Neurol.Zentralbl. 27.

Formisano, E., Kim, D.S., Di Salle, F., van de Moortele, P.F., Ugurbil, K., Goebel, R., 2003. Mirror-symmetric tonotopic maps in human primary auditory cortex. Neuron 40, 859 – 869.

Fullerton, B.C., Pandya, D.N., 2007. Architectonic analysis of the auditory-related areas of the superior temporal region in human brain. J. Comp. Neurol. 504, 470 – 498.

Gage, N.M., Juranek, J., Filipek, P.A., Osann, K., Flodman, P., Isenberg, A.L., Spence, M.A., 2009. Rightward hemispheric asymmetries in auditory language cortex in children with autistic disorder: an MRI investigation. J. Neurodev. Disord. 1, 205 – 214.

Galaburda, A., Sanides, F., 1980. Cytoarchitectonic organization of the human auditory cortex. J. Comp. Neurol. 190, 597 – 610.

Golestani, N., Price, C.J., Scott, S.K., 2011. Born with an ear for dialects? Structural

plasticity in the expert phonetician brain. J. Neurosci. Off. J. Soc. Neurosci. 31, 4213 – 4220.

Hackett, T.A., Barkat, T.R., OBrien, B.M.J., Hensch, T.K., Polley, D.B., 2011. Linking topography to tonotopy in the mouse auditory thalamocortical circuit. J. Neurosci. Off. J. Soc. Neurosci. 31, 2983 – 2995.

Hackett, T.A., Preuss, T.M., Kaas, J.H., 2001. Architectonic identification of the core region in auditory cortex of macaques, chimpanzees, and humans. J. Comp. Neurol. 441, 197 – 222.

Howard, M.A., Volkov, I.O., Abbas, P.J., Damasio, H., Ollendieck, M.C., Granner, M.A., 1996. A chronic microelectrode investigation of the tonotopic organization of human auditory cortex. Brain Res. 724, 260 – 264.

Hubl, D., Dougoud-Chauvin, V., Zeller, M., Federspiel, A., Boesch, C., Strik, W., Dierks, T., Koenig, T., 2010. Structural analysis of Heschl's gyrus in schizophrenia patients with auditory hallucinations. Neuropsychobiology 61, 1 – 9.

Humphries, C., Liebenthal, E., Binder, J.R., 2010. Tonotopic organization of human auditory cortex. NeuroImage 50, 1202 – 1211.

Kaas, J.H., Hackett, T.A., 2000. Subdivisions of auditory cortex and processing streams in primates. Proc. Natl. Acad. Sci. 97, 11793 – 11799.

Leonard, C.M., Eckert, M.A., Lombardino, L.J., Oakland, T., Kranzler, J., Mohr, C.M., King, W.M., Freeman, A., 2001. Anatomical risk factors for phonological dyslexia. Cereb. Cortex N. Y. N 1991 11, 148 – 157.

Leonard, C.M., Puranik, C., Kuldau, J.M., Lombardino, L.J., 1998. Normal variation in the frequency and location of human auditory cortex landmarks. Heschl's gyrus: where is it? Cereb. Cortex N. Y. N 1991 8, 397 – 406.

Marques, J.P., Kober, T., Krueger, G., van der Zwaag, W., Van de Moortele, P.-F., Gruetter, R., 2010. MP2RAGE, a self bias-field corrected sequence for improved segmentation and T1-mapping at high field. NeuroImage 49, 1271 – 1281.

Morel, A., Garraghty, P.E., Kaas, J.H., 1993. Tonotopic organization, architectonic fields, and connections of auditory cortex in macaque monkeys. J. Comp. Neurol. 335, 437 – 459.

Morel, A., Kaas, J.H., 1992. Subdivisions and connections of auditory cortex in owl monkeys. J. Comp. Neurol. 318, 27 – 63.

Morosan, P., Rademacher, J., Schleicher, A., Amunts, K., Schormann, T., Zilles, K., 2001. Human Primary Auditory Cortex: Cytoarchitectonic Subdivisions and Mapping into a Spatial Reference System. NeuroImage 13, 684 – 701.

Penhune, V.B., Zatorre, R.J., MacDonald, J.D., Evans, A.C., 1996. Interhemispheric anatomical differences in human primary auditory cortex: probabilistic mapping and volume measurement from magnetic resonance scans. Cereb. Cortex N. Y. N 1991 6, 661 – 672.

Petkov, C.I., Kayser, C., Augath, M., Logothetis, N.K., 2006. Functional Imaging Reveals Numerous Fields in the Monkey Auditory Cortex. PloS Biol 4, e215.

Petkov, C.I., Logothetis, N.K., Obleser, J., 2009. Where are the human speech and voice regions, and do other animals have anything like them? Neurosci. Rev. J. Bringing Neurobiol. Neurol. Psychiatry 15, 419 – 429.

Phillips, D.P., Semple, M.N., Calford, M.B., Kitzes, L.M., 1994. Level-dependent representation of stimulus frequency in cat primary auditory cortex. Exp. Brain Res. Exp. Hirnforsch. Expérimentation Cérébrale 102, 210 – 226.

Rademacher, J., Caviness, V.S., Steinmetz, H., Galaburda, A.M., 1993. Topographical Variation of the Human Primary Cortices: Implications for Neuroimaging, Brain Mapping, and Neurobiology. Cereb. Cortex 3, 313 – 329.

Rademacher, J., Morosan, P., Schormann, T., Schleicher, A., Werner, C., Freund, H.J., Zilles, K., 2001. Probabilistic mapping and volume measurement of human primary auditory cortex. NeuroImage 13, 669 – 683.

Rajimehr, R., Tootell, R.B.H., 2009. Does retinotopy influence cortical folding in primate visual cortex? J. Neurosci. Off. J. Soc. Neurosci. 29, 11149 – 11152.

Rauschecker, J.P., Tian, B., Pons, T., Mishkin, M., 1997. Serial and parallel processing in rhesus monkey auditory cortex. J. Comp. Neurol. 382, 89 – 103.

Recanzone, G.H., Guard, D.C., Phan, M.L., 2000. Frequency and intensity response properties of single neurons in the auditory cortex of the behaving macaque monkey. J. Neurophysiol. 83, 2315 – 2331.

Rivier, F., Clarke, S., 1997. Cytochrome oxidase, acetylcholinesterase, and NADPH-diaphorase staining in human supratemporal and insular cortex: evidence for multiple auditory areas. NeuroImage 6, 288 – 304.

Romani, G.L., Williamson, S.J., Kaufman, L., 1982. Tonotopic organization of the human auditory cortex. Science 216, 1339 – 1340.

Sadagopan, S., Wang, X., 2008. Level invariant representation of sounds by populations of neurons in primary auditory cortex. J. Neurosci. Off. J. Soc. Neurosci. 28, 3415 – 3426.

Schneider, P., Andermann, M., Wengenroth, M., Goebel, R., Flor, H., Rupp, A., Diesch, E., 2009. Reduced volume of Heschl's gyrus in tinnitus. NeuroImage 45, 927 – 939.

Schneider, P., Scherg, M., Dosch, H.G., Specht, H.J., Gutschalk, A., Rupp, A., 2002. Morphology of Heschl's gyrus reflects enhanced activation in the auditory cortex of musicians. Nat. Neurosci. 5, 688 – 694.

Schreiner, C.E., Winer, J.A., 2007. Auditory cortex mapmaking: principles, projections, and plasticity. Neuron 56, 356 – 365.

Sereno, M.I., Dale, A.M., Reppas, J.B., Kwong, K.K., Belliveau, J.W., Brady, T.J., Rosen, B.R., Tootell, R.B., 1995. Borders of multiple visual areas in humans revealed by functional magnetic resonance imaging. Science 268, 889 – 893.

Speck, O., Stadler, J., Zaitsev, M., 2008. High resolution single-shot EPI at 7T. Magma N. Y. N 21, 73 – 86.

Striem-Amit, E., Hertz, U., Amedi, A., 2011. Extensive cochleotopic mapping of human auditory cortical fields obtained with phase-encoding FMRI. PloS One 6, e17832.

Sweet, R.A., Dorph-Petersen, K.-A., Lewis, D.A., 2005. Mapping auditory core, lateral belt, and parabelt cortices in the human superior temporal gyrus. J. Comp. Neurol. 491, 270 – 289.

Talavage, T.M., Sereno, M.I., Melcher, J.R., Ledden, P.J., Rosen, B.R., Dale, A.M., 2004. Tonotopic organization in human auditory cortex revealed by progressions of frequency sensitivity. J. Neurophysiol. 91, 1282 – 1296.

Tanji, K., Leopold, D.A., Ye, F.Q., Zhu, C., Malloy, M., Saunders, R.C., Mishkin, M.,

2010. Effect of sound intensity on tonotopic fMRI maps in the unanesthetized monkey. NeuroImage 49, 150 – 157.

Van der Zwaag, W., Francis, S., Head, K., Peters, A., Gowland, P., Morris, P., Bowtell, R., 2009. fMRI at 1.5, 3 and 7 T: Characterising BOLD signal changes. NeuroImage 47, 1425 – 1434.

Van der Zwaag, W., Gentile, G., Gruetter, R., Spierer, L., Clarke, S., 2011. Where sound position influences sound object representations: a 7-T fMRI study. NeuroImage 54, 1803 – 1811.

Van Essen, D.C., 1997. A tension-based theory of morphogenesis and compact wiring in the central nervous system. Nature 385, 313 – 318.

Von Economo, C., Horn, L., 1930. Über Winddungsrelief, Masse und Rindenarchitektonik der Supratemporalfläche, ihre individuellen und ihre Seitenunterschiede. Z. Ges. Neurol. Psychiatr. 130, 678 – 757.

Von Economo, C., Koskinas, G.N., 1925. Die Cytoarchitektonik der Grosshirnrinde des erwachsenen Menschen., Berlin: Springer. ed.

Wallace, M.N., Johnston, P.W., Palmer, A.R., 2002. Histochemical identification of cortical areas in the auditory region of the human brain. Exp. Brain Res. Exp. Hirnforsch. Expérimentation Cérébrale 143, 499 – 508.

Warrier, C., Wong, P., Penhune, V., Zatorre, R., Parrish, T., Abrams, D., Kraus, N., 2009. Relating structure to function: Heschl's gyrus and acoustic processing. J. Neurosci. Off. J. Soc. Neurosci. 29, 61 – 69.

Wengenroth, M., Blatow, M., Bendszus, M., Schneider, P., 2010. Leftward Lateralization of Auditory Cortex Underlies Holistic Sound Perception in Williams Syndrome. PloS One 5, e12326.

Wong, P.C.M., Warrier, C.M., Penhune, V.B., Roy, A.K., Sadehh, A., Parrish, T.B., Zatorre, R.J., 2008. Volume of Left Heschl's Gyrus and Linguistic Pitch Learning. Cereb. Cortex N. Y. N 1991 18, 828 – 836.

Woods, D.L., Stecker, G.C., Rinne, T., Herron, T.J., Cate, A.D., Yund, E.W., Liao, I., Kang, X., 2009. Functional Maps of Human Auditory Cortex: Effects of Acoustic Features and Attention. PloS One 4, e5183.

3.2 Tuning in to sound: frequency-selective attentional filter in human primary auditory cortex.

Sandra Da Costa, Lee M Miller, Wietske Van der Zwaag, Stephanie Clarke and Melissa Saenz

This article has been published in Journal of Neuroscience in January 2013 (Da Costa et al., 2013).

Ackowledgements

This work was supported by a Swiss National Science Foundation Grant 3200030-124897 to S.C. and IZK0Z3_139473/1 to Micah Murray, and by the Centre d'Imagerie BioMédicale of the Université de Lausanne, Université de Genève, Hôpitaux Universitaires de Genève et de Lausanne, Ecole Polytechnique Fédérale de Lausanne, and the Leenaards and Louis-Jeantet Foundations. We thank Micah Murray for hosting the visit of L.M.M., leading to our collaboration.

Abstract

Cocktail parties, busy streets, and other noisy environments pose a difficult challenge to the auditory system: how to focus attention on selected sounds while ignoring others? Neurons of primary auditory cortex, many of which are sharply tuned to sound frequency, could help solve this problem by filtering selected sound information based on frequency-content. To investigate whether this occurs, we used high-resolution fMRI at 7 Tesla to map the fine-scale frequency-tuning (1.5 mm isotropic resolution) of primary auditory areas A1 and R in six human participants. Then, in a selective attention experiment, participants heard low- (250 Hz) and high- (4000 Hz) frequency streams of tones presented at the same time (dual-stream) and were instructed to focus attention onto one stream versus

the other, switching back and forth every 30 s. Attention to low-frequency tones enhanced neural responses within low-frequency-tuned voxels relative to high, and when attention switched the pattern quickly reversed. Thus, like a radio, human primary auditory cortex is able to tune into attended frequency channels and can switch channels on demand.

Introduction

The "cocktail party" problem (Cherry, 1953) refers to the challenge of auditory selective attention: how to focus attention onto selected sounds in a noisy background? In studies of visual attention, much evidence points toward a "feature-based" mechanism by which attention to a particular visual feature enhances the response of visual cortical neurons tuned to that feature, thus strengthening the neural representation of attended stimuli relative to unattended stimuli (Maunsell and Treue, 2006; Saenz et al., 2002; Treue and Martnez Trujillo, 1999). In the auditory system, the most ubiquitous feature to which cortical neurons are tuned is sound frequency. Here we test whether frequency-tuned units of human primary areas A1 and R are modulated by selective attention to preferred versus nonpreferred sound frequencies in the dynamic manner needed to account for human listening abilities. Such an early-stage filtering mechanism could contribute to downstream selection of spectrally complex auditory stimuli like speech. Previous human studies suggest that attention modulates responses in the region of primary auditory cortex (EEG: Hillyard et al., 1973; Woldorff et al., 1993; Woods et al., 1984. MEG: Fujiwara et al., 1998. fMRI: Jäncke et al., 1999; Rinne et al., 2008. EcoG: Bidet-Caulet et al., 2007) including frequency-specific enhancement (Oh et al., 2013; Paltoglou et al., 2009). Other fMRI studies suggest that attentional modulation occurs predominantly in secondary, and not primary, auditory cortical areas (Ahveninen et al., 2011; Petkov et al., 2004; Woods et al., 2010). Differences across studies may relate to the variety of spatial, featural, and multisensory attentional tasks used. However, previous human studies have not performed fine-scale frequency mappings needed to identify A1 and R in individual subjects (as we aim to do here with high-resolution fMRI).

Single-neuron recordings in A1 of rats and ferrets show that attention to a target tone amid distractor sounds reshapes the frequency-tuning profiles of individual neurons (Atiani et

al., 2009; David et al., 2012; Fritz et al., 2003, 2005; Jaramillo and Zador, 2011). While the specific modulatory effects vary (see Discussion), attention tends to enhance the contrast between responses to target and non-target frequencies. One caveat is that the animals require many weeks of specific task training and thus the effects potentially involve long-term learning mechanisms, in addition to the flexible and transient attentional mechanisms needed to account for dynamic human listening skills.

Here, we test for attentional modulation of frequency-tuned units in human primary auditory cortex using a two-step approach. First, we use high-resolution fMRI at 7T to map the fine-scale frequency tuning of human primary auditory areas hA1 and hR in individual subjects. Second, we test whether frequency-tuned units are modulated by attention to preferred versus nonpreferred frequencies in a dynamic selective attention task. The results demonstrate robust frequency-specific attentional modulation in primary auditory cortex – these effects outweighed more modest effects of spatial attention and were large relative to stimulus-driven changes.

Materials and Methods

Six subjects (ages 25 – 40, 2 males) with no known hearing deficit participated after giving written, informed consent. Experimental procedures were approved by the Ethics Committee of the Faculty of Biology and Medicine of the University of Lausanne.

MRI data acquisition and data analysis

Blood oxygenation level-dependent (BOLD) functional imaging was performed with an actively shielded 7 Tesla Siemens MAGNETOM scanner (Siemens Medical Solutions) located at the Centre d'Imagerie BioMédicale in Lausanne, Switzerland. The increased signal-to-noise ratio and available BOLD associated with ultra-high magnetic field systems ($>$ 3 T) allow the use of smaller voxel sizes in fMRI. The spatial specificity of the BOLD signal is improved because the signal strength of venous blood is reduced due to a shorted relaxation time, restricting activation signals to cortical gray matter (van der

Zwaag et al., 2009, 2011). fMRI data were acquired using an 8-channel head volume RF-coil (RAPID Biomedical GmbH) and a continuous EPI pulse sequence with sinusoidal read-out (1.5 x1.5 mm in-plane resolution, slice thickness = 1.5 mm, TR = 2000 ms, TE = 25ms, flip angle = 47°, slice gap = 1.57 mm, matrix size = 148 x 148, field of view 222 x 222, 30 oblique slices covering the superior temporal plane). A T1-weighted high-resolution 3D anatomical image (resolution = 1 x 1 x 1 mm, TR = 5500 ms, TE = 2.84 ms, slice gap = 1 mm, matrix size = 256 x 240, field of view = 256 x 240) was acquired for each subject using the MP2RAGE pulse sequence optimized for 7T MRI (Marques et al., 2010).

Standard fMRI data preprocessing steps were performed with BrainVoyager QX v2.3 software and included linear trend removal, temporal high-pass filtering, and motion correction. Spatial smoothing was not applied. Functional time-series data were interpolated into 1 x 1 x 1mm volumetric space and registered to each subjects 3D Talairach-normalized anatomical dataset. Cortical surface meshes were generated from each subjects anatomical dataset using automated segmentation tools in BrainVoyager QX.

Auditory stimuli

Sound stimuli were generated using MATLAB and the Psychophysics Toolbox (www.psychtoolbox.org) with a sampling rate of 44.1 kHz. Stimuli were delivered via MRI-compatible headphones (AudioSystem, NordicNeuroLab) featuring flat frequency transmission over the stimulus range. Sound intensities were adjusted to match standard equal-loudness curves (ISO 226) at phon 85: the sound intensity of each pure tone stimulus (ranging from 88 to 8000 Hz) was adjusted to approximately equal the perceived loudness of a 1000 Hz reference tone at 85 dB SPL (range of sound intensities: 8297 dB SPL). Sound levels were further attenuated ($\sim$22 dB) by protective ear plugs. Subjects reported hearing sounds clearly over background scanner noise and were instructed to keep eyes closed during fMRI scanning.

Tonotopic mapping step

For tonotopic mapping, pure tones (88, 125, 177, 250, 354, 500, 707, 1000, 1414, 2000, 2828, 4000, 5657, and 8000 Hz; half-octave steps) were presented in ordered progressions, following our previously described methods (Da Costa et al., 2011). Briefly, starting with the lowest (or highest) frequency, pure tone bursts of that frequency were presented for a 2 s block before stepping to the next consecutive frequency until all 14 frequencies had been presented. The 28 s progression was followed by a 4 s silent pause, and this 32 s cycle was repeated 15 times per 8 min scan run. Each subject participated in two scan runs (one low-to-high progression and one high-to-low progression), and resulting maps of the two runs were averaged. The frequency progressions were designed to induce a travelling wave of response across cortical tonotopic maps (Engel, 2012). Linear cross-correlation was used to determine the time-to-peak of the fMRI response wave on a per-voxel basis, and to thus assign a corresponding best frequency value to each voxel. Analyses were performed in individual-subject volumetric space and results were then projected onto same-subject cortical surface meshes.

As shown in Figure 3.6.A, two tonotopic gradients with mirror symmetry ("high-low-low-high") were clearly observed running approximately across Heschl's gyrus in both hemispheres of all subjects (Da Costa et al., 2011; Formisano et al., 2003; Humphries et al., 2010; Langers and Dijk, 2012; Striem-Amit et al., 2011; Woods et al., 2009), the more posterior "high-to-low" gradient corresponding to human A1 (hA1) and the more anterior "low-to-high" gradient corresponding to hR. In macaque auditory cortex, fields A1 and R receive parallel thalamic input and are both considered part of the primary auditory core (along with a possible third, smaller field, RT, which has not yet been reliably confirmed in the human), and the relative functions of the two fields remain unknown (Hackett, 2010). We manually outlined a contiguous patch of cortical surface containing the two primary gradients corresponding to hA1 and hR using drawing tools within BrainVoyager QX, as illustrated with dotted lines (Figure 3.6.A). The exact borders were not dependent upon the particular correlation threshold used for display since the overall pattern was observable across a large range of display thresholds. Anterior and posterior borders were drawn along the outer high-frequency representations. Lateral and medial borders were conservatively drawn to include only the medial two-thirds of Heschl's gyrus, in accordance with

human architectonics (Hackett, 2010; Rivier and Clarke, 1997). Tonotopic responses extending onto the lateral end of Heschl's gyrus may include non-primary belt regions. The border between hA1 and hR was drawn across the length of the low-frequency gradient reversal.

Once selected on the cortical surface, the hA1 and hR regions were projected into the same-subjects 1 x 1 x 1 mm interpolated volumetric space to generate 3D regions of interest (ROIs). The 3D ROIs were generated with a width of 3 mm (-1 mm to +2 mm from the white/gray matter boundary). All volumetric voxels (1 x 1 x 1 mm interpolated) falling within the 3D ROIs were labelled with a best-frequency map value, and were subsequently analyzed in the selective attention experiment. Data analysis for the selective attention experiment was thus performed in volumetric space without loss of the acquired spatial resolution.

Selective attention (dual-stream experiment

During the selective attention experiment (Figure. 3.6.B), the same subjects attended to one of two competing tonal streams presented simultaneously to different earsone stream consisted of low-frequency tone bursts (250 Hz) and the other, high (4000 Hz). Ear-side, i.e., whether low-frequency tones were presented to the left or right side, was counterbalanced across runs. By design, this allowed the comparison of any effects of frequency-specific attention ("attend high" vs "attend low" collapsed across sides) to effects of spatial-selective attention ("attend contralateral" vs "attend ipsilateral" collapsed across frequencies). Every 30 s, subjects were cued to switch attention from one stream to the other. The brief auditory cue, appearing at the beginning of each block, was the MAC OSX system voice saying "low" or"high". Each scan run consisted of twelve 30 s blocks (6 per condition), and there were four scan runs per subject. The physical stimulus did not change across compared conditions, only the attentional state.

Each stream had a temporal pattern similar to Morse code making the task comparable to tuning into one of two competing tonal conversations at a time: patterns consisted of pseudorandomly intermixed long (300 ms) and short duration (75 ms) ramped tone bursts separated by blank intervals (75 ms). In each stream independently, the patterns were

presented in a series of two-interval forced choice trails (2-IFC). During each trial, a randomly generated 5- or 6-element pattern (interval 1) was presented followed by a second 5- or 6-element pattern (interval 2) that was either identical to the first or a shuffled permutation of the first, and subjects made a "same" or "different" judgment within the cued attended stream only. The duration of interval 1was up to 1350 ms (depending on the generated pattern) and the second interval started 2 s after onset of interval 1 (minimum interstimulus interval of 750 ms). Subjects had 1 s after the offset of interval 2 to enter their response by pressing one of two keys with the right hand. A new trial began every 4.7 s and each 30 s block had six trials. The sequence of the first interval, and whether the second interval was the same or different, was independently randomized in each stream every trial. Thus, subjects could perform the task only by attending to the cued stream. The starting condition was counter-balanced across subjects.

Before scanning, subjects participated in a brief training session (30 min). The patterns in the 2-IFC task could be either 5- or 6-element in length (6 being more difficult) and were for adjusted during training per subject to achieve performance that was well-above chance but not at ceiling. The number of elements used was then fixed per subject: 4 of the 6 subjects were given 6-element sequences. Percent correct performance was the same for attend high and attend low trials during fMRI scanning (See Results), indicating no difference in task difficulty across conditions.

Single-stream experiment

Next, we asked: How does attending to one of the two concurrent frequency streams compare with hearing that frequency stream alone (i.e., complete disappearance of the ignored stimulus)? In the same subjects, we ran a second version of the experiment (single-stream experiment) in which the stimuli and task were the same as the first experiment except that the ignored stream was physically removed during each block. The stimulus physically alternated between a single attended high-frequency stream (4000 Hz) in one ear and a single attended low-frequency stream (250 Hz) in the other ear: "high versus low". Hence, response modulations would include both stimulus-driven and attentional effects. Each subject performed four runs of the single-stream experiment alternately interleaved with the four runs of the dual-stream experiment. Single-stream runs were

counterbalanced for ear-side and starting block in the same manner as the dual-stream experiment.

Results

Figure 3.7.A plots fMRI time courses recorded during the selective attention (dual-stream) experiment, across subjects and hemispheres (n = 12). Specifically, time courses were extracted from all volumetric primary auditory cortex voxels (hA1 and hR combined) labelled as having best frequencies of 250 Hz in red and 4000 Hz in blue on a per-subject, per-hemisphere basis based on the individuals own tonotopic mapping (mean number of 250 Hz-tuned voxels: 320 $\pm$ 140 SD; 4000 Hz-tuned voxels: 115 $\pm$ 55 SD across subjects and hemispheres). Each plotted time courses is an average of the 12 extracted time courses (one per-subject, per-hemisphere). As can be appreciated by eye, the responses of 4000 Hz-tuned voxels increased during the attend high condition and decreased during the attend low condition, while in 250 Hz-tuned voxels, the opposite pattern of modulation was seen. The stimulus itself and task difficulty did not change across blocks (task performance: attend low blocks = 89.3 $\pm$ 9.1% SD; attend high blocks = 87.3 $\pm$ 7.4% SD across subjects, p = 0.59, paired t-test), and thus we attribute this modulation in primary auditory cortex to frequency-selective attention.

Next, we show response modulation not only within the 250 and 4000 Hz best-frequency voxels, but across all primary auditory cortex voxels with all frequency preferences (from 88 to 8000 Hz in half-octave bins). The bars in Figure 3.7.B indicate the mean difference between attend high blocks and attend low blocks (adjusted 4 s for hemodynamic delay) across all voxel bins (means and SE bars computed over individual responses per-subject, per-hemisphere, n = 12). Overall, the responses of frequency-tuned units were enhanced by attention to preferred versus non-preferred frequencies. Response modulations were highly significant in 250 Hz and 4000 Hz voxels ($p < 0.0005$ and $p < 0.00005$, respectively, t test) and Figure 3.7.B shows the overall tuning profile of the frequency attention-effect. Data from hA1 and hR voxels from both hemispheres are combined here since the pattern of modulation was qualitatively similar and individually significant when analyzed separately in hA1 and hR voxels (A1, $p < 0.001$ and $p < 0.01$; R, $p < 0.001$ and

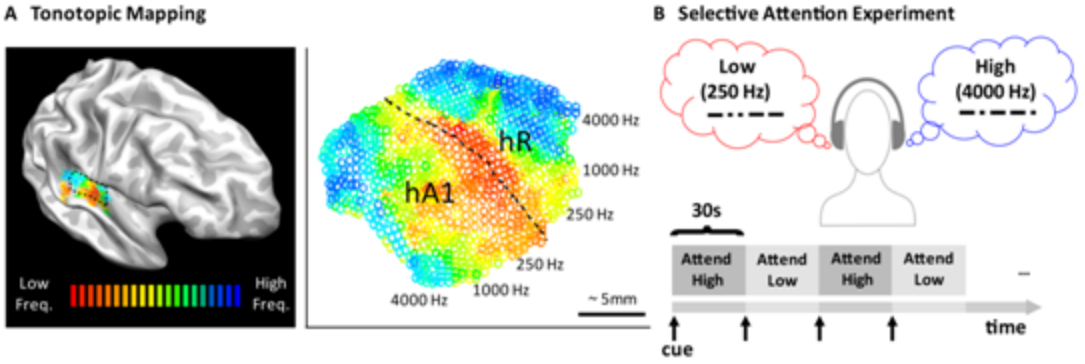

Figure 3.6: A. Tonotopic mapping was used to indentify primary auditory cortex in each subject individually (n = 6). In each hemisphere (n = 12), two mirror-symmetric gradients (high-to-low and low-to-high) corresponding the primary areas hA1 and hR were manually outlined on the medial two- thirds of Heschl's gyrus (one same right hemisphere shown). Each voxel within the selected region was labeled according to its preferred frequency between 88 and 8000 Hz in half-octave steps. **B.** Next, in the selective attention (dual-stream) experiment, low (250 Hz)- and high (4000 Hz)-frequency patterned tonal streams were presented concurrently to different ears. Subjects were cued to attend to only one stream at a time, alternating the attended stream every 30 s (blocks of attend high vs attend low). A 2-IFC experiment was used to focus attention on the cue stream (see Materials and Methods). The stimulus itself did not change across blocks, only the attentional state. Ear-side was counterbalanced across runs allowing the comparison of effects of frequency-specific attention (attend high vs attend low collapsed across sides) to effects of spatial-selective attention (attend contralateral vs attend ipsilateral collapsed across frequencies).

$p < 0.001$ for 250 Hz and 4000 Hz voxels, respectively) and in left and right hemispheres (LH, $p < 0.005$ and $p < 0.01$; RH, $p < 0.01$ and $p < 0.005$ for 250 Hz and 4000 Hz voxels). Further, to verify the reliability of our manual ROI selection, we subsequently had three experimenters (S.D.C., W.V.D.Z., and M.S.) independently draw the primary auditory cortex ROI: inter-rater overlap was high (RH, 0.87; LH, 0.84; Dice coefficient), and the pattern of results was unchanged when we reanalyzed only those voxels which overlapped all three selections ($p < 0.0001$ and $p < 0.00001$ and for 250 Hz and 4000 Hz voxels, respectively).

The data plotted so far compare responses to attend high versus attend low conditions, regardless of stimulus side. Next, we look at the effect of attending to contralateral versus ipsilateral sides, regardless of stimulus frequency. Figure 3.7.C plots the mean difference

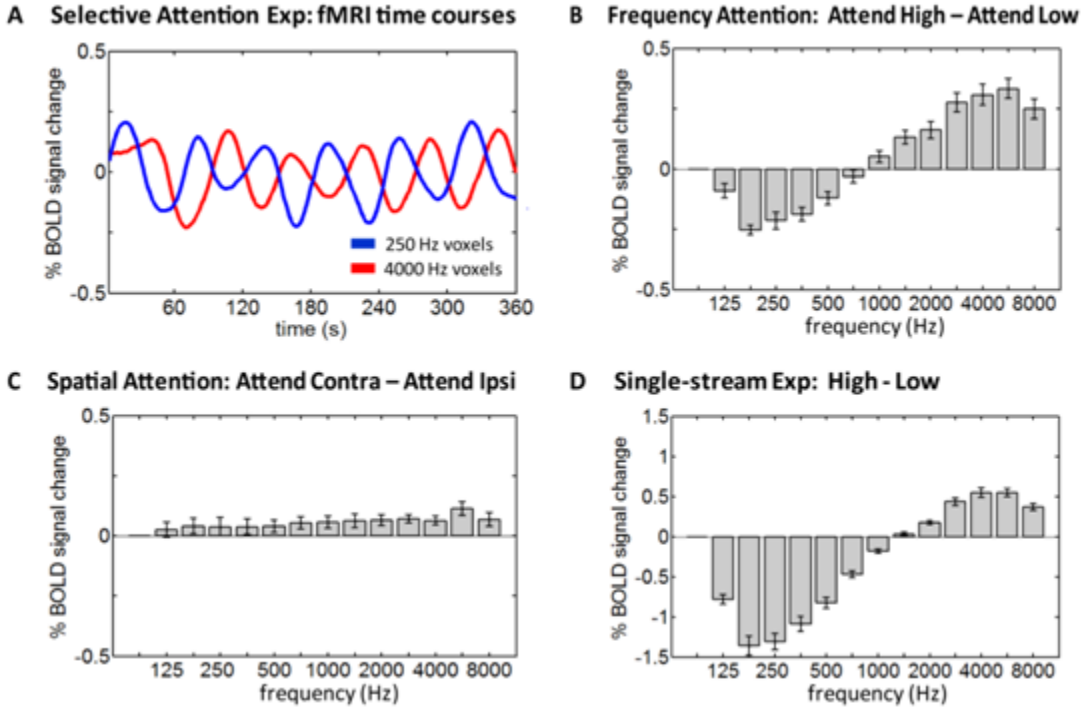

Figure 3.7: A. Mean fMRI time courses during the dual-stream selective attention experiment (across all subjects and hemispheres, n = 12) smoothed with a Gaussian (half-width 8 s). Time courses were extracted from all voxels of primary auditory cortex labeled as preferring 250 Hz (light gray) and 4000 Hz (dark gray) in each subject and hemisphere based on individual subject tonotopic mappings.The responses of 4000 Hz-preferring voxels increased during attend high blocks and decreased during attend low blocks, and vice versa for 250 Hz-preferring voxels. **B.** Frequency attention. Bars show the mean difference in response between attend high and attend low blocks across all voxel bins in primary auditory cortex with all frequency preferences. **C.** Spatial attention. Bars show the mean difference in response between attend contralateral and attend ipsilateral blocks. **D.** Modulation in single-stream experiment. Bars show the mean difference in response between high and low blocks measured in separate scans in which the stimulus physically alternated between high-only and low-only streams. Note change in y-axis scale. Comparing the amplitudes in **B** and **C**, feature-selective attention outweighed effects of spatial attention by a factor of 5. Comparing the amplitudes of **B** and **D**, frequency attention modulation was 18.6% as large as stimulus-driven modulation in 250 Hz voxels and 56.2% as large in 4000 Hz voxels, a robust modulatory effect. Error bars show SEM across all subjects and hemispheres, n = 12.

in response between attend contralateral and attend ipsilateral blocks across all voxel bins. A general response increase for attending the contralateral side is observed (spatial attention effect). The profiles of frequency-attention and spatial-attention effects are different:

the effects of frequency-selective attention (Figure 3.7.B) are largest in voxels near the frequencies used (250 and 4000 Hz) and taper off gradually in voxels tuned to neighboring frequencies, while the effects of spatial attention (Figure 3.7.C) are similar in magnitude across voxels with all frequency preferences. The effects of frequency-selective attention outweighed the more modest effects of spatial-selective attention by a factor of 4.9 in 250 Hz voxels and a factor 5.8 in 4000 Hz voxels.

Finally, we address the question: how does focusing attention onto one of two competing stimuli compare with making the ignored stimulus physically disappear? In separate interleaved experimental runs (single-stream experiment), the stimulus physically alternated between a single attended high-frequency stream in one ear and a single attended low-frequency stream in the other ear (high vs low). Figure 3.7.D plots the mean difference in response between high and low blocks in the single-stream experiment across all voxel bins. Task scores indicated no difference in difficulty across blocks (low = 94.2 $\pm$ 3.8% SD, high = 93.9 $\pm$ 2.6% SD across subjects, p = 0.8, paired t test). Next, we compare the modulation amplitudes of Figure 3.7.B (in which only attentional state alternated) to the modulation amplitudes of Figure 3.7.D (in which the physical stimulus alternated). In 250 Hz voxels, we see that attentional modulation was 18.6% as large as modulation due to physically alternating the stimulus; and in 4000 Hz voxels it was 56.2% as large. The difference in percentages between 250 Hz and 4000 Hz voxels reflects the denominator: the modulation due to physically alternating the stimulus was stronger in low-frequency voxels compared with high-frequency voxels, consistent with previous reports of weaker BOLD responses to high-frequency stimuli for reasons not fully understood (Langers and Dijk, 2012). In either case, frequency-selective attention can be regarded as a powerful modulatory effect.

Discussion

We demonstrated that neural activity within human primary auditory cortex (hA1 and hR) is strongly and dynamically modulated by attention to preferred versus nonpreferred sound frequencies. These effects of frequency-attention outweighed more modest effects of spatial-attention by a factor of $\sim$5 and were up to 56% as large as when physically

removing the competing stimulus. The frequency-attention effect was largest in voxels near the specific attended frequencies (250 Hz and 4000 Hz) and tapered off gradually in voxels tuned to neighboring frequencies. The results suggest that, like a radio, primary auditory cortex can tune into attended frequency channels and can rapidly switch channels to meet task demands.

These results are consistent with the previous human fMRI study by Paltoglou et al. (2009) that showed frequency-specific attentional modulation of auditory cortex, although with a less detailed frequency mapping. Interestingly, Oh et al. (2012) demonstrated frequency-specific modulation of auditory cortex during imagery of low- versus high-frequency tones, which may rely on related mechanisms of top-down modulation. Our study adds to the previous findings by performing high-resolution, fine-scaled frequency mappings which allow us to (1) unambiguously identify primary auditory cortical fields, and (2) characterize the tuning of attentional effects as a function of frequency preference. Our findings are also novel in that the experimental design allowed comparison of frequency-attention effects to spatial attention and stimulus-driven effects.

The degree of attentional modulation observed in a region likely depends on the extent to which the underlying neurons encode the features of the attended target, and it may not be surprising that we observed greater modulation to shifts in attended frequency compared with shifts in attended location. Across many species, primary auditory cortex contains a fine-grained representation of sound frequency and is organized tonotopically (Bartlett et al., 2011; Bitterman et al., 2008; Guo et al., 2012), but spatial tuning is notably broad and a cortical topographic organization has not been found (Recanzone et al., 2000). Unilaterally presented sounds are known to induce a significant bilateral fMRI response in human auditory cortex (van der Zwaag et al., 2011). However modestly, we did observe spatial attention effects in A1 and R; and previous studies have shown spatially-driven attentional modulation in auditory cortex (Rinne et al., 2008, 2012). It is possible that spatial attentional modulation would be greater with a task that required more use of spatial information.

Our results (both dual stream and single stream) showed a fairly broad frequency-tuning at the voxel level, larger than what is expected of some individual neurons. This broad tun-

ing could be related to a population level mixture of narrowly and broadly tuned neurons ($\sim$ 104 – 105 neurons per cubic mm in cortex). In rat A1 the precise tonotopic organization of middle cortical layers is degraded in the superficial and deep cortical layers, where many irregularly tuned neurons are found (Guo et al., 2012). Additionally, broadened frequency-tuning is expected at high stimulus sound intensities (Guo et al., 2012; Tanji et al., 2010), an effect which originates at the basilar membrane. However, it should be noted that sharp frequency tuning, on the order of 1/12th of an octave, was found to suprathreshold sound stimuli in a large proportion of A1 single neurons in alert humans (intra-cranial depth electrodes, Bitterman et al., 2008), and in awake-behaving marmosets (Bartlett et al., 2011). Thus we expect that some component of our population BOLD response in humans arises from sharply frequency-tuned neurons.

Comparison to single-neuron studies of auditory attention

The observed attentional modulation in the BOLD response could reflect both neural enhancement and suppression, and recent findings from single-neuron recordings in animals emphasize the role of both in the modulation of A1 receptive fields. For example, in ferret A1, individual frequency-tuning profiles were rapidly reshaped when animals attended to target tones amid distractor sounds (Atiani et al., 2009; David et al., 2012; Fritz et al., 2003, 2005, 2007). In many cases, neurons tuned near the target frequency showed enhanced responsiveness to best frequency and those tuned to background frequencies showed suppression, but, interestingly, target frequency suppression could be evoked under different behavioral contexts (David et al., 2012). In rat A1, neurons showed enhanced responses during attention to target tones matching the neurons best frequency (Jaramillo and Zador, 2011), but also showed broad suppression during performance of an auditory task compared with passive listening (Otazu et al., 2009). Thus, it seems that A1 uses multiple strategies, not limited to target response enhancement, to sharpen the representation of attended stimuli relative to background. It is not straightforward to relate these single-neuron findings in animals to BOLD population results in humans, except to say that a combination of attention-related excitatory and inhibitory mechanisms could contribute to the observed BOLD modulation. One difference between our study and the single-neuron studies cited here is that the effects in animals followed many weeks of specific task training and could persist minutes to hours after task completion (Fritz et

al., 2003, 2007). Thus, the effects in animals possibly depend upon long-term learning mechanisms, in addition to short-term flexible attentional mechanisms. Our study demonstrates dynamic and transient (target shifting every 30 s) attentional modulation of A1 and R using a task that required only limited training in humans.

Comparison to feature-based attention in visual cortex

Our findings are broadly consistent with "feature-based" models of attention, from the visual cortex literature, which propose that responses are enhanced in neurons whose feature-selectivity matches the current attentional focus (Maunsell and Treue, 2006; Saenz et al., 2002; Treue and Martnez Trujillo, 1999). In visual cortex, feature-based attention has been shown to modulate both stimulus-evoked responses and spontaneous baseline activity in the absence of a stimulus (macaque single unit: Luck et al., 1997; Reynolds et al., 1999; human fMRI: Serences and Boynton, 2007). Thus, feature-based attention could serve both to strengthen the neuronal representation of an attended target and/or increase the detectability of an anticipated target if its features are known in advance. Likewise it is possible that attention to a sound frequency could modulate the baseline activity of auditory cortex neurons in the absence of a stimulus.

Broader significance

Frequency is one featural cue out of several, including position, trajectory, timbre, intensity, and temporal cues, that likely contribute to speech selection (Zion-Golumbic and Schroeder, 2012). Responses to attended speech patterns are enhanced and responses to unattended speech patterns suppressed at higher levels of auditory cortex (Kerlin et al., 2010; Mesgarani and Chang, 2012) and age-related deficits in speech comprehension in noise are linked to impaired attentional mechanisms in older adults (Passow et al., 2012). Spectral filtering by attention may be an important function of the primary auditory cortex, contributing to downstream selection of spectrally complex auditory streams such as speech.

References

Ahveninen, J., Hämäläinen, M., Jääskeläinen, I.P., Ahlfors, S.P., Huang, S., Lin, F.-H., Raij, T., Sams, M., Vasios, C.E., Belliveau, J.W., 2011. Attention-driven auditory cortex short-term plasticity helps segregate relevant sounds from noise. Proc. Natl. Acad. Sci. 108, 4182 – 4187.

Atiani, S., Elhilali, M., David, S.V., Fritz, J.B., Shamma, S.A., 2009. Task difficulty and performance induce diverse adaptive patterns in gain and shape of primary auditory cortical receptive fields. Neuron 61, 467 – 480.

Bartlett, E.L., Sadagopan, S., Wang, X., 2011. Fine frequency tuning in monkey auditory cortex and thalamus. J. Neurophysiol. 106, 849 – 859.

Bidet-Caulet, A., Fischer, C., Besle, J., Aguera, P.-E., Giard, M.-H., Bertrand, O., 2007. Effects of selective attention on the electrophysiological representation of concurrent sounds in the human auditory cortex. J. Neurosci. Off. J. Soc. Neurosci. 27, 9252 – 9261.

Bitterman, Y., Mukamel, R., Malach, R., Fried, I., Nelken, I., 2008. Ultra-fine frequency tuning revealed in single neurons of human auditory cortex. Nature 451, 197 – 201.

Cherry, E.C., 1953. Some experiments on the recognition of speech, with one and two ears. J Acoust Soc Am 975 – 979.

Da Costa, S., van der Zwaag, W., Marques, J.P., Frackowiak, R.S.J., Clarke, S., Saenz, M., 2011. Human Primary Auditory Cortex Follows the Shape of Heschl's Gyrus. J. Neurosci. 31, 14067 – 14075.

David, S.V., Fritz, J.B., Shamma, S.A., 2012. Task reward structure shapes rapid receptive field plasticity in auditory cortex. Proc. Natl. Acad. Sci. U. S. A. 109, 2144 – 2149.

Engel, S.A., 2012. The development and use of phase-encoded functional MRI designs. NeuroImage 62, 1195 – 1200.

Formisano, E., Kim, D.S., Di Salle, F., van de Moortele, P.F., Ugurbil, K., Goebel, R., 2003. Mirror-symmetric tonotopic maps in human primary auditory cortex. Neuron 40, 859 – 869.

Fritz, J., Shamma, S., Elhilali, M., Klein, D., 2003. Rapid task-related plasticity of spectrotemporal receptive fields in primary auditory cortex. Nat. Neurosci. 6, 1216 – 1223.

Fritz, J.B., Elhilali, M., David, S.V., Shamma, S.A., 2007. Auditory attention–focusing the searchlight on sound. Curr. Opin. Neurobiol. 17, 437 – 455.

Fritz, J.B., Elhilali, M., Shamma, S.A., 2005. Differential dynamic plasticity of A1 receptive fields during multiple spectral tasks. J. Neurosci. Off. J. Soc. Neurosci. 25, 7623 – 7635.

Fujiwara, N., Nagamine, T., Imai, M., Tanaka, T., Shibasaki, H., 1998. Role of the primary auditory cortex in auditory selective attention studied by whole-head neuromagnetometer. Brain Res. Cogn. Brain Res. 7, 99 – 109.

Guo, W., Chambers, A.R., Darrow, K.N., Hancock, K.E., Shinn-Cunningham, B.G., Polley, D.B., 2012. Robustness of cortical topography across fields, laminae, anesthetic states, and neurophysiological signal types. J. Neurosci. Off. J. Soc. Neurosci. 32, 9159 – 9172.

Hackett, T.A., 2011. Information flow in the auditory cortical network. Hear. Res. 271, 133 – 146.

Hillyard, S.A., Hink, R.F., Schwent, V.L., Picton, T.W., 1973. Electrical signs of selective attention in the human brain. Science 182, 177 – 180.

Humphries, C., Liebenthal, E., Binder, J.R., 2010. Tonotopic organization of human auditory cortex. NeuroImage 50, 1202 – 1211.

Jäncke, L., Mirzazade, S., Shah, N.J., 1999. Attention modulates activity in the primary and the secondary auditory cortex: a functional magnetic resonance imaging study in human subjects. Neurosci. Lett. 266, 125 – 128.

Jaramillo, S., Zador, A.M., 2011. The auditory cortex mediates the perceptual effects of acoustic temporal expectation. Nat. Neurosci. 14, 246 – 251.

Kerlin, J.R., Shahin, A.J., Miller, L.M., 2010. Attentional gain control of ongoing cortical speech representations in a cocktail party. J. Neurosci. Off. J. Soc. Neurosci. 30, 620 – 628.

Langers, D.R.M., Dijk, P. van, 2012. Mapping the Tonotopic Organization in Human Auditory Cortex with Minimally Salient Acoustic Stimulation. Cereb. Cortex 22, 2024 – 2038.

Luck, S.J., Chelazzi, L., Hillyard, S.A., Desimone, R., 1997. Neural mechanisms of spatial selective attention in areas V1, V2, and V4 of macaque visual cortex. J. Neurophysiol. 77, 24 – 42.

Maunsell, J.H.R., Treue, S., 2006. Feature-based attention in visual cortex. Trends Neurosci. 29, 317 – 322.

Mesgarani, N., Chang, E.F., 2012. Selective cortical representation of attended speaker in multi-talker speech perception. Nature 485, 233 – 236.

Oh, J., Kwon, J.H., Yang, P.S., Jeong, J., 2013. Auditory imagery modulates frequency-specific areas in the human auditory cortex. J. Cogn. Neurosci. 25, 175 – 187.

Otazu, G.H., Tai, L.-H., Yang, Y., Zador, A.M., 2009. Engaging in an auditory task suppresses responses in auditory cortex. Nat. Neurosci. 12, 646 – 654.

Paltoglou, A.E., Sumner, C.J., Hall, D.A., 2009. Examining the role of frequency specificity in the enhancement and suppression of human cortical activity by auditory selective attention. Hear. Res. 257, 106 – 118.

Passow, S., Westerhausen, R., Wartenburger, I., Hugdahl, K., Heekeren, H.R., Lindenberger, U., Li, S.-C., 2012. Human aging compromises attentional control of auditory perception. Psychol. Aging 27, 99 – 105.

Petkov, C.I., Kang, X., Alho, K., Bertrand, O., Yund, E.W., Woods, D.L., 2004. Attentional modulation of human auditory cortex. Nat. Neurosci. 7, 658 – 663.

Recanzone, G.H., Guard, D.C., Phan, M.L., 2000. Frequency and intensity response properties of single neurons in the auditory cortex of the behaving macaque monkey. J. Neurophysiol. 83, 2315 – 2331.

Reynolds, J.H., Chelazzi, L., Desimone, R., 1999. Competitive mechanisms subserve attention in macaque areas V2 and V4. J. Neurosci. Off. J. Soc. Neurosci. 19, 1736 – 1753.

Rinne, T., Balk, M.H., Koistinen, S., Autti, T., Alho, K., Sams, M., 2008. Auditory selective attention modulates activation of human inferior colliculus. J. Neurophysiol. 100, 3323 – 3327.

Rinne, T., Koistinen, S., Talja, S., Wikman, P., Salonen, O., 2012. Task-dependent activations of human auditory cortex during spatial discrimination and spatial memory tasks.

NeuroImage 59, 4126 – 4131.

Rivier, F., Clarke, S., 1997. Cytochrome oxidase, acetylcholinesterase, and NADPH-diaphorase staining in human supratemporal and insular cortex: evidence for multiple auditory areas. NeuroImage 6, 288 – 304.

Saenz, M., Buracas, G.T., Boynton, G.M., 2002. Global effects of feature-based attention in human visual cortex. Nat. Neurosci. 5, 631 – 632.

Serences, J.T., Boynton, G.M., 2007. Feature-based attentional modulations in the absence of direct visual stimulation. Neuron 55, 301 – 312.

Striem-Amit, E., Hertz, U., Amedi, A., 2011. Extensive cochleotopic mapping of human auditory cortical fields obtained with phase-encoding FMRI. PloS One 6, e17832.

Tanji, K., Leopold, D.A., Ye, F.Q., Zhu, C., Malloy, M., Saunders, R.C., Mishkin, M., 2010. Effect of sound intensity on tonotopic fMRI maps in the unanesthetized monkey. NeuroImage 49, 150 – 157.

Treue, S., Martínez Trujillo, J.C., 1999. Feature-based attention influences motion processing gain in macaque visual cortex. Nature 399, 575 – 579.

Van der Zwaag, W., Francis, S., Head, K., Peters, A., Gowland, P., Morris, P., Bowtell, R., 2009. fMRI at 1.5, 3 and 7 T: Characterising BOLD signal changes. NeuroImage 47, 1425 – 1434.

Van der Zwaag, W., Gentile, G., Gruetter, R., Spierer, L., Clarke, S., 2011. Where sound position influences sound object representations: a 7-T fMRI study. NeuroImage 54, 1803 – 1811.

Woldorff, M.G., Gallen, C.C., Hampson, S.A., Hillyard, S.A., Pantev, C., Sobel, D., Bloom, F.E., 1993. Modulation of early sensory processing in human auditory cortex during auditory selective attention. Proc. Natl. Acad. Sci. 90, 8722 – 8726.

Woods, D.L., Herron, T.J., Cate, A.D., Yund, E.W., Stecker, G.C., Rinne, T., Kang, X., 2010. Functional properties of human auditory cortical fields. Front. Syst. Neurosci. 4, 155.

Woods, D.L., Hillyard, S.A., Hansen, J.C., 1984. Event-related brain potentials reveal similar attentional mechanisms during selective listening and shadowing. J. Exp. Psy-

chol. Hum. Percept. Perform. 10, 761 – 777.

Woods, D.L., Stecker, G.C., Rinne, T., Herron, T.J., Cate, A.D., Yund, E.W., Liao, I., Kang, X., 2009. Functional Maps of Human Auditory Cortex: Effects of Acoustic Features and Attention. PloS One 4, e5183.

Zion-Golumbic, E., Schroeder, C.E., 2012. Attention modulates speech-tracking at a cocktail party. Trends Cogn. Sci. 16, 363 – 364.

3.3 Semantic representation within early-stage auditory areas: a 7T fMRI repetition effect study

Da Costa Sandra, Bourquin Nathalie, Knebel Jean-François, Van der Zwaag Wietske, Saenz Melissa, Clarke Stephanie

This article is currently in preparation for submission.

Acknowledgements

This work was supported by a Swiss National Science Foundation Grant 3200030-124897 to S.C. and was done in collaboration with the Centre d'Imagerie BioMédicale of the Université de Lausanne, Université de Genève, Hôpitaux Universitaires de Genève et de Lausanne, Ecole Polytechnique Fédérale de Lausanne, and the Leenaards and Louis-Jeantet Foundations.

Abstract

Environmental sounds are highly complex sounds, whose processing depends on top-down and bottom-up processing. The regions involved in their recognition are classically assed with repetition effect paradigms. A repeated exposure to a sound of the same sound source yields a lower neuronal activity in their semantic representation than the initial exposure. Here, we assessed repetition effects to environmental sounds within primary and non-primary early-stage auditory areas, which were first identified by means of tonotopic mapping. Repeated presentations of sounds from the same sources, as compared to different sources, gave sufficient repetition suppression effects within posterior and medial non-primary areas of the right hemisphere. Thus, parts of the planum temporale and medial Heschl's gyrus are likely to carry semantic representations.

Introduction

Human primary auditory cortex (PAC) always colocalize with the medial two-thirds of Heschl's gyrus (HG) in the temporal plane and does not seem to be restricted by architectonic borders (Galaburda and Sanides, 1980; Morosan et al., 2001; Rademacher et al., 2001; Rivier and Clarke, 1997). Using functional magnetic resonance imaging (fMRI), several studies showed a common continuous mapping of preferred frequencies in monkeys (Baumann et al., 2010; Petkov et al., 2006) and in humans (Da Costa et al., 2011; De Martino et al., 2013; Formisano et al., 2003; Humphries et al., 2010; Moerel et al., 2012; Striem-Amit et al., 2011; Talavage et al., 2000, 2004; Woods et al., 2009). Primary subfields are organised in frequency gradients from high to low (A1) and low to high (R) frequencies, with a frequent low frequency cluster at the union of A1and R. Another gradient from high to low frequencies (RT) is consistently found in monkeys and less often in humans (for review, see Baumann et al., 2013; Saenz and Langers, 2013; Talavage et al., 2013).

At ultra-high field (7 Tesla), signal-to-noise ratio (SNR) and BOLD signal are increased, which supports small voxel size imaging. Also, the signal strength of venous blood is reduced because of the short relaxation times, restricting activation signals to cortical gray matter and thus improving spatial specificity (van der Zwaag et al., 2009a, 2009b). All together, these technical advances are beneficial for fMRI-based tonotopic mapping of the relatively small individual human fields which requires high spatial resolution (Da Costa et al., 2011; De Martino et al., 2013; Formisano et al., 2003; Moerel et al., 2012; Yacoub et al., 2007).

Environmental sounds (such as voices, natural sounds, human non-vocalizations, musical instruments, vehicles and animals) are highly complex sounds categorized extremely fast (70 ms after stimulus onset, Murray et al., 2006) and without effort due to the top-down and bottom-up interactions (Lewis et al., 2009) along hierarchical ventral and dorsal pathways (Griffiths and Warren, 2004; Warren et al., 2002). Environmental sounds activate primary (Altmann et al., 2010; Andics et al., 2013; Belin et al., 2000; Bidet-Caulet et al., 2005; Bourquin et al., 2012; Doehrmann et al., 2008; Engel et al., 2009; Leaver and Rauschecker, 2010; Moerel et al., 2012; Sharda and Singh, 2012; van der

Zwaag et al., 2011; Woods et al., 2011) and non-primary auditory areas (Altmann et al., 2007; Belin et al., 2000; Bergerbest et al., 2004; Bourquin et al., 2012; De Lucia et al., 2010, 2012; Doehrmann et al., 2008; Latinus and Taylor, 2012; Leaver and Rauschecker, 2010; Murray et al., 2006; Viceic et al., 2006; Woods et al., 2011; Zatorre and Belin, 2001). Most of these studies used repetition suppression paradigms (Grill-Spector et al., 1999, 2006) where immediate repetition of the stimulus induced a reduction of activity in stimulus-specific regions in a bottom-up manner. The hierarchical model of sound recognition postulates that early stages decompose auditory information according to acoustical spectrotemporal features, whereas later stages are more dedicated to semantic processing (Altmann et al., 2010). Thus, semantic repetition effects should be absent in early-stage auditory areas, in particular in belt areas.

While no repetition priming effects are expected in the primary or belt regions, several of the previously mentioned studies observed repetition priming effects within primary and belt areas (Altmann et al., 2007a, 2007b, 2010; Belin et al., 2000; Bergerbest et al., 2004; Bidet-Caulet et al., 2005; Doehrmann et al., 2008; Engel et al., 2009; Latinus et al., 2011; Leaver and Rauschecker, 2010; Moerel et al., 2012, 2013; Sharda and Singh, 2012; Woods et al., 2011). This discrepancy between the model and repetition priming results could be explained by (1) the involvement of belt areas in the recognition pathway, which implies that these areas already code for sound meaning and display repetition priming effects or (2) semantic repetition priming effects, which occur outside the hierarchical organised pathways, indicating possibly the existence of two parallel sound recognition pathways. Here, we have tested these hypotheses with high-resolution functional auditory imaging of environmental sounds processing within primary and non-primary auditory cortex regions.

Materials and Methods

Subjects

Ten subjects (6 female, mean ages 23.9 $\pm$ 3.7) with normal hearing and no history of neurological or psychiatric illness participated in the study. Written, informed consent forms were signed by all subjects after a brief oral description of the protocol. The

Ethics Committee of the Faculty of Biology and Medicine of the University of Lausanne approved all experimental procedure. Eight subjects were right-handed, one left-handed and one ambidextrous.

MRI data acquisition and data analyis

Imaging was performed with an actively shielded 7 Tesla Siemens MAGNETOM scanner (Siemens Medical Solutions, Erlangen, Germany) located at the Centre dImagerie BioMédicale (CIBM) in Lausanne, Switzerland. Functional data was acquired using an 32-channel head volume rf-coil (RAPID Biomedical, Germany) and an EPI pulse sequence with sinusoidal read-out (Speck et al., 2008; 1.5 x 1.5 mm in-plane resolution, slice thickness = 1.5 mm, TR = 2000 ms, TE = 25 ms, flip angle = 47°, slice gap = 1.57 mm, matrix size = 148 x 148, field of view 222 x 222, 30 oblique slices covering the superior temporal plane, first three EPI images discarded). The sinusoidal shape of the readout gradients reduces the acoustic noise produced by the scanner. A T1-weighted high-resolution (resolution = 1 x 1 x 1 mm, TR = 5500 ms, TE = 2.84 ms, TI1 = 2350 ms, TI2 = 0 ms, slice gap = 1 mm, matrix size = 256 x 240, field of view = 256 x 240) 3-D anatomical image was acquired for each subject using the MP2RAGE pulse sequence optimized for 7T (Marques et al., 2010). Anatomical images were used to co-register to functional scans and to generate of cortical surface representations.

Preprocessing steps were performed with BrainVoyager QX v2.3 software and included standard linear trend removal, temporal high-pass filtering, motion correction, but no spatial smoothing. Functional time-courses were interpolated into 1 x 1 x 1 mm volumetric space and registered to each subjects 3D Talairach-normalized anatomical dataset. Cortical surface meshes were generated from each subjects anatomical using automated segmentation tools of the program. Data analysis for the repetition priming experiment was performed in volumetric space using a GLM approach. A group-averaged contrast sound vs. rest was generated using cortex-based alignment (Goebel et al., 2006). This is a non-rigid alignment of cortical surface meshes across individuals based on the gyral and sulcal folding patterns. Each subjects cortical surface meshes were aligned to a target mesh (separately for left and right hemispheres) which had intermediate HG anatomy (partial HG duplication in the left hemisphere and a large single gyrus in the right hemisphere). All

alignments were visually inspected.

Auditory stimuli

Sound stimuli were generated using MATLAB and the Psychophysics Toolbox (www.psychtoolbox.org). Stimuli were delivered binaurally via MRI-compatible headphones (Insert Earphones, SensiMetrics, MA, USA) featuring flat frequency transmission from 100 Hz to 8 kHz. Sound intensities were adjusted to match standard equal-loudness curves (ISO 226) at phon 95: the sound intensity of each pure tone stimulus (ranging from 88 to 8000 Hz) was adjusted to approximately equal the perceived loudness of a 1000 Hz reference tone at 95 dB SPL (range of sound intensities: 87-101 dB SPL). Sound levels were further attenuated ($\sim$35 dB) by silicone ear plugs (Etymotic Research Inc., ER38-15SM). Subjects reported hearing sounds clearly over background scanner noise and were instructed to keep their eyes closed during fMRI scanning.

Tonotopic mapping

Pure tones (88, 125, 177, 250, 354, 500, 707, 1000, 1414, 2000, 2828, 4000, 5657, and 8000 Hz; half-octave steps with a sampling rate of 44.1 kHz) were presented in ordered progressions, following our previously described methods (Da Costa et al., 2011, 2013). Each subject performed two tonotopic sessions with ascending and descending progressions (low to high and high to low frequencies, respectively). Pure tone bursts were presented for a 2 s block in consecutive steps until all 14 frequencies had been presented. The 28 s progression was followed by a 4 s silent pause, and this 32 s cycle was repeated 15 times per 8 min scan run. Resulting maps of the two runs were averaged. This paradigm is designed to induce travelling waves of response across cortical tonotopic maps (Engel, 2012). Linear cross-correlation was used to determine the time-to-peak of the fMRI response wave on a per-voxel basis, and to thus assign a corresponding best frequency value to each voxel. Analyses were performed in individual-subject volumetric space and results were then projected onto same-subject cortical surface meshes.

Similar to the example shown in Figure 3.8.B, two tonotopic gradients with mirror symmetry ("high-low-low-high") were clearly observed in both hemispheres of all subjects

(Da Costa et al., 2011, 2013; Formisano et al., 2003; Humphries et al., 2010; Langers and Dijk, 2012; Moerel et al., 2012; Striem-Amit et al., 2011; Woods and Alain, 2009), A1 is defined by the more posterior "high-to-low" gradient corresponding and R by the more anterior "low-to-high" gradient. In macaque auditory cortex, fields A1 and R receive parallel thalamic input and are both considered part of the primary auditory core.

fMRI repetition suppression experiment

Environmental sounds of 500 ms were extracted from BBC sound effects (following Bourquin et al., 2013) using Adobe Audition (Adobe Systems Software Ireland Ltd.). Amplitudes, sampling frequencies and linear rise/fall times were normalized with the same routine for all sounds (16 bits, 44.1 kHz, 50 ms rise/fall times). Monophonic sounds were duplicated into stereophonic sounds and tested with a sound recognition task in five subjects outside the MRI. This constrains our dataset to sounds that were correctly named with high confidence by all subjects. Sounds were manually classified, according to their number of repeats, into two groups: repetition group (REP group, i.e. eight or more different exemplars) and control group (CTRL group, i.e. less than eight exemplars, max seven). Sounds subsets of each group were randomly selected and frequency distributions were compared using t-tests. Differing sounds were then removed from the database. This operation was performed several times until less than 1% of significant differences between subsets was obtained (for more details see Aeschlimann et al., 2008 and Knebel et al., 2008). This procedure yielded a total of 323 environmental sounds (64 REP sounds and 259 CTRL sounds). Semantic categories (animal vocalizations, human-made sounds, tools, music instruments, and natural scene-like sounds) were equally distributed in both groups. Sounds from the REP group were never repeated in the CTRL group.

Subjects listened passively to sounds during fMRI acquisitions. A block design with alternating blocks of sounds of the same semantic category (REP) and sounds of different semantic categories (CTRL) was presented. REP blocks were made of eight different repetitions of the same semantic object (i.e. eight baby cries of different babies), with in total 8 REP clocks or 64 REP sounds per run. CTRL blocks had 8 different exemplars of different categories randomly selected at the beginning of each run (8 different semantic objects x 8 blocks = 64 out of the 259 CTRL sounds). Sounds were presented bilaterally

during 500 ms with an ISI of 1500 ms during 16 s and followed by a 14 s silent pause at the end of each block. Each fMRI run consisted of 16 blocks of 30 s (8 REP and 8 CTRL, 8 minutes in total). Two runs, with the same sequence of sounds, were acquired both before and after tonotopic mapping runs. Sound onsets were synchronized with the scanner trigger.

Fixed-effect multi-subject GLM group analysis of all individual time-courses highlighted regions preferring *environmental sounds vs. rest* (Figure 3.8.A). This contrast was used to define group average regions of interest (see further in the text and Figures 3.8.B and 3.15.A).

Individual ROIs

Individual tonotopic maps used to define subject-specific ROIs. Maps created with an intermediate threshold ($r > 0.13$, equivalent to $p = 0.05$) in order to obtain a region of activation that covered most of the superior temporal gyrus (STG). We then manually outlined a contiguous patch of interest (general auditory cortex ROI, AC; LH: 1400.87 mm^2 $\pm$ 321.35, and RH: 1364.58 mm^2 $\pm$ 189.15) of cortical surfaces including the two primary gradients, surrounding non-primary areas, and planum temporale (PT) using drawing tools within BrainVoyager QX (external outlines in Figure 3.9). This patch of interest was subdivided in the following steps: first, primary subfields A1 and R were localized, and the anterior and posterior borders thereof were drawn along the outer high-frequency representations, while lateral and medial borders were set so as to cover only the medial two-thirds of Heschl's gyrus (in accordance with human architectonics; Hackett et al., 2011; Rivier and Clarke, 1997). The border between A1 and R was then drawn perpendicular to the low-frequency gradient reversal. Exact borders of A1 and R were not dependent upon the particular correlation threshold. Second, we divided the non-primary area surrounding A1 and R into eight subfields. The common border between A1 and R was extended until the outlines of AC, dividing it into anterior and posterior parts. The same was done for the anterior and posterior borders of the primary subfields. This resulted in six small fields along Heschl's gyrus and two moderate ones, anterior and posterior to Heschl's gyrus, which were finally divided along the posterior-anterior axis into medial and lateral subfields. In consequence, our initial AC region was subdivided into ten fields

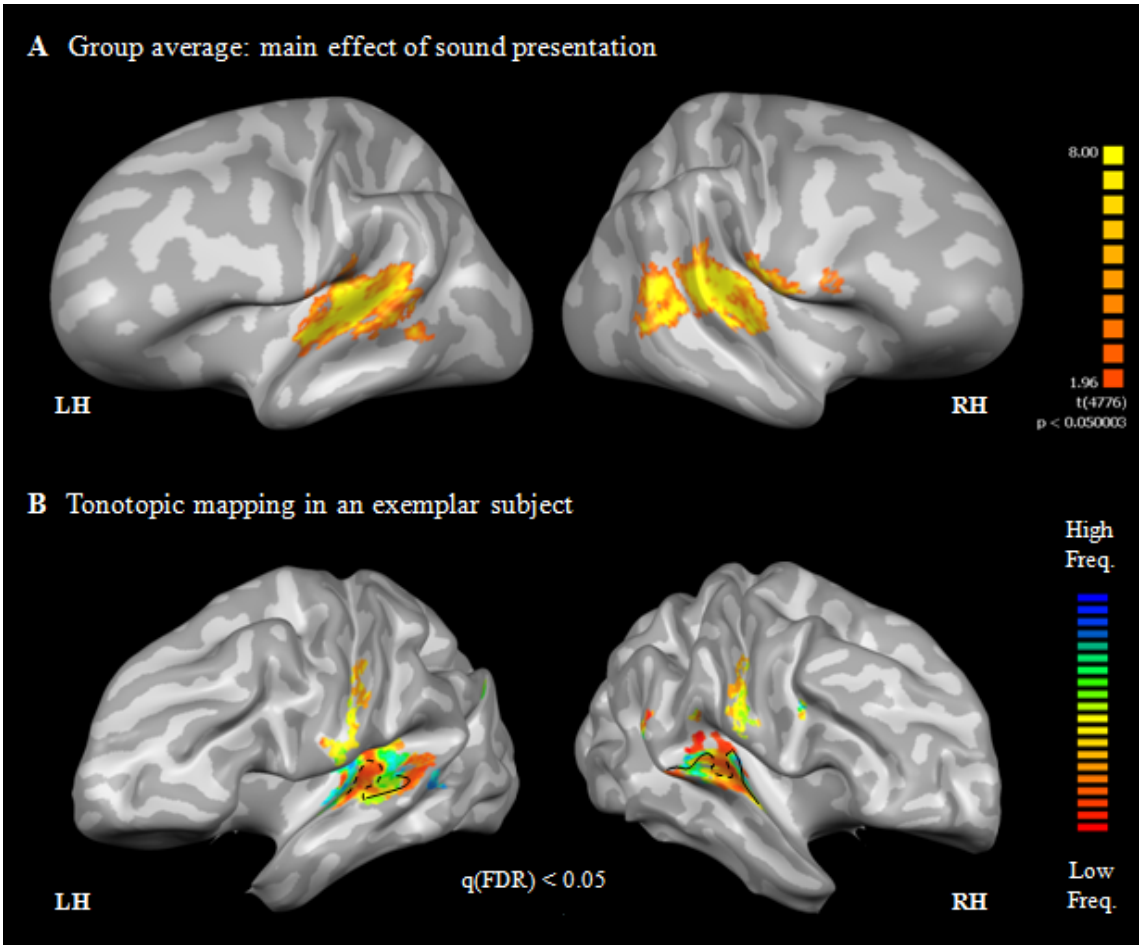

Figure 3.8: A. Main effect of environmental sound presentations during the repetition suppression experiment displayed on a reference brain. Fixed-effect multi-subject GLM group analysis of all individual time-courses highlighted regions preferring *environmental sounds vs. rest* bilateral STG, right posterior STS and posterior MTG (see Table 3.2). **B.** Exemplar individual tonotopic map (FDR corrected $q < 0.05$, $r > 0.20$). In each hemisphere, two mirror-symmetric gradients (high-to-low and low-to-high) corresponding the primary areas A1 and R run across Heschl's gyrus (black solid lines) or the intermediate sulcus (dashed lines).

per hemisphere which were named according to their position along posterior-anterior and medial-lateral axes: *M1, L1, M2, A1, L2, M3, R, L3, M4, and L4* (fore more details, see Table 3.1 and Figure 3.9). L1 and M1 are found in the anterior portion of the planum temporale; L2 and L3 on lateral Heschl's gyrus; M2, M3 and M4 in the insula; and L4 in the planum polare. In total, twenty individual ROIs covering primary and non-primary

auditory cortices were defined based on the tonotopic maps.

Labels	**Talairach coordinates [x ± std y ± std z ± std]**	**Mean areas (mm^3) ± std**	**Corresponding area**
right A1	[44 ± 4 - 20 ± 3 9 ± 2]	145.71 ± 27.00	PAC
right R	[44 ± 4 - 21 ± 3 10 ± 2]	133.35 ± 31.58	PAC
right L1	[56 ± 4 - 28 ± 4 12 ± 3]	212.07 ± 126.06	LA
right L2	[57 ± 3 - 17 ± 3 7 ± 3]	125.97 ± 24.99	ALA
right L3	[52 ± 4 - 10 ± 3 4 ± 2]	148.14 ± 20.16	ALA – AA
right L4	[44 ± 4 - 10 ± 5 0 ± 3]	213.67 ± 97.77	AA
right M1	[46 ± 4 - 30 ± 2 16 ± 3]	136.31 ± 33.29	PA
right M2	[38 ± 3 - 29 ± 2 16 ± 3]	67.35 ± 20.57	–
right M3	[34 ± 2 - 25 ± 2 14 ± 3]	65.75 ± 20.41	–
right M4	[35 ± 3 - 20 ± 2 7 ± 4]	119.92 ± 71.61	∼ MA
S1a	[56 ± 4 - 39 ± 4 13 ± 3]	308.11	–
S1b	[56 ± 6 - 39 ± 6 5 ± 3]	362.59	–
C1	[44 ± 5 - 53 ± 6 21 ± 5]	747.17	–
left A1	[-40 ± 3 - 24 ± 3 9 ± 2]	138.67 ± 30.27	PAC
left R	[-39 ± 3 - 21 ± 3 9 ± 2]	106.00 ± 25.05	PAC
left L1	[-52 ± 4 - 29 ± 4 11 ± 3]	246.53 ± 69.66	LA
left L2	[-52 ± 3 - 18 ± 3 6 ± 2]	140.07 ± 38.11	ALA
left L3	[-47 ± 4 - 11 ± 4 4 ± 2]	165.28 ± 38.47	ALA – AA
left L4	[-40 ± 4 - 12 ± 6 0 ± 3]	209.44 ± 105.22	AA
left M1	[-40 ± 3 - 34 ± 3 14 ± 3]	155.71 ± 59.12	PA
left M2	[-34 ± 2 - 30 ± 2 15 ± 3]	62.58 ± 22.41	–
left M3	[-31 ± 2 - 26 ± 2 15 ± 3]	59.66 ± 15.78	–
left M4	[-32 ± 2 - 20 ± 2 8 ± 4]	100.23 ± 48.17	∼ MA

Table 3.1: Mean Talaraich coordinates of all ROIs with standard deviations, and their corresponding areas defined by cytoarchitechtonic studies (Rivier and Clarke, 1997; Wallace et al. 2002). PAC: primary auditory cortex; LA: lateral auditory area; ALA: anterolateral auditory area; AA: anterior auditory area; PA: posterior area; MA: medial auditory area.

These regions of cortical surfaces were projected into the same-subjects 1 x 1 x 1 mm interpolated volumetric space to generate 3D regions of interest (ROIs). The 3D ROIs were generated with a width of 2 mm (-1 mm to 1 mm from the vertex centre). Individual time-

courses from the 3D-ROIS were subsequently analyzed in the repetition effect experiment.

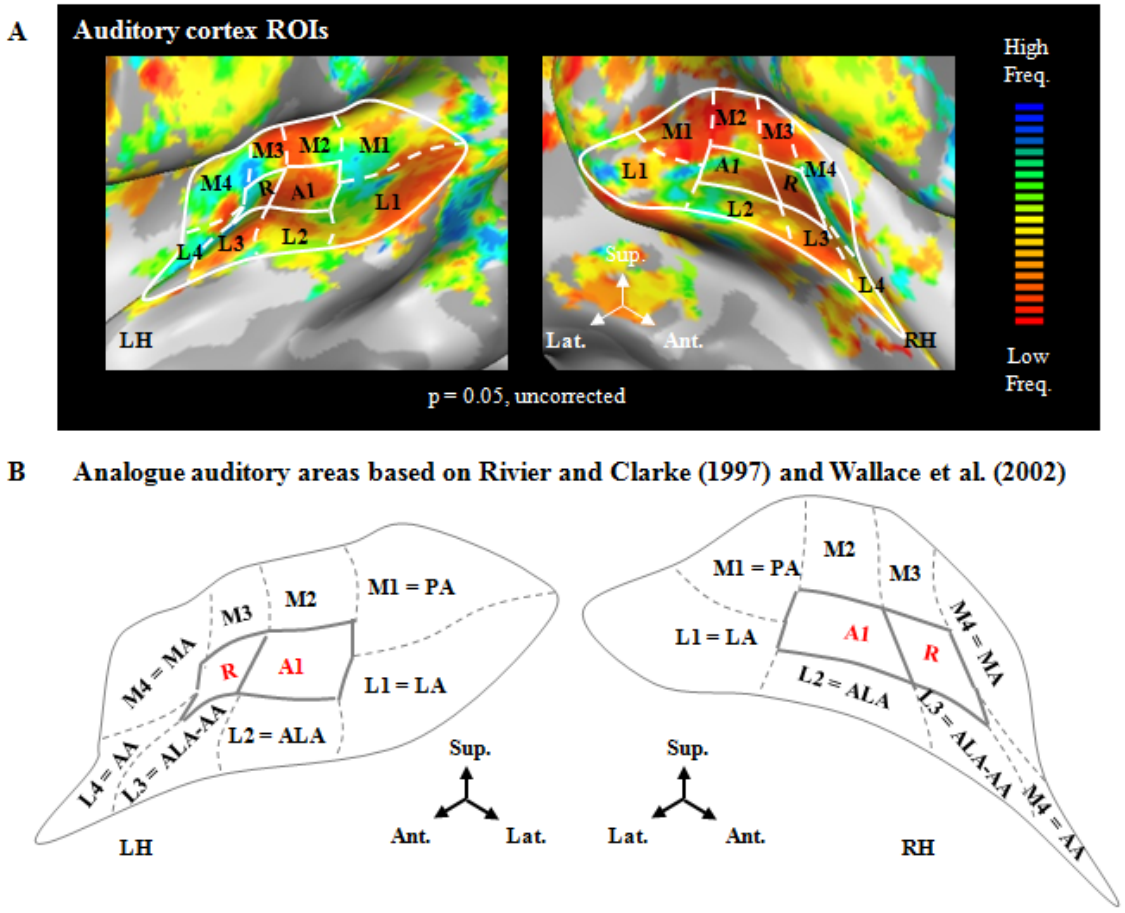

Figure 3.9: Auditory cortex ROIs. A. Primary and secondary areas of an exemplar subject (same areas than in Figure 3.8.B). Tonotopic mapping was used to indentify primary and secondary auditory cortex (AC) in each hemisphere at a threshold of p = 0.05. The AC was then subdivided according borders of primary areas A1 and R into 10 ROIs per hemisphere: *M1, L1, M2, A1, L2, M3, R, L3, M4, and L4*. **B.** Corresponding regions according to Rivier and Clarke (1997) and Wallace et al. (2002).

Group ROIs

Group average contrast *environmental sounds vs. rest* was set at threshold $p < 0.05$. Activation outside AC was found in the bilateral posterior superior temporal gyrus (STG),

posterior middle temporal gyrus (MTG) and precentral gyrus. Only right MTG and STG survived to Bonferroni correction ($p < 0.05$), other activated regions were considered due to partial volume effects. Thus, we manually outlined a continuous patch of interest and split it into anterior and posterior regions (S1a, posterior STG, and S1b, posterior MTG; purple and pink patches in Figure 3.15.A; S1a area: 362.59 mm^2; S1b area: 308.11 mm^2). We also delineated a third, control, region (C1, green patch; C1 area: 747.17 mm^2) that did not show any activation for *environmental sounds vs. rest*. This region should show no repetition effect at all. C1 was selected posterior to S1a and S1b, of the same size as the S1a/S1b clusters and overlapping with the right angular gyrus. As for individual ROIs, the group ROIs were labelled with their region name and projected into the reference brain 1 x 1 x 1 mm interpolated volumetric space. Individual time courses of these regions were subsequently analyzed in the repetition suppression experiment.

Time-course analysis

Functional individual time-courses were extracted for each voxel, ROI and hemisphere. Using home-made Matlab scripts, they were baseline corrected and averaged in space and in time, separating conditions, in order to have two final time-courses (one for REP and one for CTRL, with 15 time points each) per ROI, hemisphere and subject. These later ones were then averaged across subjects and used in the remaining analysis.

Plateau definition

We assumed that whether the sound was followed by a repetition or not, the hemodynamic response will have the same behaviour at onset, only the plateau will differ between CTRL and REP conditions. BOLD signal intensities of consecutive time frames were subtracted pairwise to calculate their relative slopes ($t_{n+1} - t_n$). We tested our hypothesis on the slope values using paired t-tests against 0. Positive p values indicate a rise period, negative values a decay and null values a plateau (Figure 3.10). We restricted our results in time to a minimum of two consecutive time frames.

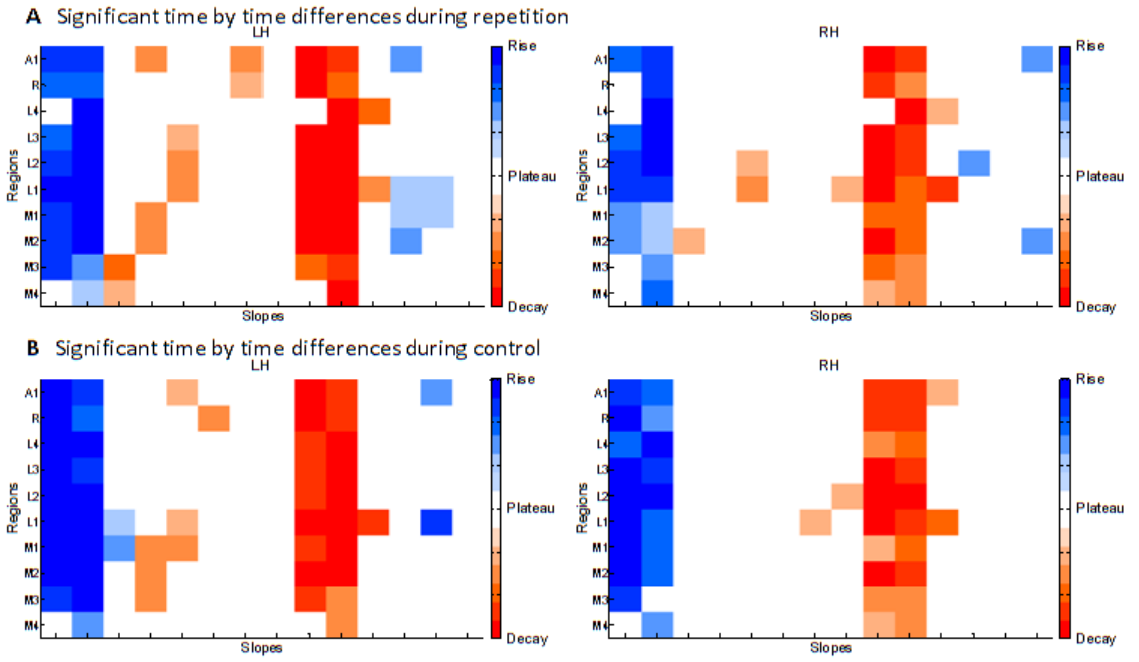

Figure 3.10: Plateau definition during repetition (A) and control (B). BOLD signal dynamics illustrate the slope between two consecutive time-points. Paired t-tests pointed out three different periods: rise from 2 to 6 s, plateau from 6 to 18 s, and decay from 18 to 22 s. Shades of blue correspond to positive slopes (rise), orange-red to negative slopes (decay) and white to flat curves.

Results

Main effect of environmental sounds

Group analysis of all individual time-courses of the repetition suppression experiment (Figure 3.8.A) highlighted several clusters preferring environmental sounds vs. rest in bilateral superior temporal gyrus (STG), right posterior superior temporal sulcus (STS), bilateral posterior middle temporal gyrus (MTG) and precentral gyrus. However, only bilateral STG, right posterior STS and right posterior MTG survived Bonferroni correction ($p < 0.05$, see Table 3.2).

Early-stage auditory areas

Individual phase-encoding analysis of the time-courses of the tonotopy runs reproduced the same mirror-symmetric tonotopic gradients (Figure 3.8.B and Figure 3.9.A) as

Region	Talairach coordinates [x, y, z]	t score	p value
right STG	[62 -25 14]	14.07	$p < 0.01$
right posterior STG	[57 -35 14]	10.83	$p < 0.01$
right posterior MTG	[61 -32 04]	7.89	$p < 0.01$
left STG	[-39 -31 10]	14.62	$p < 0.01$

Table 3.2: Main effect of environmental sounds. Centroid coordinates of activation clusters, t scores and p values. Only regions surviving a Bonferroni correction at 0.05 were considered.

previously published with other subjects (Da Costa et al., 2011). The "high-low-low-high" reversals colocalise with primary areas A1 and R and were used as reference to parcel the tonotopic patch of activity into the remaining auditory areas (Table 3.1 and Figure 3.9).

Time frame by time frame paired t-tests revealed significant differences ($p < 0.05$, uncorrected) in slopes during the same time periods for all conditions and hemispheres: a rise between 2 – 6 s, a plateau between 6 – 18 s, and a decay between 18 – 22 s (Figure 3.10).

A 2 x 2 ANOVA on individual repetition suppression time-courses revealed a main effect of condition for L1, M1 and M2 ROIs between 16 – 18 s after block onset (Figure 3.11.A) and a main effect of hemisphere for M1 ROI between 14 – 18 s (Figure 3.11.B), respectively. An interaction Hemisphere x Condition was found in A1, M1, M2 and M3 between 10 – 18 s (Figure 3.11.C).

Repetition effects in auditory-related areas

Group average repetition suppression time-courses are plotted for each condition (REP: blue line; CTRL: red line) and ROI inside the right (Figure 3.12) and left supratemporal plane (Figure 3.13). Irrespective of number of repetitions, we found BOLD signal gradients along posterior-to-anterior and medial-to-lateral axes in both hemispheres: postero-lateral fields showed greater changes in time than antero-medial ones.

Time frame by time frame paired t-tests revealed significant differences ($p < 0.05$, uncorrected) between conditions for L1, M1, M2, and M3 ROIs in the right hemisphere between 10 – 22 s after block onset (Table 3.3 and Figure 3.14.A, right) and between hemispheres for M1 and M2 between 8 – 18 s (Figure 3.14.B, left) during REP blocks. No significant differences were found between conditions in left hemisphere ROIs or between hemispheres during control.

Group ROIs outside the supratemporal plane

Group average repetition suppression time-courses of C1, S1a and S1b are plotted for each condition in Figure 3.15. As expected, C1 did not show any repetition effect and thus our paradigm was inducing suppression only in regions processing auditory objects. S1a and S1b showed both the same tendency, however S1b had clearly higher BOLD response during REP blocks.

Discussion

We measured response modulation by environmental sounds in primary and secondary auditory areas. All sounds induced activation in bilateral superior temporal gyrus, right posterior middle and superior temporal gyrus. A closer inspection revealed semantic repetition effects within posterior-medial early-stage auditory areas of the right hemisphere. Sound repetition suppression effects have been measured previously in the superior temporal plane along the ventral pathway, preferentially in the left hemisphere. However these semantic priming effects were not related to activity within belt areas but more to a hierarchical assemblage of semantic representations along the ventral pathway. Here, we hypothesised the existence of a distinct semantic pathway for environmental sounds processing.

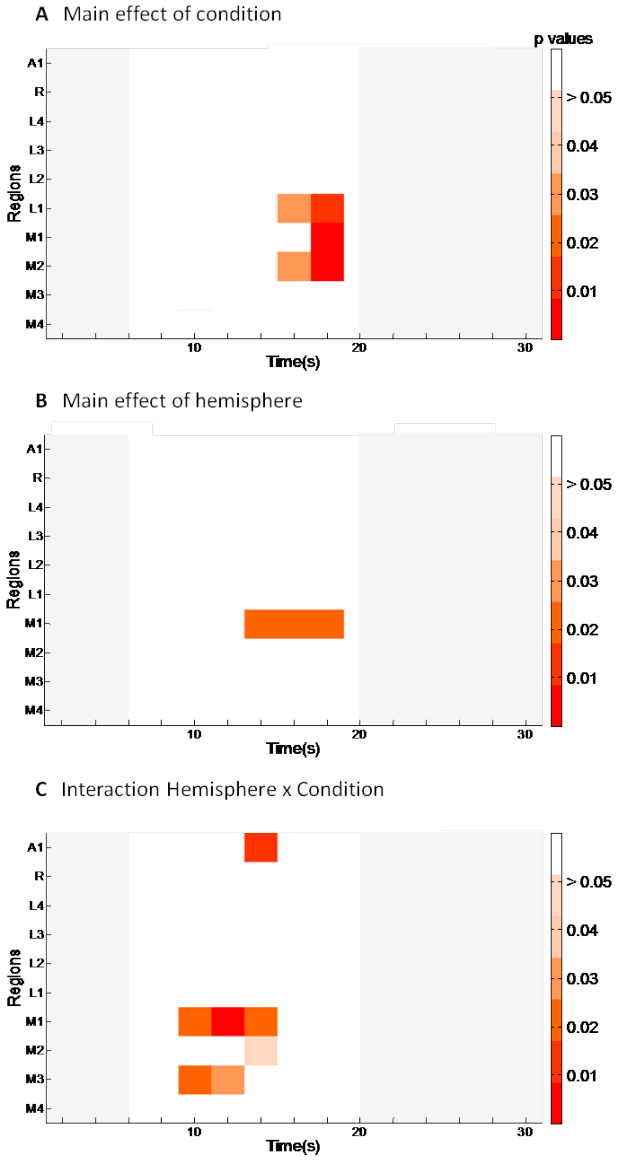

Figure 3.11: Time frame by time frame 2x2 ANOVA. A. Main effect of condition was found in M1 18 s after block onset ($p < 0.05$, uncorrected). **B.** Main effect of hemisphere also highlighted the same ROI between 14 – 18 s ($p < 0.05$, uncorrected). **C.** Hemisphere x Condition interaction was found in AC, M1, and M3 between 10 – 18 s ($p < 0.05$, uncorrected). Differences during rise and decay periods (grey boxes) were not taken in account. We considered only results with a minimum of two consecutive time frames and three adjacent areas statistically different within the time window defined in Figure 3.10.

A Group average time courses in the right primary auditory areas

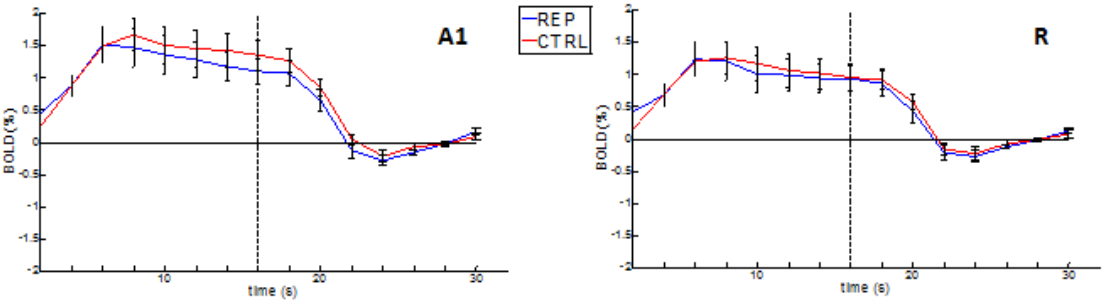

B Group average time courses in the right non-primary auditory areas

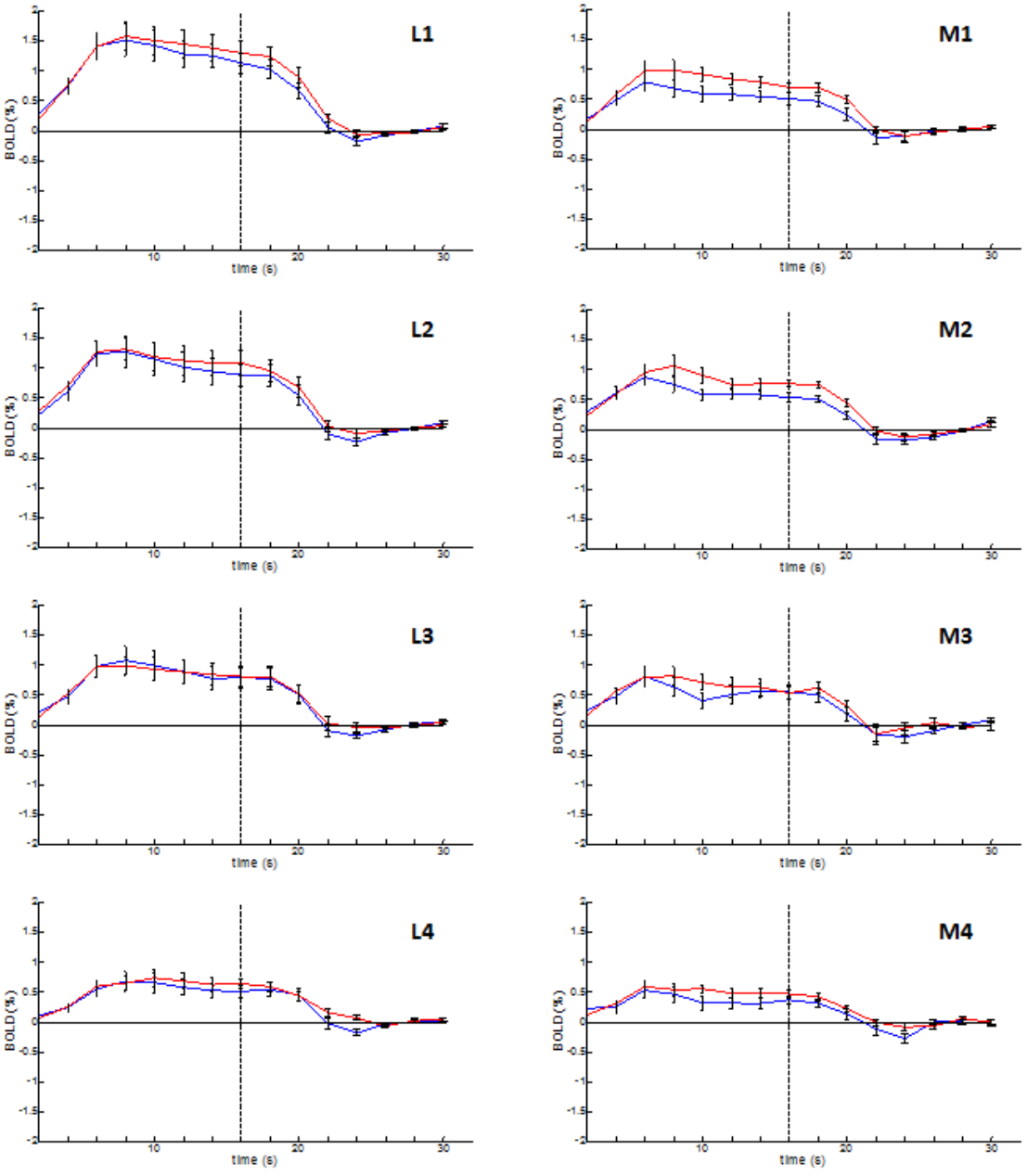

Figure 3.12: Group average time-courses of the two conditions in right hemisphere ROIs. BOLD signal changes (in %) were plotted across time points of the block. Error bars represented standard errors across all subjects. A. BOLD signal changes in primary auditory areas A1 and R. **B.** BOLD signal changes in non-primary areas. Blue and red lines stand for repetition and control time-courses, respectively. Dashed lines marked the end of the stimuli presentation. See materials and methods for more details.

Figure 3.13: Group average time-courses of the two conditions in left hemisphere ROIs. BOLD signal changes (in %) were plotted across time points of the block. Error bars represented standard errors across all subjects. A. BOLD signal changes in primary auditory areas A1 and R. **B.** BOLD signal changes in non-primary areas. Blue and red lines stand for repetition and control time-courses, respectively. Dashed lines marked the end of the stimuli presentation. See materials and methods for more details.

A Group average time courses in the left primary auditory areas

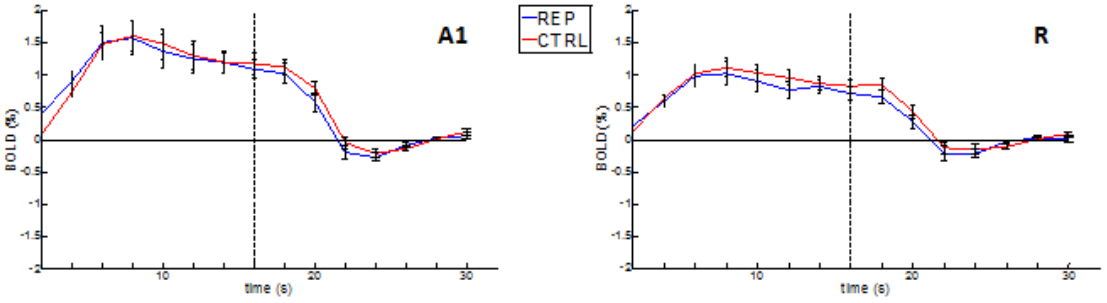

B Group average time courses in the left non-primary auditory areas

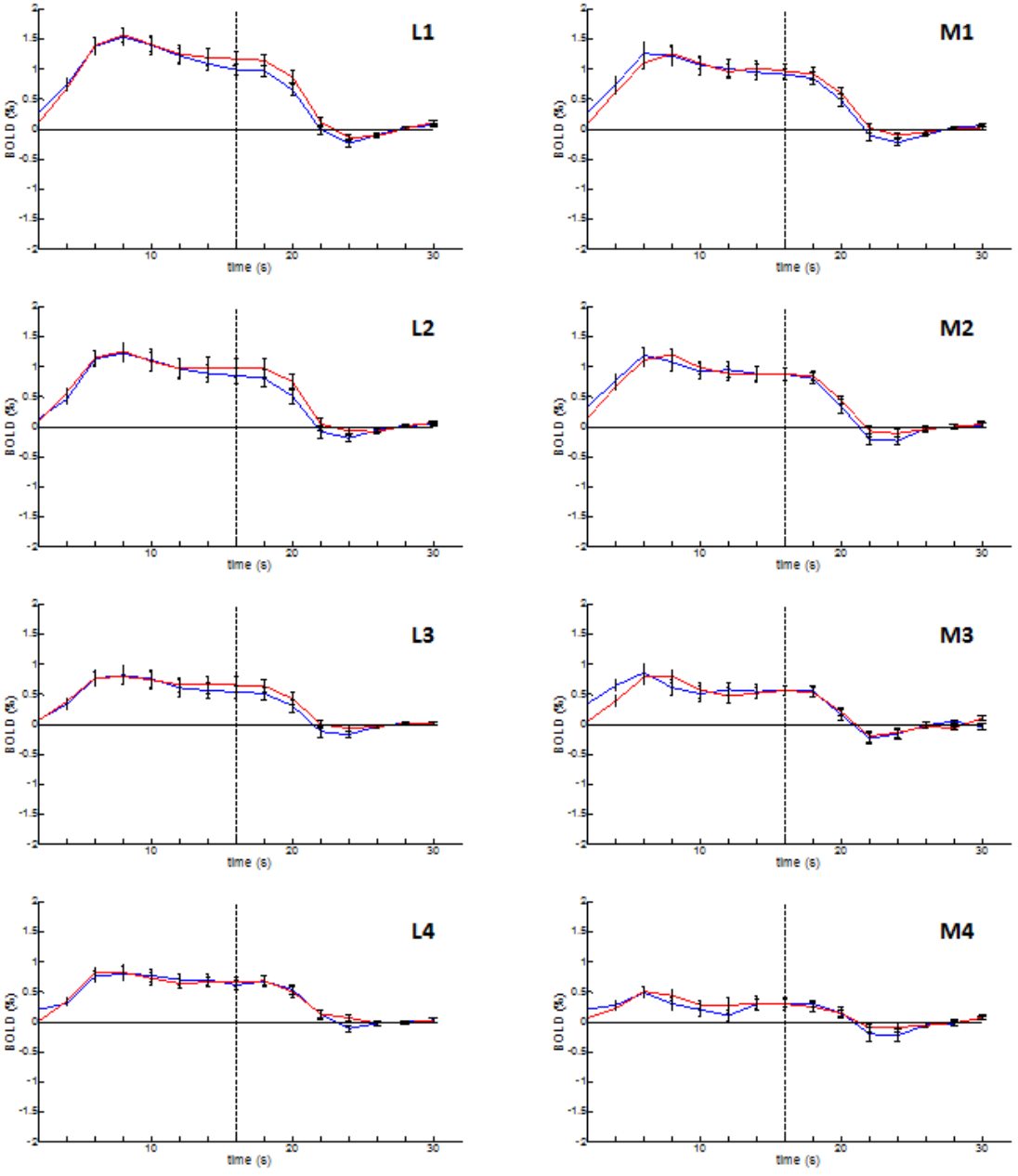

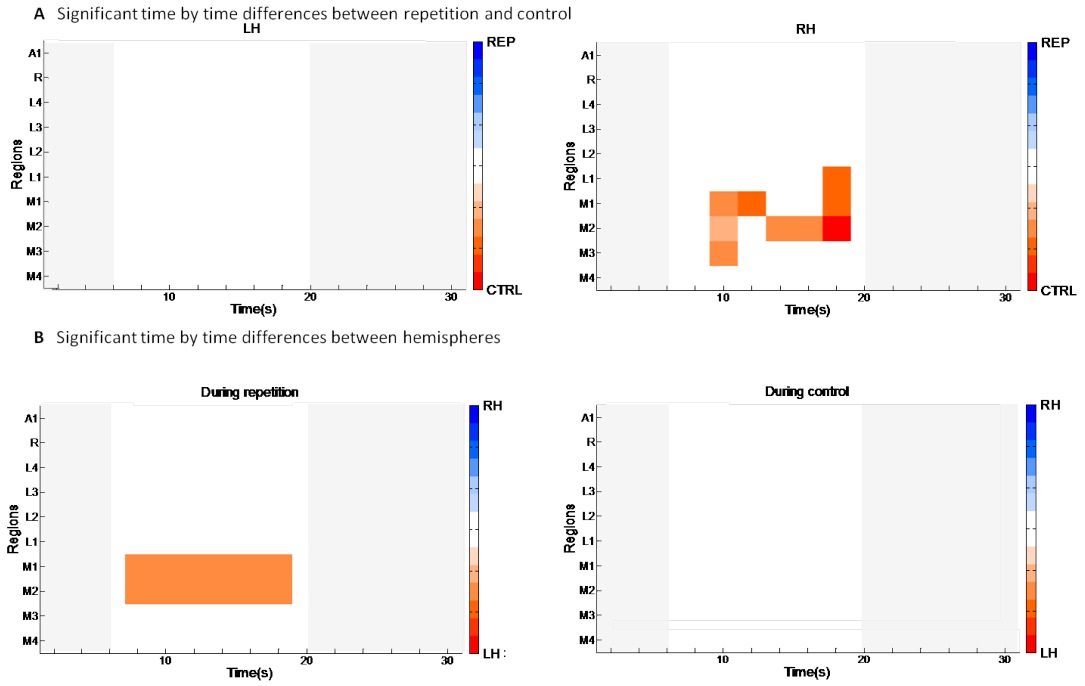

Figure 3.14: **A.** Significant differences between REP and CTRL blocks ($p < 0.05$) in the right (RH) and left hemisphere (LH). Time by time paired t-tests showed higher activity in right L1, M1, M2 and M3 ROIs between 10 – 18 s. No significant differences were found in the left hemisphere. **B.** Significant differences between hemispheres during REP (left) and CTRL (right) blocks. M1 and M2 ROIs responded more to REP blocks in the left hemisphere between 8 – 18 s. No significant differences were found for CTRL blocks. Shades of blue correspond to REP blocks **(A)** or RH **(B)** and orange-red to CTRL blocks **(A)** or LH **(B)**. We considered valid results only if a minimum of two consecutive time frames were statistically different. We considered only results with a minimum of two consecutive time frames and three adjacent areas statistically different.

Dual pathway for sound recognition

Our results showed greater activity for environmental sounds in posterior-medial early-stage areas corresponding to or near the anterior planum temporal, which is considered a computational hub for auditory information (Griffiths and Warren, 2004). Moreover, these areas were also related to sound recognition (Altmann et al., 2007, 2010; Andics et al., 2013; Belin et al., 2000; Bergerbest et al., 2004; Bourquin et al., 2012; Engel et al., 2009; Lewis and Talkington, 2012; Lewis et al., 2009; Lucia et al., 2010; Remedios et al., 2009; Sharda and Singh, 2012; van der Zwaag et al., 2011; Viceic et al., 2006; Woods et al., 2011; and Table 3.3), but are also in contradiction with other seminal repetition prim-

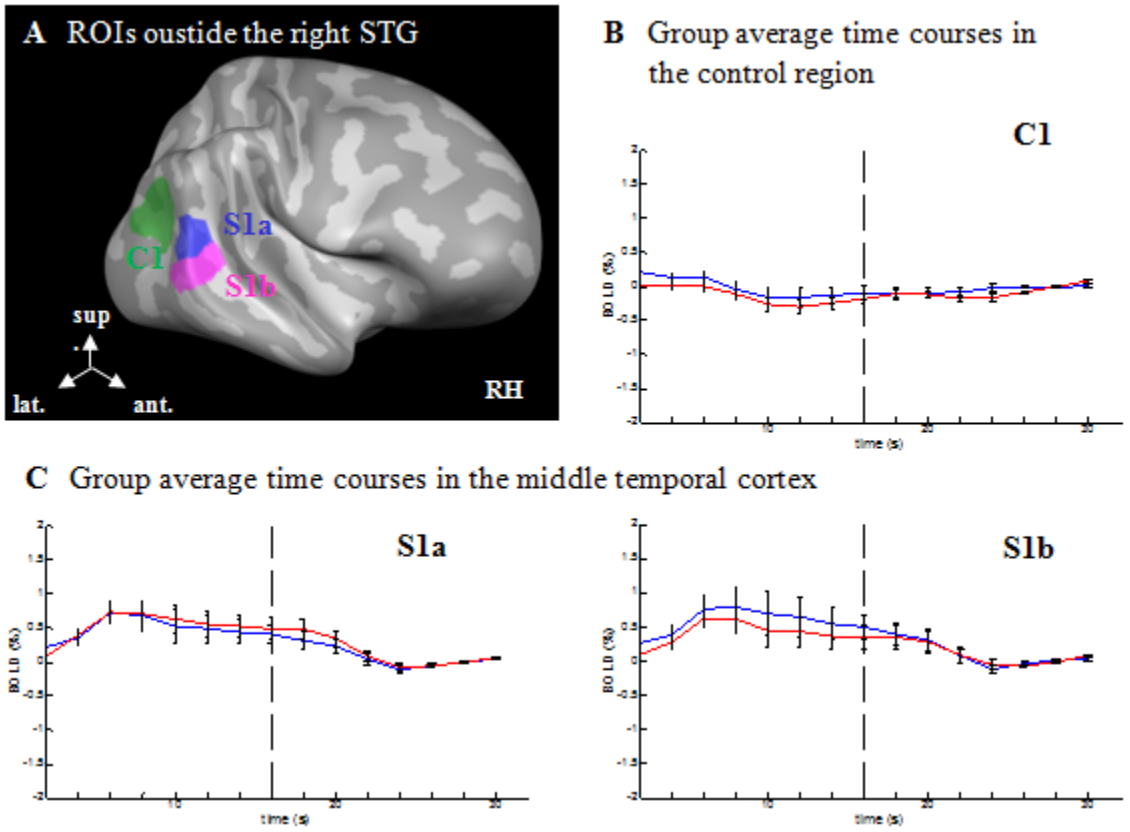

Figure 3.15: ROIs outside right auditory cortex. **A.** Group average contrast *environmental sounds vs. rest* showed activation in the right posterior MTG. This region was split into anterior and posterior regions (S1a, in purple, and S1b in pink). We also delineated a third region (C1, in green) which did not pop out with the former contrast in order to check if our paradigm was specific for repetition suppression. **B.** Group average time-course in C1. **C.** Group average time-course in S1a and S1b. **B-C.** BOLD signal changes (in %) were plotted across time points of the block. Error bars represented standard errors across all subjects. Blue and red lines stand for repetition and control time-courses, respectively. See materials and methods for more details.

ing studies (Altmann et al., 2007a, 2007b, 2010; De Lucia et al., 2010; Doehrmann et al., 2008; Riecke et al., 2011; Scott, 2005; Staeren et al., 2009). It is commonly assumed that the left superior temporal plane is more semantic and the right more acoustic (Murray et al., 2008; Schönwiesner et al., 2005). Recently, Angenstein and Brechmann (2013) stated that previous lateralization effects could be due to top-down task-related modulation (Angenstein and Brechmann, 2013). Our results are related to passive listening of environmental sounds, thus, previous results in the left hemisphere could be due to the

experiment task more than bottom-up processing per se. Moreover, activation in the right posterior-medial belt areas could perfectly confirm a rapid early semantic recognition of well-known sounds. Thus, the information will enter in the superior temporal plane by primary auditory areas and then pass to posterior-medial areas before getting into the ventral pathway areas such as right MTG.

Technical considerations

We attribute the discrepancies between our results and previous studies to a lack of spatial resolution in the superior temporal plane. The imaging studies previously mentioned did all apply spatial smoothing (2 to 6 mm FWHM) and were acquired at low (Belin et al., 2000; Bergerbest et al., 2004; Woods et al., 2011) or high field strengths (Altmann et al., 2007a, 2007b, 2010; Bidet-Caulet et al., 2005; Doehrmann et al., 2008; Engel et al., 2009; Latinus and Taylor, 2012; Leaver and Rauschecker, 2010; Moerel et al., 2012; Sharda and Singh, 2012; Staeren et al., 2009) with large voxels size (2-3 mm or more). Our high resolution findings are close to results from Altmann et al. (2008, adaptation in the right lateral HG), so we can speculate that high temporal and spatial resolution is mandatory for such fast and subtle early-stage processing.

Limitations

Our fMRI experiment was designed for a simple contrast analysis. Retrospectively, the stimulus onset could have been jittered in order to sample the hemodynamic response more densely. The gain in spatial and temporal resolution provided by the continuous 7T imaging strategy should be sufficient.

Our regions of interest are manually defined according to the preferred frequency gradients. As we can see in Figure 3.8.B, a third low frequency (red) cluster is found anteriorly to R. This third high-to-low frequency reversal could be the homologue of the RT areas in the monkey (Rauschecker et al., 1997). Thus, our parcellation could be more elaborated on the anterior side of HG, with three regions instead of two (M4 and L4). Alternatively,

to overcome this experimenter-related definition, we could take advantage of high resolution imaging to acquire high resolution individual R1 maps, as has been done previously at lower field strength (Dick et al., 2012; Lutti et al., 2013), though that would only help in the definition of A1 and R and still define a manual threshold as the T1 maps have slow-varying borders, much like the tonotopic maps. However, the overlap between myelin and tonotopic maps would help to consolidate region definitions.

Finally, repeated and non-repeated environmental sounds had similar spectral intensities. However, we did not control for spectral distributions of consecutive blocks. Thus, our results could also be related to sensitivity to acoustic changes instead of semantics per se (Latinus et al., 2011), although the long gap between blocks and the presence of the scanner sound makes such a history effect unlikely.

Future directions and conclusions

In this study, we considered frequency preferences and semantic processing separately. One could investigate a hypothetical link between frequency distributions and categories distributions by computing category-specific correlations. Or, otherwise, we could evaluate time courses variations related to semantic processing in different frequency bins.

Our results give some evidences for a dual semantic processing pathway in auditory belt areas. These areas could behave differently if environmental sounds are perceived at different spatial positions. One could speculate that spatial semantic processing will involve posterior-lateral belt areas in the dorsal pathway. Thus, posterior belt areas would be where ventral and dorsal pathways cross-over.

Furthermore, recent results from our lab showed attention modulation effects in primary auditory areas during pure tones processing (Da Costa et al., 2013). One could hypothesize that (1) attention could also modulate auditory belt areas during semantic processing and that (2) this effect should be different in strength than in primary auditory areas.

Finally, several cognitive processes are impaired or slowed down with age. Grady et al (2011) showed evidence for decreased adaptation effects in elderly people during sound location and identity processing with environmental sounds (Grady et al., 2011). This experiment was performed at high field. Thus, these effects could be precisely due to downregulation of posterior-medial belt areas related to aging.

References

Aeschlimann, M., Knebel, J.-F., Murray, M.M., Clarke, S., 2008. Emotional pre-eminence of human vocalizations. Brain Topogr. 20, 239 – 248.

Altmann, C.F., Bledowski, C., Wibral, M., Kaiser, J., 2007a. Processing of location and pattern changes of natural sounds in the human auditory cortex. NeuroImage 35, 1192 – 1200.

Altmann, C.F., Doehrmann, O., Kaiser, J., 2007b. Selectivity for Animal Vocalizations in the Human Auditory Cortex. Cereb. Cortex 17, 2601 – 2608.

Altmann, C.F., Júnior, C.G. de O., Heinemann, L., Kaiser, J., 2010. Processing of spectral and amplitude envelope of animal vocalizations in the human auditory cortex. Neuropsychologia 48, 2824 – 2832.

Andics, A., Gál, V., Vicsi, K., Rudas, G., Vidnyánszky, Z., 2013. FMRI repetition suppression for voices is modulated by stimulus expectations. NeuroImage 69, 277 – 283.

Angenstein, N., Brechmann, A., 2013. Division of labor between left and right human auditory cortices during the processing of intensity and duration. NeuroImage 83, 1 – 11.

Baumann, S., Griffiths, T.D., Rees, A., Hunter, D., Sun, L., Thiele, A., 2010. Characterisation of the BOLD response time course at different levels of the auditory pathway in non-human primates. NeuroImage 50, 1099 – 1108.

Baumann, S., Petkov, C.I., Griffiths, T.D., 2013. A unified framework for the organization of the primate auditory cortex. Front. Syst. Neurosci. 7, 11.

Belin, P., Zatorre, R.J., Lafaille, P., Ahad, P., Pike, B., 2000. Voice-selective areas in human auditory cortex. Nature 403, 309 – 312.

Bergerbest, D., Ghahremani, D.G., Gabrieli, J.D.E., 2004. Neural Correlates of Auditory Repetition Priming: Reduced fMRI Activation in the Auditory Cortex. J. Cogn. Neurosci. 16, 966 – 977.

Bidet-Caulet, A., Voisin, J., Bertrand, O., Fonlupt, P., 2005. Listening to a walking human activates the temporal biological motion area. NeuroImage 28, 132 – 139.

Bourquin, N.M.-P., Spierer, L., Murray, M.M., Clarke, S., 2012. Neural plasticity associated with recently versus often heard objects. NeuroImage 62, 1800 – 1806.

Bourquin, N.M.-P., Murray, M.M., Clarke, S., 2013. Location-independent and location-linked representations of sound objects. NeuroImage 73, 40 – 49.

Da Costa, S., van der Zwaag, W., Marques, J.P., Frackowiak, R.S.J., Clarke, S., Saenz, M., 2011. Human Primary Auditory Cortex Follows the Shape of Heschl's Gyrus. J. Neurosci. 31, 14067 – 14075.

Da Costa, S., van der Zwaag, W., Miller, L.M., Clarke, S., Saenz, M., 2013. Tuning In to Sound: Frequency-Selective Attentional Filter in Human Primary Auditory Cortex. J. Neurosci. 33, 1858 – 1863.

De Lucia, M., Cocchi, L., Martuzzi, R., Meuli, R.A., Clarke, S., Murray, M.M., 2010. Perceptual and semantic contributions to repetition priming of environmental sounds. Cereb. Cortex 20, 1676 – 1684.

De Lucia, M., Tzovara, A., Bernasconi, F., Spierer, L., Murray, M.M., 2012. Auditory perceptual decision-making based on semantic categorization of environmental sounds. NeuroImage 60, 1704 – 1715.

De Martino, F., Moerel, M., van de Moortele, P.-F., Ugurbil, K., Goebel, R., Yacoub, E., Formisano, E., 2013a. Spatial organization of frequency preference and selectivity in the human inferior colliculus. Nat. Commun. 4, 1386.

De Martino, F., Zimmermann, J., Muckli, L., Ugurbil, K., Yacoub, E., Goebel, R., 2013b. Cortical Depth Dependent Functional Responses in Humans at 7T: Improved Specificity with 3D GRASE. PloS One 8, e60514.

Dick, F., Tierney, A.T., Lutti, A., Josephs, O., Sereno, M.I., Weiskopf, N., 2012. In Vivo Functional and Myeloarchitectonic Mapping of Human Primary Auditory Areas. J. Neurosci. 32, 16095 – 16105.

Doehrmann, O., Naumer, M.J., Volz, S., Kaiser, J., Altmann, C.F., 2008. Probing category selectivity for environmental sounds in the human auditory brain. Neuropsychologia 46, 2776 – 2786.

Engel, L.R., Frum, C., Puce, A., Walker, N.A., Lewis, J.W., 2009. Different categories of living and non-living sound-sources activate distinct cortical networks. NeuroImage 47, 1778 – 1791.

Engel, S.A., 2012. The development and use of phase-encoded functional MRI designs. NeuroImage 62, 1195 – 1200.

Formisano, E., Kim, D.S., Di Salle, F., van de Moortele, P.F., Ugurbil, K., Goebel, R., 2003. Mirror-symmetric tonotopic maps in human primary auditory cortex. Neuron 40, 859 – 869.

Galaburda, A., Sanides, F., 1980. Cytoarchitectonic organization of the human auditory cortex. J. Comp. Neurol. 190, 597 – 610.

Goebel, R., Esposito, F., Formisano, E., 2006. Analysis of functional image analysis contest (FIAC) data with brainvoyager QX: From single-subject to cortically aligned group general linear model analysis and self-organizing group independent component analysis. Hum. Brain Mapp. 27, 392 – 401.

Grady, C.L., Charlton, R., He, Y., Alain, C., 2011. Age differences in fMRI adaptation for sound identity and location. Front. Hum. Neurosci. 5, 24.

Griffiths, T.D., Warren, J.D., 2004. What is an auditory object? Nat. Rev. Neurosci. 5, 887 – 892.

Grill-Spector, K., Kushnir, T., Edelman, S., Avidan, G., Itzchak, Y., Malach, R., 1999. Differential Processing of Objects under Various Viewing Conditions in the Human Lateral Occipital Complex. Neuron 24, 187 – 203.

Grill-Spector, K., Henson, R., Martin, A., 2006. Repetition and the brain: neural models of stimulus-specific effects. Trends Cogn. Sci. 10, 14 – 23.

Hackett, T.A., Barkat, T.R., O'Brien, B.M.J., Hensch, T.K., Polley, D.B., 2011. Linking topography to tonotopy in the mouse auditory thalamocortical circuit. J. Neurosci. Off. J. Soc. Neurosci. 31, 2983 – 2995.

Humphries, C., Liebenthal, E., Binder, J.R., 2010. Tonotopic organization of human auditory cortex. NeuroImage 50, 1202 – 1211.

Knebel, J.-F., Toepel, U., Hudry, J., le Coutre, J., Murray, M.M., 2008. Generating controlled image sets in cognitive neuroscience research. Brain Topogr. 20, 284 – 289.

Langers, D.R.M., Dijk, P. van, 2012. Mapping the Tonotopic Organization in Human Auditory Cortex with Minimally Salient Acoustic Stimulation. Cereb. Cortex 22, 2024 – 2038.

Latinus, M., Crabbe, F., Belin, P., 2011. Learning-induced changes in the cerebral processing of voice identity. Cereb. Cortex 21, 2820 – 2828.

Latinus, M., Taylor, M.J., 2012. Discriminating male and female voices: differentiating pitch and gender. Brain Topogr. 25, 194 – 204.

Leaver, A.M., Rauschecker, J.P., 2010. Cortical Representation of Natural Complex Sounds: Effects of Acoustic Features and Auditory Object Category. J. Neurosci. 30, 7604 – 7612.

Lewis, J.W., Talkington, W.J., Walker, N.A., Spirou, G.A., Jajosky, A., Frum, C., Brefczynski-Lewis, J.A., 2009. Human Cortical Organization for Processing Vocalizations Indicates Representation of Harmonic Structure as a Signal Attribute. J. Neurosci. 29, 2283 – 2296.

Lewis, J.W., Talkington, W.J., 2012. Auditory object salience: human cortical processing of non-biological action sounds and their acoustic signal attributes. Front. Syst. Neurosci. 6, 27.

Lucia, M.D., Clarke, S., Murray, M.M., 2010. A Temporal Hierarchy for Conspecific Vocalization Discrimination in Humans. J. Neurosci. 30, 11210 – 11221.

Lutti, A., Dick, F., Sereno, M.I., Weiskopf, N., 2013. Using high-resolution quantitative mapping of R1 as an index of cortical myelination. NeuroImage. Epub.

Marques, J.P., Kober, T., Krueger, G., van der Zwaag, W., Van de Moortele, P.-F., Gruetter, R., 2010. MP2RAGE, a self bias-field corrected sequence for improved segmentation and T1-mapping at high field. NeuroImage 49, 1271 – 1281.

Moerel, M., De Martino, F., Formisano, E., 2012. Processing of natural sounds in human auditory cortex: tonotopy, spectral tuning, and relation to voice sensitivity. J. Neurosci.

Off. J. Soc. Neurosci. 32, 14205 – 14216.

Moerel, M., De Martino, F., Santoro, R., Ugurbil, K., Goebel, R., Yacoub, E., Formisano, E., 2013. Processing of natural sounds: characterization of multipeak spectral tuning in human auditory cortex. J. Neurosci. Off. J. Soc. Neurosci. 33, 11888 – 11898.

Morosan, P., Rademacher, J., Schleicher, A., Amunts, K., Schormann, T., Zilles, K., 2001. Human Primary Auditory Cortex: Cytoarchitectonic Subdivisions and Mapping into a Spatial Reference System. NeuroImage 13, 684 – 701.

Murray, M.M., Camen, C., Gonzalez Andino, S.L., Bovet, P., Clarke, S., 2006. Rapid brain discrimination of sounds of objects. J. Neurosci. Off. J. Soc. Neurosci. 26, 1293 – 1302.

Murray, M.M., Camen, C., Spierer, L., Clarke, S., 2008. Plasticity in representations of environmental sounds revealed by electrical neuroimaging. NeuroImage 39, 847 – 856.

Petkov, C.I., Kayser, C., Augath, M., Logothetis, N.K., 2006. Functional Imaging Reveals Numerous Fields in the Monkey Auditory Cortex. PloS Biol 4, e215.

Rademacher, J., Morosan, P., Schormann, T., Schleicher, A., Werner, C., Freund, H.J., Zilles, K., 2001. Probabilistic mapping and volume measurement of human primary auditory cortex. NeuroImage 13, 669 – 683.

Rauschecker, J.P., Tian, B., Pons, T., Mishkin, M., 1997. Serial and parallel processing in rhesus monkey auditory cortex. J. Comp. Neurol. 382, 89 – 103.

Remedios, R., Logothetis, N.K., Kayser, C., 2009. An auditory region in the primate insular cortex responding preferentially to vocal communication sounds. J. Neurosci. Off. J. Soc. Neurosci. 29, 1034 – 1045.

Riecke, L., Walter, A., Sorger, B., Formisano, E., 2011. Tracking vocal pitch through noise: neural correlates in nonprimary auditory cortex. J. Neurosci. Off. J. Soc. Neurosci. 31, 1479 – 1488.

Rivier, F., Clarke, S., 1997. Cytochrome oxidase, acetylcholinesterase, and NADPH-diaphorase staining in human supratemporal and insular cortex: evidence for multiple auditory areas. NeuroImage 6, 288 – 304.

Saenz, M., Langers, D.R.M., 2013. Tonotopic mapping of human auditory cortex. Hear.

Res. Epub.

Schönwiesner, M., Rübsamen, R., von Cramon, D.Y., 2005. Hemispheric asymmetry for spectral and temporal processing in the human antero-lateral auditory belt cortex. Eur. J. Neurosci. 22, 1521 – 1528.

Scott, S.K., 2005. Auditory processing–speech, space and auditory objects. Curr. Opin. Neurobiol. 15, 197 – 201.

Sharda, M., Singh, N.C., 2012. Auditory perception of natural sound categories An fMRI study. Neuroscience 214, 49 – 58.

Speck, O., Stadler, J., Zaitsev, M., 2008. High resolution single-shot EPI at 7T. Magma N. Y. N 21, 73 – 86.

Staeren, N., Renvall, H., De Martino, F., Goebel, R., Formisano, E., 2009. Sound Categories Are Represented as Distributed Patterns in the Human Auditory Cortex. Curr. Biol. 19, 498 – 502.

Striem-Amit, E., Hertz, U., Amedi, A., 2011. Extensive cochleotopic mapping of human auditory cortical fields obtained with phase-encoding FMRI. PloS One 6, e17832.

Talavage, T.M., Ledden, P.J., Benson, R.R., Rosen, B.R., Melcher, J.R., 2000. Frequency-dependent responses exhibited by multiple regions in human auditory cortex. Hear. Res. 150, 225 – 244.

Talavage, T.M., Sereno, M.I., Melcher, J.R., Ledden, P.J., Rosen, B.R., Dale, A.M., 2004. Tonotopic organization in human auditory cortex revealed by progressions of frequency sensitivity. J. Neurophysiol. 91, 1282 – 1296.

Talavage, T.M., Gonzalez-Castillo, J., Scott, S.K., 2013. Auditory neuroimaging with fMRI and PET. Hear. Res. Epub.

Van der Zwaag, W., Francis, S., Head, K., Peters, A., Gowland, P., Morris, P., Bowtell, R., 2009a. fMRI at 1.5, 3 and 7 T: Characterising BOLD signal changes. NeuroImage 47, 1425 – 1434.

Van der Zwaag, W., Marques, J.P., Lei, H., Just, N., Kober, T., Gruetter, R., 2009b. Minimization of Nyquist ghosting for echo-planar imaging at ultra-high fields based on a negative readout gradient strategy. J. Magn. Reson. Imaging JMRI 30, 1171 – 1178.

Van der Zwaag, W., Gentile, G., Gruetter, R., Spierer, L., Clarke, S., 2011. Where sound position influences sound object representations: a 7-T fMRI study. NeuroImage 54, 1803 – 1811.
Viceic, D., Fornari, E., Thiran, J.-P., Maeder, P.P., Meuli, R., Adriani, M., Clarke, S., 2006. Human auditory belt areas specialized in sound recognition: a functional magnetic resonance imaging study. Neuroreport 17, 1659 – 1662.

Warren, J.D., Zielinski, B.A., Green, G.G.R., Rauschecker, J.P., Griffiths, T.D., 2002. Perception of sound-source motion by the human brain. Neuron 34, 139 – 148.

Woods, D.L., Alain, C., 2009. Functional imaging of human auditory cortex. Curr. Opin. Otolaryngol. Head Neck Surg. 17, 407 – 411.

Woods, D.L., Stecker, G.C., Rinne, T., Herron, T.J., Cate, A.D., Yund, E.W., Liao, I., Kang, X., 2009. Functional Maps of Human Auditory Cortex: Effects of Acoustic Features and Attention. PloS One 4, e5183.

Woods, D.L., Herron, T.J., Cate, A.D., Kang, X., Yund, E.W., 2011. Phonological processing in human auditory cortical fields. Front. Hum. Neurosci. 5, 42.

Yacoub, E., Shmuel, A., Logothetis, N., Ugurbil, K., 2007. Robust detection of ocular dominance columns in humans using Hahn Spin Echo BOLD functional MRI at 7 Tesla. NeuroImage 37, 1161 – 1177.

Zatorre, R.J., Belin, P., 2001. Spectral and Temporal Processing in Human Auditory Cortex. Cereb. Cortex 11, 946 – 953.

3.4 Tonotopic Gradients in Human Primary Auditory Cortex: concurring evidence from 7T and 3T fMRI

Sandra Da Costa, Melissa Saenz, Stephanie Clarke, Wietske van der Zwaag

This article is currently in preparation for submission.

Acknowledgements

This work was supported by the Swiss National Science Foundation Grant 3200030-124897 to S.C. and done in collaboration with the Centre d'Imagerie BioMédicale of the Université de Lausanne, Université de Genève, Hôpitaux Universitaires de Genève et de Lausanne, Ecole Polytechnique Fédérale de Lausanne, and the Leenaards and Louis-Jeantet Foundations. We also thank Eleonora Fornari and Giovanni Battistella for their help with the 3T acquisitions.

Abstract

Functional magnetic resonance imaging (fMRI) techniques have dramatically evolved during the past twenty years. Specifically, ultra-high magnetic fields (7T and more) and rf-coil improvements facilitated recent results in the auditory processing field such as mapping of clear tonotopic gradients in primary cortices (Da Costa et al., 2011) and in the inferior colliculus (De Martino et al., 2013). However, 7T scanners are, for the moment, not yet used for clinical diagnosis and mostly reside in external institutions, sometimes close to hospitals but not directly at patients bed. Thus, clinical functional and structural studies are mainly using hospital-based high fields systems (3T). Here, we acquired tonotopic maps in 5 subjects at 3T and 7T in order to evaluate the consistency of a tonotopic mapping paradigm between scanners. Mirror-symmetric gradients within the primary

auditory cortex were highly similar at 7T and 3T across renderings at different spatial resolutions. Thus, the tonotopic paradigm is robust and suitable for tonotopic studies, also at 3T, allowing a reliable identification of the primary auditory cortex.

Introduction

Human primary auditory cortex (PAC, Brodmanns area 41) was initially identified based on its dense cellular structure (koniocortex), myelin content, and thalamic connectivity in postmortem brains (Brodmann, 1909; Campbell, 1905; Fleschig, 1908; von Economo and Horn, 1930; von Economo and Koskinas, 1925). However, PAC is still not easily identified in the living human brain. Human PAC definition differs in size, shape and extend across studies but PAC always colocalizes with the medial two-thirds of Heschl's gyrus (HG, approximately 3 cm) in the temporal plane and is not restricted by gyral architectonic borders (Galaburda and Sanides, 1980; Morosan et al., 2001; Rademacher et al., 2001; Rivier and Clarke, 1997). HG is highly variable across individuals and hemispheres, it can be either single, partially or completely duplicated (Rademacher et al., 1993). Using functional magnetic resonance imaging (fMRI), several studies showed a common continuous mapping of preferred frequencies in monkeys (Baumann et al., 2010; Petkov et al., 2006) and in humans (Da Costa et al., 2011; Formisano et al., 2003; Humphries et al., 2010; Striem-Amit et al., 2011; Talavage et al., 2000, 2004; Woods et al., 2009), independent of gyrification. Primary subfields are organised in frequency gradients from high to low (A1) and low to high (R) frequencies, with a consistent low frequency cluster at the union of A1 and R. Another gradient from high to low frequencies (RT) appeared consistently in monkey, but less often in humans (for review see Baumann et al., 2013; Saenz and Langers, 2013; Talavage et al., 2013).

fMRI tonotopic mapping of individual relatively small human fields requires high spatial resolution which is more easily achieved at high field (Da Costa et al., 2011; De Martino et al., 2013b; Formisano et al., 2003; Moerel et al., 2012; Yacoub et al., 2007). Ultra high field scanners (7T) allow increased signal-to-noise ratio (SNR) and BOLD signal, and thus small voxel sizes. Short relaxation times reduces venous blood signal and activation signal is restricted to cortical gray matter with a benefit for spatial specificity

(van der Zwaag et al., 2009). However, among the more than 35 human 7T scanners spread around the world (Ugurbil, 2012) and used in research, only a few are available for clinical applications. Most of these infrastructures are used in research institutions far away from the patients bed and doctors office. So today lower field scanners (3T) are prominently used for patients in acute phase or with large disabilities. Several lower field imaging studies showed tonotopic maps in healthy subjects (Engelien et al., 2002; Humphries et al., 2010; Schönwiesner et al., 2002; Seifritz et al., 2006; Talavage et al., 2000, 2004; Upadhyay et al., 2007; Woods et al., 2009; Yang et al., 2000) or tinnitus patients (Langers, 2013; Langers et al., 2012). Some of these studies looked at individual data, but their broader activations were insufficient to explore tonotopic variations without smoothing (Humphries et al., 2010; Langers and Dijk, 2012; Langers, 2013; Moerel et al., 2012; Schönwiesner et al., 2002; Upadhyay et al., 2007). However, there are still open questions on primary auditory cortex plasticity which can be solved only with clinical imaging at lower fields. Here, we acquired tonotopic maps in five subjects at both 3T and 7T using an efficient travelling wave paradigm in order to evaluate the consistency of the maps between scanners.

Materials and Methods

Subjects

Five subjects (2 male, 3 female, ages 26 – 40) were scanned after providing written, informed consent. None of the subjects had hearing deficits or neurological or psychiatric illnesses. The ethics Committee of the Faculty of Biology and Medicine of the University of Lausanne approved all experimental procedures.

MRI data acquisition

Functional imaging was performed with actively shielded 7T Siemens MAGNETOM and 3T Siemens MAGNETOM TRIO whole-body scanners (Siemens Medical Solutions) located at the Centre d'Imagerie BioMédicale (CIBM) and the Centre Hospitalier Universitaire Vaudois (CHUV) in Lausanne, Switzerland.

7T data were acquired using an 8-channel head volume rf-coil (RAPID Biomedical, Germany). An EPI pulse sequence with sinusoidal read-out was used for fMRI data as described in (Da Costa et al., 2011); with the following parameters : 1.5 x 1.5 mm in-plane resolution, slice thickness = 1.5 mm, TR = 2000 ms, TE = 25 ms, flip angle = 47°, slice gap = 1.57 mm, bandwidth = 1877 Hz, matrix size = 148 x 148, field of view (FOV) 222 x 222 mm, 30 oblique slices covering the superior temporal plane, first three EPI images discarded). The use of a sinusoidal shape of the readout gradients reduces the level of acoustic noise introduced by the scanner image acquisition.

3T data were acquired using a 12-channel head volume rf-coil (RAPID Biomedical, Germany). fMRI data were acquired using the same EPI pulse sequences, using differing spatial resolution (1.8 and 2.4 mm isotropic voxels) to compensate the drop in SNR. A TR of 2000 ms, flip angle 80 and slice gap of 10% were used for both acquisitions. For the 1.8 mm isotropic data, TE = 39 ms, matrix size 108 x 108, FOV 194 x 194 mm and bandwidth 759 Hz/Px were used. 25 slices were acquired per volume to reach identical coverage to the 7T acquisition. For the 2.4 mm isotropic data, TE = 40 ms, matrix size 80 x 80, FOV 192 x 192 mm and bandwidth 762 Hz/PX were used. 19 slices were acquired per volume to reach identical coverage to the 7T acquisitions. The readout bandwidth was kept constant for the two 3T acquisitions to achieve identical acoustical noise properties in both runs.

T1-weighted high-resolution 3-D individual anatomical images were acquired for each subject and field strength using the MP2RAGE pulse sequence (7T: resolution = 1 x 1 x 1 mm, TR = 5500 ms, TE = 2.84 ms, slice gap = 1 mm, TI1 = 0 ms, TI2 = 2350 ms, matrix size = 256 x 240, field of view = 256 x 240; Marques et al., 2010; 3T: resolution = 1 x 1 x 1 mm, TR = 5000 ms, TE = 2.89 ms, slice gap = 1 mm, TI1 = 0 ms, TI2 = 1850 ms, matrix size = 256 x 240, field of view = 256 x 240).

Auditory stimuli

MATLAB (The Mathworks, R2008b) and the Psychophysics Toolbox (www.psychtoolbox.org) were used to generate sound stimuli with a sampling rate of 44.1 kHz. They

were presented to the subjects via MRI-compatible headphones (AudioSystem, Nordic-NeuroLab, same system in both scanners) with flat frequency transmission from 8 Hz to 35 kHz. Subjects were asked to keep their eyes closed during the entire experiment.

The stimulus design was built up in order to have a travelling wave of activity across the auditory cortex (Engel, 2012). Progressions of pure tones from 88 to 8000 Hz in half-octave steps (88, 125, 177, 250, 354, 500, 707, 1000, 1414, 2000, 2828, 4000, 5657, and 8000 Hz) were presented as in our previous experiment (Da Costa et al., 2011, 2013). Each progression started with pure tone bursts of the lowest frequency during 2 seconds, and then stepped to the next consecutive frequency until the highest one was reached, or, alternatively, a descending progression was used (8000 to 88 Hz). Each cycle consisted of a 28 s progression followed by a 4 s silent pause and was repeated 30 times in total (15 times per scan run). For each subject, two functional runs were acquired (one low-to-high and one high-to-low progression) at 7T (1.5 mm resolution) and four functional runs at 3T (1.8 and 2.4 mm resolution, both high to low and low to high). Results were averaged across high-to-low and low-to-high runs in the individual anatomical space. The sound system was calibrated and sound intensities were adjusted according to standard equal-loudness curves (ISO 226, phon 65, equal perceived volume across all frequencies). The scanner noise was attenuated by approximately 30 dB by the headphones and foam padding around the head. All tones were clearly perceived over the background noise by all subjects.

Analysis

Data analysis and display were done using Brain Voyager QX software v2.3 (Brain Innovation) and MATLAB. Preprocessing steps included linear trend removal, temporal high-pass filtering and motion correction. No spatial smoothing was applied. Functional time-series were registered with each subjects Talairach-normalized anatomical data and interpolated to a 1 x 1 x 1 mm^3 volumetric space. Functional-to-anatomical coregistrations were all visually verified. Anatomical images were segmented in BrainVoyager QX. Cortical surface meshes were generated and minimally inflated (100 steps) in order to facilitate the view of the temporal plane.

Voxel-by-voxel linear cross-correlations were performed individually in the volumetric space. The initial 2-seconds sound block onset within the progression was convolved with the hemodynamic response function (HRF) and shifted successively every TR to generate 14 time-lagged functions. Voxels were colour-coded according to the best fitting lag function (higher correlation value). Individual resulting maps were projected onto cortical surface meshes, without applying spatial smoothing. A tonotopic map of an exemplar control subject is displayed in Figure 3.16 with a statistical threshold of $r < 0.13$ ($p = 0.05$, uncorrected).

Primary areas definition

A cortical patch containing A1 and R was manually outlined in the partially-inflated surface meshes using drawing tools within BrainVoyager QX, as illustrated with dotted lines (Figure 3.16.B). Anterior and posterior borders were drawn along the middle of high-frequency representations, and lateral and medial borders were restricted to the medial two-thirds of HG (Rivier and Clarke, 1997; Hackett, 2011). While this is our best estimation of the expected location of PAC, the lateral border may include nonprimary belt areas. The common border between A1 and R was drawn along the low-frequency gradient (from medial to lateral). Our goal was to compare tonotopic maps at different fields and resolutions in each subject. To this end, we used the individual patch of interest defined with the 7T functional data to extract cortical surface data spanning the two primary gradients in each hemisphere of the two 3T resolutions. Each individual cortical surface ($n = 10$) was displayed with gyral borders overlaid (Figure 3.17).

Tonotopic spatial layouts

Once exported into Matlab, each vertex included in the each patch was linked to five values: the three axis coordinates (x, y, and z), a best-fitting lag value (corresponding to preferred frequency) and a curvature value. Coordinates were collapsed across the z-dimension and displayed projected onto the x-y plane. All voxels of the patch were plotted as open circles with a colour scale representing the best-fitting lag value. No statistical threshold was applied.

Frequency distribution

3D regions of interest (ROIs) were generated by projecting A1 and R cortical surfaces onto the individual 1 x 1 x 1 mm interpolated volumetric space. All voxels within the subjects ROIs were labelled according to the best-frequency map value and extracted for each hemisphere and resolutions.Tonotopic maps were quantified in percentage of best-fitting lag values per total number of voxels in each hemisphere, and plotted in bar graphs. The same colour code was used as for the tonotopic spatial layout maps.

Frequency-related time-course variations

The time courses from all voxels within the subjects ROIs were labelled according to the best-frequency map value and extracted for each hemisphere and resolutions. Once exported into Matlab, each time-course was normalized, grouped into frequency bins of same best-frequency value, and then averaged.

Results

As shown in Figure 3.16, "high-low-low-high" tonotopic gradients were clearly measured across HG in both individual hemispheres. Posterior high-to-low and anterior low-to-high gradients corresponds to human A1 and R, respectively.

The extent of the regions with significant main effect of tones differed between resolutions and field strength (at a fixed threshold of p = 0.05, uncorrected, Figure 3.16.B and 3.16.C). Regions with a significant main effect of tones were comparable for the 1.5 mm/7T acquisition (mean area RH: 1490 $mm^2 \pm 750$; mean area LH: 1035 $mm^2 \pm 379$) and the 2.4 mm/3T acquisition (mean area RH: 1771 $mm^2 \pm 287$; mean area LH: 1261 $mm^2 \pm 447$). Patch sizes for the 1.8 mm/3T acquisition (mean area RH: 661 $mm^2 \pm 293$; mean area LH: 579 $mm^2 \pm 198$) were half of either of these.

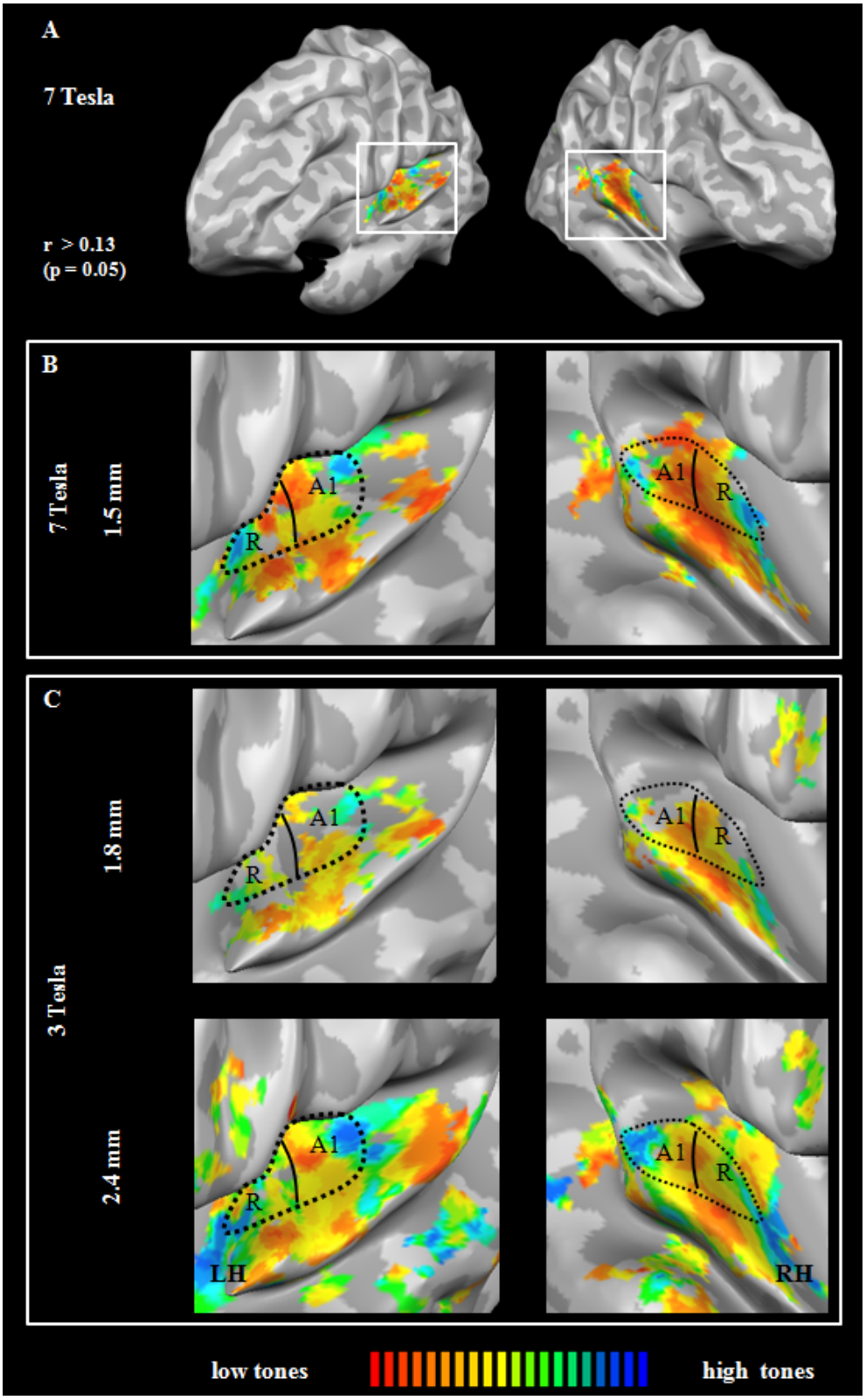
A
7 Tesla
r > 0.13
(p = 0.05)
B
7 Tesla
1.5 mm
A1
R
A1
R
C
1.8 mm
A1
R
A1
R
3 Tesla
2.4 mm
A1
R
LH
A1
R
RH
low tones
high tones

Figure 3.16: Tonotopic maps in the primary auditory cortex of subject 2. A. Color-coded tonotopic maps were projected onto each subjects cortical surface meshes (minimally inflated). Mirror-symmetric tonotopic gradients (high-to-low-low-to-high) were observed for all subjects, resolutions and field strengths. Posterior (high-to-low) and anterior (low-to-high) maps delimited A1 and R areas (dotted lines). **B-C.** Enlargement of the region delimited by the white squares. Individual tonotopic maps in the left and right hemispheres ($r > 0.13$, $p = 0.05$) at 7T **(B)** and 3T **(C)**. RH: right hemisphere; LH: left hemisphere.

Figure 3.17: Spatial layout of primary auditory areas relative to HG. Primary surface patches were selected from cortical surface meshes and plotted with HG borders (solid lines: first temporal sulcus and Heschl's sulcus) and intermediate sulcus (dashed lines) in case of partial (*) or complete duplications (**). Open circles show overlapping voxels in the collapsed z-dimension. Colour scale indicates best-fitting lag value of each point with low frequencies in red and high frequencies in blue. Gyral and sulcal borders were estimated from the curvature values and overlaid on tonotopic maps (for more details, see Da Costa et al., 2011).

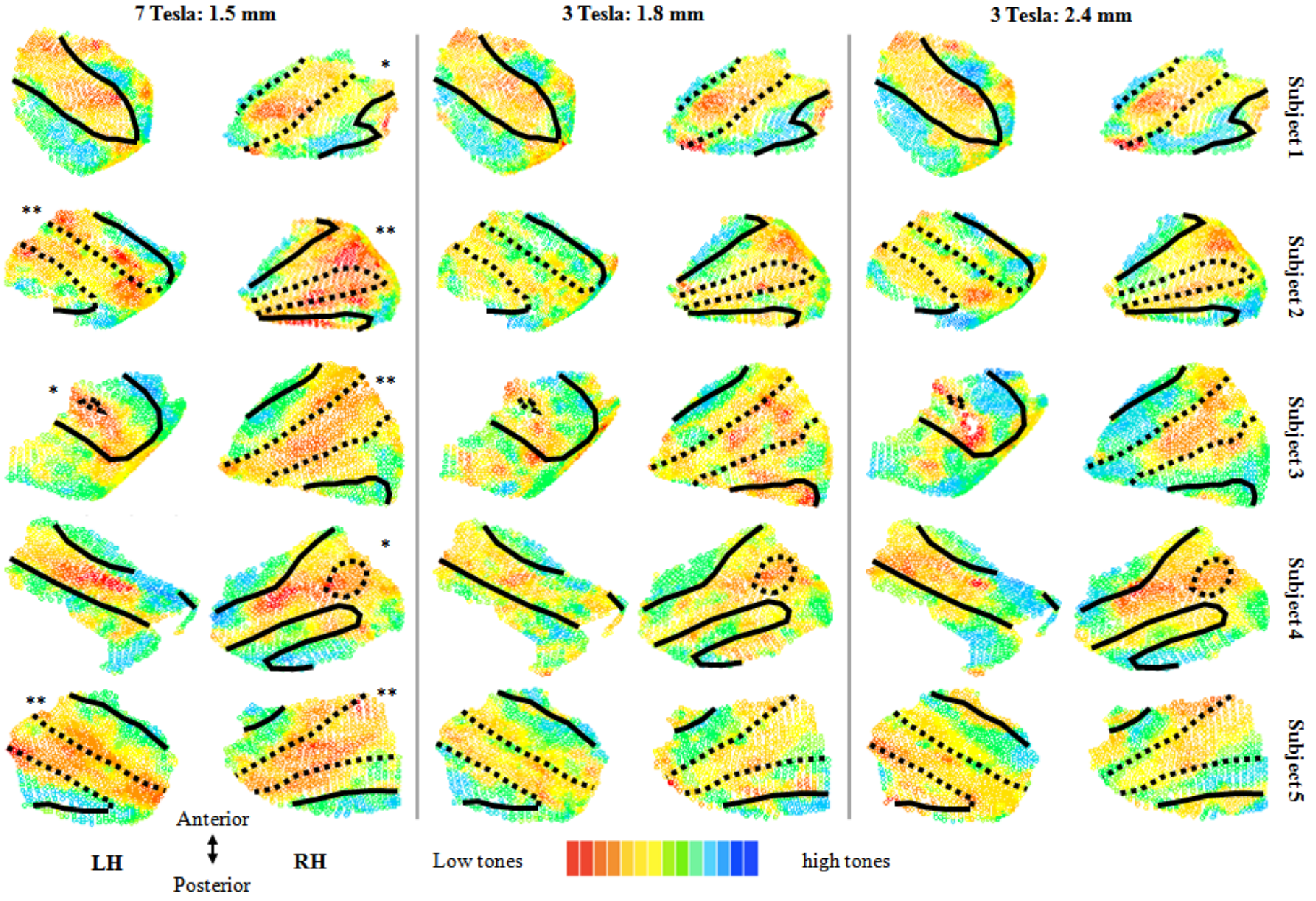
7 Tesla: 1.5 mm
3 Tesla: 1.8 mm
3 Tesla: 2.4 mm
Subject 1
Subject 2
Subject 3
Subject 4
Subject 5
*
**
*
**
*
**
*
**
Anterior
LH
RH
Posterior
Low tones
high tones

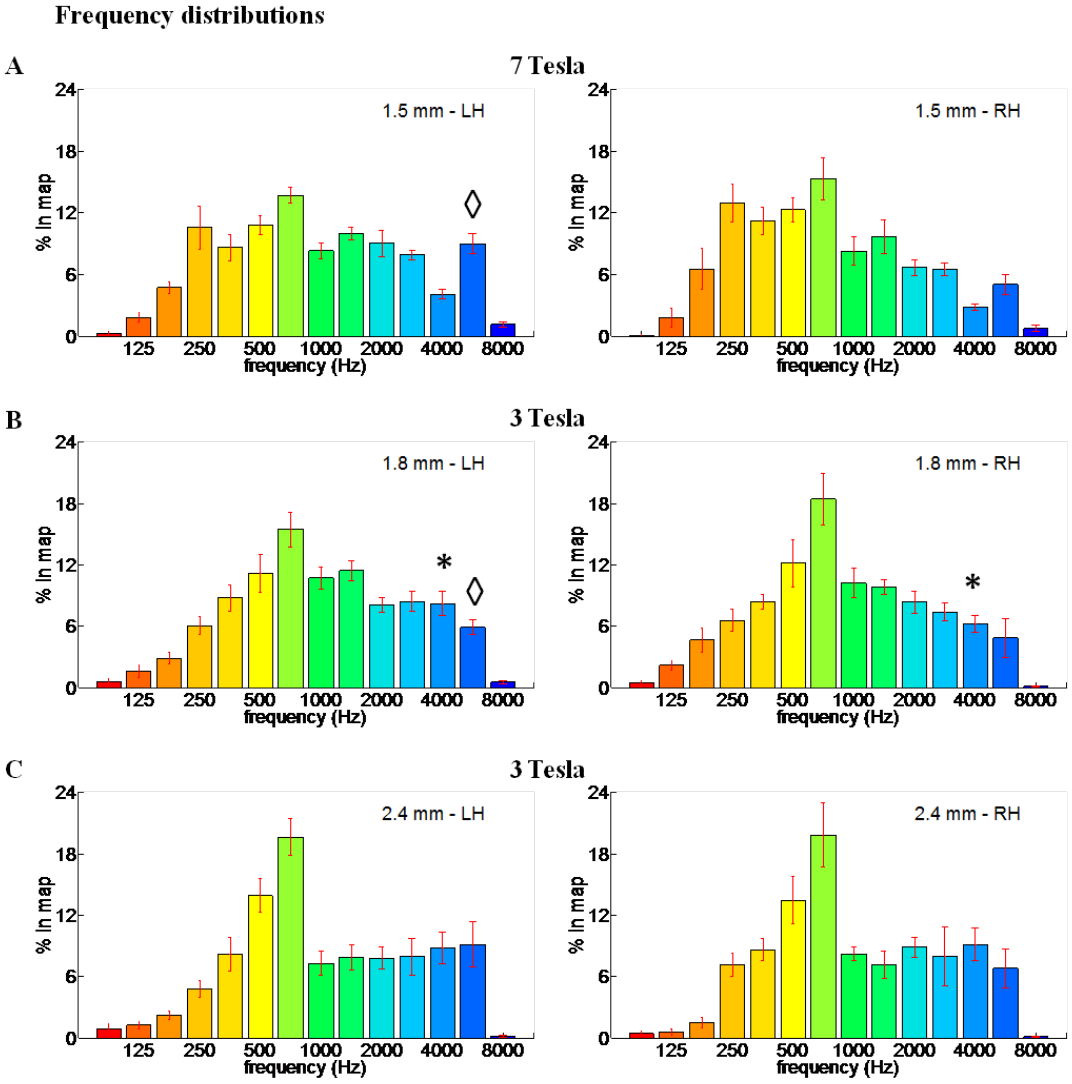

Figure 3.18: Frequency distributions in left and right hemispheres at 1.5 mm/7T (A), 1.8mm/3T (B), and 2.4mm/3T (C). Tonotopic average maps were quantified in percentages of best-fitted frequency per total number of voxels. Each bar represents the percentage of voxels dedicated to a specific frequency and error bars the standard errors across subjects and runs. Frequency distributions peak around 707 Hz in all resolutions, field strengths and hemispheres (with sharper peak at 3 than 7 Tesla). Paired t-tests between frequencies showed significant differences between hemispheres in the 1.8mm/3T maps for 4000 Hz (*, $p < 0.01$, uncorrected) and between 1.5mm/7T and 1.8mm/3T maps for 2828 Hz ($\diamond$, $p < 0.01$, uncorrected).

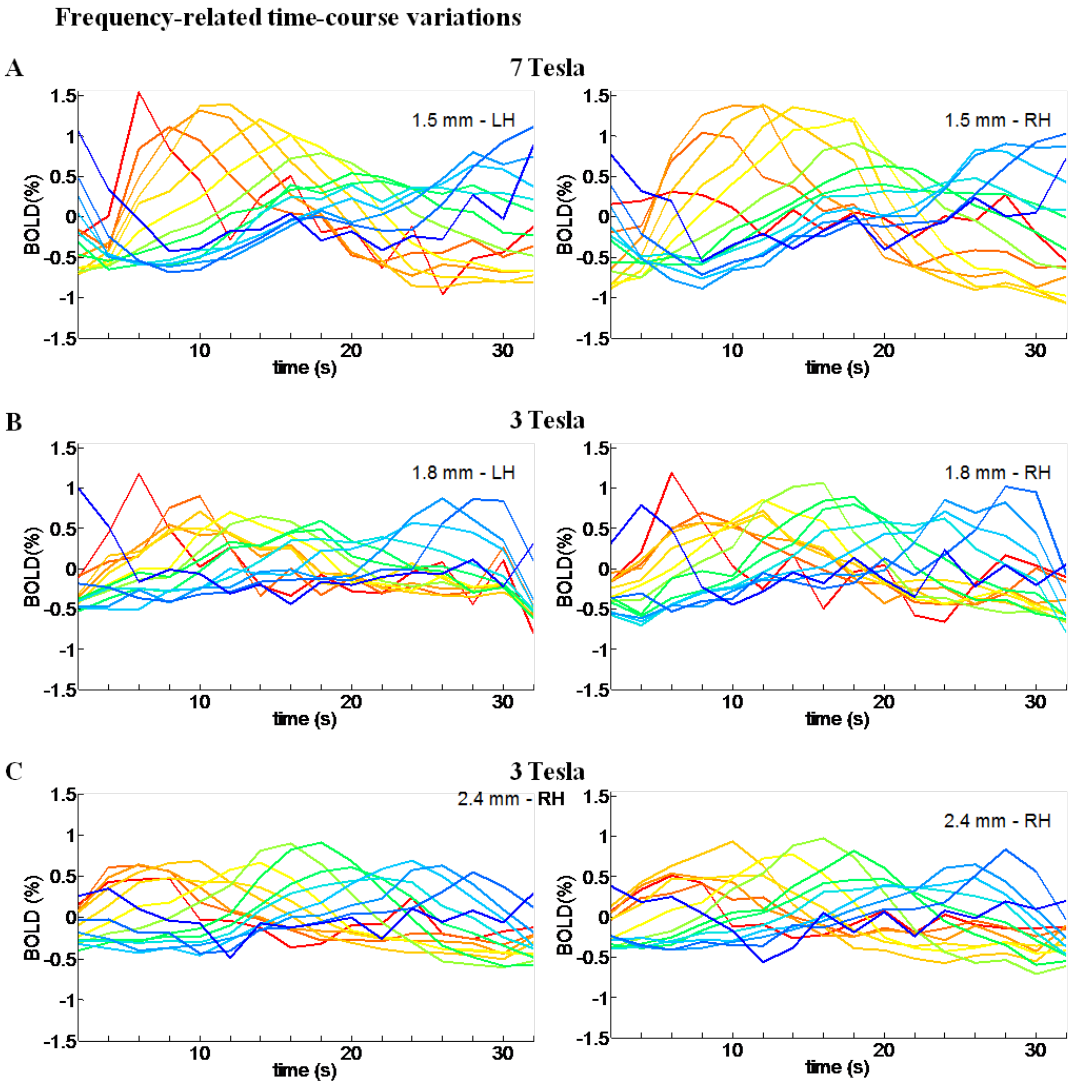

Figure 3.19: Frequency-related time course variations for the low-to-high runs averaged according to preferred frequency at 1.5 mm/7T (A), 1.8mm/3T (B), and 2.4mm/3T (C). Time courses of the low-to-high runs were extracted for each best-fitted lag value and averaged across blocks, according preferred frequency and across subjects. BOLD signal changes responses peak first for low frequencies voxels than for high frequencies, then return to baseline. The same analysis was done for the high-to-low runs with reverse pattern (figure not shown). Consistent with our design, this pattern perfectly reproduces a travelling wave of response.

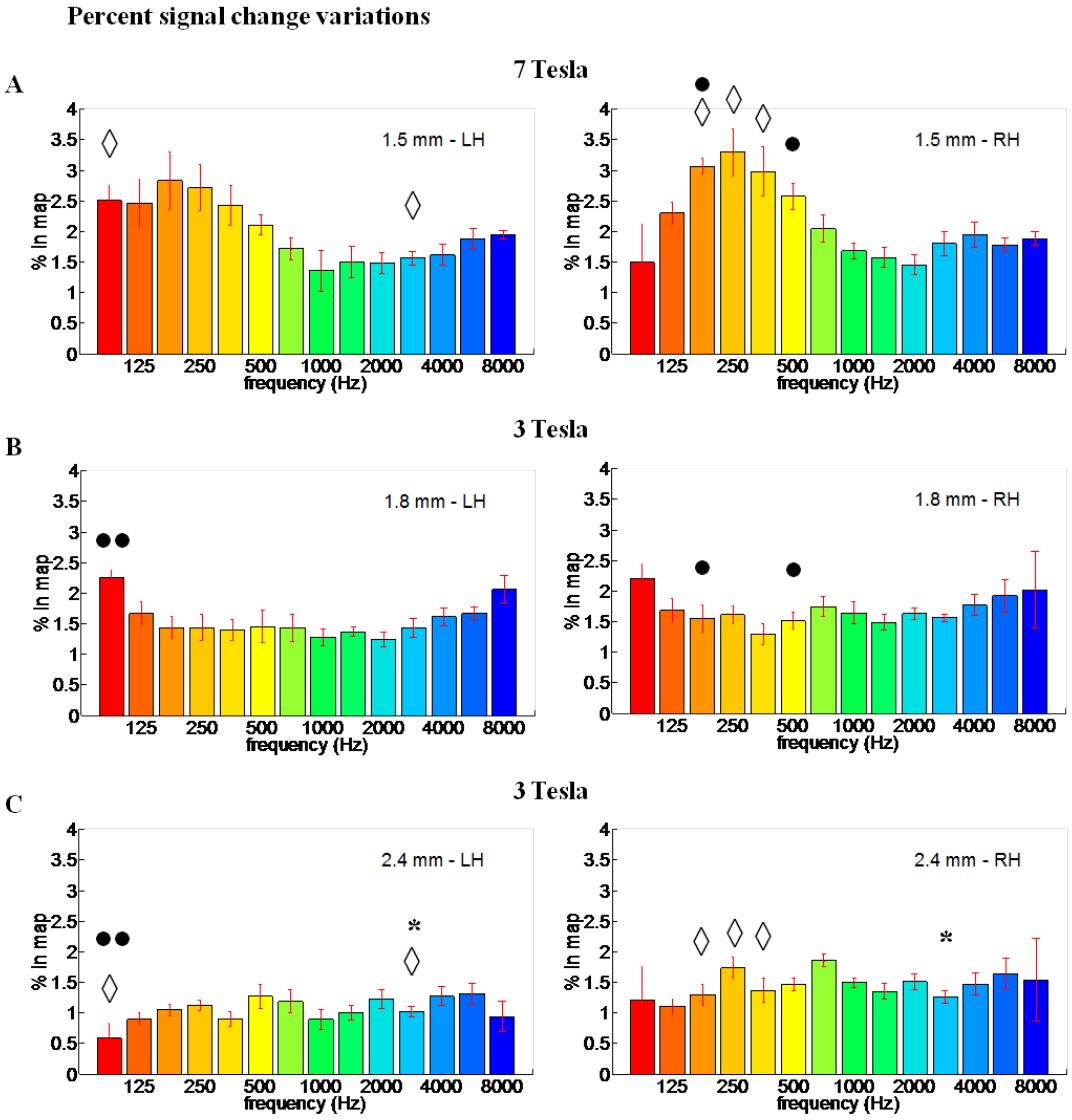

Figure 3.20: Percent signal changes variations in left and right hemisphere at 1.5 mm/7T (A), 1.8mm/3T (B), and 2.4mm/3T (C). Amplitude ratios from frequency-related time courses are displayed in percent signal changes (PSC) variations per frequency bin. A significant difference was found between hemispheres only at 2.4 mm for 2828 Hz (*, $p < 0.01$, uncorrected). Other significant differences appeared between 1.5mm/7T and 2.4mm/3T for 88 and 2828 Hz in the left hemisphere and from 177 to 354 Hz in the right hemisphere ($\diamond$, $p < 0.01$, uncorrected), between 1.5mm/7T and 1.8mm/3T only in the right hemisphere for 135 and 500 Hz($\bullet$, $p < 0.01$, uncorrected) and between 1.8mm/3T and 2.4mm/3T only in the left hemisphere for 88 Hz ($\bullet\bullet$,$p < 0.01$, uncorrected). Error bars represent standard errors across subjects.

On Heschl's gyrus, the activation pattern was highly similar between 7T and 3T acquisitions (Figure 3.17). Ordered tonotopic high-low-low-high progressions with reversal at mid-HG and clear iso-frequency stripes along the long axis of HG were apparent in all frequency maps independent of spatial resolution or field strength.

In Figure 3.18, each bar represents the percentage of voxels dedicated to a specific frequency and the error bars the standard errors across subjects. Preferred frequency distributions peaked around 707 Hz in all resolutions and field strengths (with a sharper peak at 3T than at 7T, Figure 3.18.B and 3.18.C). A frequency-by-frequency 3 x 2 (resolution x hemisphere) ANOVA on the preferred frequency distributions revealed a main effect of resolution ($p < 0.05$, uncorrected). Paired t-tests between resolutions showed significant differences in the left hemisphere 5657 Hz bin between 1.5 and 1.8 mm ($p < 0.01$, uncorrected, $\diamond$ in Figure 3.18.A and 3.18.B). Significant differences between hemispheres were found only in the 1.8mm/3T distributions for the 4000 Hz ($p < 0.01$, uncorrected, * in Figure 3.18.B).

Mean time course per frequency bin was plotted against time with the same colour code as in frequency distributions plots (Figure 3.19). Consistent with our stimulus design, frequency-related BOLD responses reproduce a travelling wave of activity along time evolution: as expected, low frequencies voxels peaked earlier than high frequencies voxels for the low-to-high runs. The opposite pattern (high first and low last) was found for the high-to-low runs (figure not shown).

Amplitude ratios between the maximum and the minimum of the frequency-related time courses were computed and plotted in bar graphs with the same colour code (Figure 3.20). Error bars represent standard errors across subjects. PSC values were overall larger at 7T than 3T, as expected (van der Zwaag et al., 2009). PSC variations changed between resolutions and scanners. BOLD signal amplitudes formed a dip near background scanner noise frequency (corresponding to the readout bandwidth and therefore acoustic signal peak of the sequence, 1877 Hz) at 7T, whereas both resolutions showed moderately flat distributions with moderate tendency of peak around 707 Hz at 3T. A longer TE was used at 3T than at 7T, as the grey matter T2* and thus optimal TE for BOLD fMRI is significantly longer at 3T. So the read-out gradients could be switched slower, moving max-

imum scanner noise contributions to approximately 750 Hz. A frequency-by-frequency 3 x 2 (Resolution x Hemisphere) ANOVA on PSC variations showed, a main effect of resolution ($p < 0.05$, uncorrected, from 88 to 500 Hz and for 2828 and 8000 Hz), a main effect of hemisphere ($p < 0.05$, uncorrected, for 707, 1000 and 2000 Hz), but no interaction Resolution x Hemisphere. Paired t-tests between resolutions showed differences for several frequency PSC variations ($p < 0.01$, uncorrected; between 1.5 and 2.4 mm in LH: $\diamond$; between 1.8 and 2.4 mm in LH: $\bullet\bullet$; between 1.5 and 2.4 mm in RH: $\diamond$; and between 1.5 and 1.8 mm in RH: $\bullet$; Figure 3.20). A frequency-by-frequency paired t-test between hemispheres showed significant difference only at 2.4 mm ($p < 0.01$, uncorrected; *). The mean of the signal variations was higher in the right hemisphere but not significant ($p > 0.05$, uncorrected; mean of 1.5 mm LH: 2.08 % $\pm$ 0.38; mean of 1.5 mm RH: 2.53 % $\pm$ 0.25; mean of 1.8 mm LH: 1.55 % $\pm$ 0.28; mean of 1.8 mm RH: 1.68 % $\pm$ 0.17; mean of 2.4 mm LH: 1.05 % $\pm$ 0.14; mean of 2.4 mm RH: 1.45 % $\pm$ 0.24). Several subjects did not have any voxels with a preferred frequency corresponding to one of the two extreme frequencies (preferring voxels for 88 Hz were found for 3/5 at 1.5 mm in RH, 5/5 at 1.5 mm in LH, 5/5 at 1.8 mm in RH, 5/5 at 1.8 mm in LH, 3/5 at 2.4 mm in RH and 3/5 at 2.4 mm in LH; preferring voxels for 8000 Hz were found for 5/5 at 1.5 mm in RH, 5/5 at 1.5 mm in LH, 4/5 at 1.8 mm in RH, 5/5 at 1.8 mm in LH, 4/5 at 2.4 mm in RH and 4/5 at 2.4 mm in LH).

Discussion

Reliable tonotopic maps of sufficient resolution to distinguish frequency bands were obtained at both 3T and 7T with the proposed 16-minute scan paradigm. 3T tonotopic maps contain enough information to be used as a valid tool for future studies aiming to understand frequency representations in auditory cortex of healthy and patient subjects, at least at the spatial resolutions available at 3T.

Tonotopic gradients within primary auditory cortex

The presence of tonotopic gradients within the primary auditory cortex is consistent with previous mappings in humans at low (Dick et al., 2012; Seifritz et al., 2006; Talavage et al., 2000, 2004; Woods et al., 2010), high (Humphries et al., 2010; Langers and

Dijk, 2012; Moerel et al., 2012; Striem-Amit et al., 2011; Yang et al., 2000) or ultra-high fields (Da Costa et al., 2011; De Martino et al., 2013; Formisano et al., 2003; Moerel et al., 2013). However, the orientation of the gradient in relation to the axis of Heschl's gyrus differed between studies. Several studies revealed mirror-symmetric gradients parallel (Formisano et al., 2003; Schönwiesner et al., 2002; Seifritz et al., 2006; Talavage et al., 2000; Yang et al., 2000), perpendicular (Humphries et al., 2010; Striem-Amit et al., 2011; Talavage et al., 2004) or oblique in respect to the long axis of Heschl's gyrus (Da Costa et al., 2011; Langers and Dijk, 2012; Moerel et al., 2013; Woods et al., 2010). Our 3T tonotopic mappings run across the Heschl's gyri with a slight angle towards the lateral side of the structure, consistent with our previous results at 7T. Overall, our results are in line with the "oblique configuration model" of primary tonotopic gradients which has been confirmed in both non-human primate and human studies (Baumann et al., 2013).

Lateralization in tonotopic gradients within primary auditory cortex

The initial goal of this study was to test if the tonotopic paradigm used at 7T (Da Costa et al., 2011) was also suitable for tonotopic studies at 3T. However, our results also allowed a comparison between right and left processing of pure tone bursts. The primary auditory cortices in the healthy subject are not expected to process pure tones differently (unlike speech sounds), and thus frequency representations and signal variations are expected to be the same between hemispheres. Our results supported this definition, we found no significant differences between hemispheres for pure tone burst processing both in the frequency distributions and signal changes.

Tonotopic gradients outside primary auditory cortex

Our results showed evidence for frequency-specific gradients beyond primary areas consistent with results from other studies (Formisano et al., 2003; Humphries et al., 2010; Moerel et al., 2012, 2013; Schönwiesner et al., 2002; Talavage et al., 2000, 2004). However, these gradients are less robust at 3T, since their signal intensity is blurred by the overall noise, reducing their small size in the case of the 1.8 mm and the fact that they are less frequency-specific per se. This could explain why results differed between studies,

in addition to others aspects such as type of acquisition and paradigms. Higher SNR and resolution imaging at 7T increase the separation between BOLD signal from primary and non-primary areas. Thus, clear tonotopic gradients outside primary auditory cortex could be measured only at 7T with a reasonable statistical threshold.

Methodological issues

The major characteristics of the tonotopic maps within primary auditory cortex remained constant over field strengths and resolutions. Small differences in tonotopic maps between different spatial resolutions and field strengths could be related to several technical features. First, we used the same audio system (AudioSystem, NordicNeuroLab) in both scanners, but not the exact same device, leading to a possibility in calibration differences between sound systems. However, sound calibration was performed the same way with both pieces of equipment and subjects confirmed a clear perception of the sounds inside both scanners. Second, 3T and 7T datasets were acquired during different sessions and with different rf-coils. Even though, there might be small positioning differences between acquisitions at different scanners, these should not lead to any systematic differences between the tonotopic maps. Third, voxel size differed between acquisitions, leading to different SNR levels and partial volume effects. While SNR values between the 1.5 and 2.4 mm datasets were roughly comparable, SNR in the 1.8 mm dataset was notably lower, resulting in a marked decrease in the patch displaying a significant result to the travelling wave paradigm. Because of lower spatial resolution attainable at 3T, partial volume effects are expected to be larger at 3T than for the 7T 1.5 mm dataset. The larger voxels (especially 2.4 mm) would be less specific than smaller ones, which could explain why 3T maps had blurred and somewhat less organised (especially at 2.4 mm) frequency distributions. The gain in signal contrast combined with small voxel size contributed to finer frequency representations (and broader frequency distributions) at 7T. Nevertheless, the 3T 1.8 mm resolution tonotopic maps within primary auditory cortices gave reliable results, equivalent to tonotopic maps acquired with smaller (1.5 mm isotropic voxels, Langers and Dijk, 2012) or larger voxels size (2 or 3 mm isotropic voxels, Humphries et al., 2010; Moerel et al., 2012; Striem-Amit et al., 2011) with longer stimulus protocols. Fourth, independent of resolution and scanner used, no spatial smoothing was applied

during preprocessing or statistical analysis. Spatial smoothing increases statistical significance, but in counterpart lowers frequency-specificity, resulting in smoother tonotopic maps with broader response functions as illustrated in Moerel et al. (2012). Their 2 mm resolution acquisitions smoothed with a 3 mm FWHM resulted in frequency-specific regions as large as in our 2.4 mm tonotopic maps, but with less robust frequency representations.

Conclusion

Overall, our data demonstrated clear tonotopic gradients within primary auditory cortex without smoothing in a 16-minute scan session at 3T as well as at 7T. Thus, this passive tonotopy protocol could be used straightforwardly used as a primary auditory cortex localizer in further studies with healthy subjects. Patients with large impairments should equally be able to perform this experiment without significant effort, opening new possibilities to study auditory plasticity in new patient populations. Non-primary tonotopic gradients were more apparent at ultra high field, suggesting that the choice of field strength used should be carefully considered depending on the question of interest for a given auditory fMRI experiment.

References

Baumann, S., Griffiths, T.D., Rees, A., Hunter, D., Sun, L., Thiele, A., 2010. Characterisation of the BOLD response time course at different levels of the auditory pathway in non-human primates. NeuroImage 50, 1099 – 1108.

Baumann, S., Petkov, C.I., Griffiths, T.D., 2013. A unified framework for the organization of the primate auditory cortex. Front. Syst. Neurosci. 7, 11.

Brodmann, K., 1909. Vergleichende Lokalisationslehre der Grosshirnrinde in ihren Prinzipien dargestellt auf Grund des Zellenbaues., Leipzig: Barth. ed.

Campbell, A.W., 1905. Histological studies on the localization of cerebral function. Cambridge: University Press.

Da Costa, S., van der Zwaag, W., Marques, J.P., Frackowiak, R.S.J., Clarke, S., Saenz, M., 2011. Human Primary Auditory Cortex Follows the Shape of Heschl's Gyrus. J. Neurosci. 31, 14067 – 14075.

Da Costa, S., van der Zwaag, W., Miller, L.M., Clarke, S., Saenz, M., 2013. Tuning In to Sound: Frequency-Selective Attentional Filter in Human Primary Auditory Cortex. J. Neurosci. 33, 1858 – 1863.

De Martino, F., Moerel, M., van de Moortele, P.-F., Ugurbil, K., Goebel, R., Yacoub, E., Formisano, E., 2013a. Spatial organization of frequency preference and selectivity in the human inferior colliculus. Nat. Commun. 4, 1386.

De Martino, F., Zimmermann, J., Muckli, L., Ugurbil, K., Yacoub, E., Goebel, R., 2013b. Cortical Depth Dependent Functional Responses in Humans at 7T: Improved Specificity with 3D GRASE. PloS One 8, e60514.

Dick, F., Tierney, A.T., Lutti, A., Josephs, O., Sereno, M.I., Weiskopf, N., 2012. In Vivo Functional and Myeloarchitectonic Mapping of Human Primary Auditory Areas. J. Neurosci. 32, 16095 – 16105.

Engel, S.A., 2012. The development and use of phase-encoded functional MRI designs. NeuroImage 62, 1195 – 1200.

Engelien, A., Yang, Y., Engelien, W., Zonana, J., Stern, E., Silbersweig, D.A., 2002. Physiological Mapping of Human Auditory Cortices with a Silent Event-Related fMRI Technique. NeuroImage 16, 944 – 953.

Fleschig, P., 1908. Bemerkungen über die Hörsphäre des menschlichen Gehirns. Neurol.Zentralbl. 27.

Formisano, E., Kim, D.S., Di Salle, F., van de Moortele, P.F., Ugurbil, K., Goebel, R., 2003. Mirror-symmetric tonotopic maps in human primary auditory cortex. Neuron 40, 859 – 869.

Galaburda, A., Sanides, F., 1980. Cytoarchitectonic organization of the human auditory cortex. J. Comp. Neurol. 190, 597 – 610.

Humphries, C., Liebenthal, E., Binder, J.R., 2010. Tonotopic organization of human auditory cortex. NeuroImage 50, 1202 – 1211.

Langers, D.R.M., de Kleine, E., van Dijk, P., 2012. Tinnitus does not require macroscopic tonotopic map reorganization. Front. Syst. Neurosci. 6, 2.

Langers, D.R.M., 2013. Assessment of tonotopically organised subdivisions in human auditory cortex using volumetric and surface-based cortical alignments. Hum. Brain Mapp. Epub.

Langers, D.R.M., Dijk, P. van, 2012. Mapping the Tonotopic Organization in Human Auditory Cortex with Minimally Salient Acoustic Stimulation. Cereb. Cortex 22, 2024 – 2038.

Marques, J.P., Kober, T., Krueger, G., van der Zwaag, W., Van de Moortele, P.-F., Gruetter, R., 2010. MP2RAGE, a self bias-field corrected sequence for improved segmentation and T1-mapping at high field. NeuroImage 49, 1271 – 1281.

Moerel, M., De Martino, F., Formisano, E., 2012. Processing of natural sounds in human auditory cortex: tonotopy, spectral tuning, and relation to voice sensitivity. J. Neurosci. Off. J. Soc. Neurosci. 32, 14205 – 14216.

Moerel, M., De Martino, F., Santoro, R., Ugurbil, K., Goebel, R., Yacoub, E., Formisano, E., 2013. Processing of natural sounds: characterization of multipeak spectral tuning in human auditory cortex. J. Neurosci. Off. J. Soc. Neurosci. 33, 11888 – 11898.

Morosan, P., Rademacher, J., Schleicher, A., Amunts, K., Schormann, T., Zilles, K., 2001. Human Primary Auditory Cortex: Cytoarchitectonic Subdivisions and Mapping into a Spatial Reference System. NeuroImage 13, 684 – 701.

Petkov, C.I., Kayser, C., Augath, M., Logothetis, N.K., 2006. Functional Imaging Reveals Numerous Fields in the Monkey Auditory Cortex. PloS Biol 4, e215.

Rademacher, J., Caviness, V.S., Steinmetz, H., Galaburda, A.M., 1993. Topographical Variation of the Human Primary Cortices: Implications for Neuroimaging, Brain Mapping, and Neurobiology. Cereb. Cortex 3, 313 – 329.

Rademacher, J., Morosan, P., Schormann, T., Schleicher, A., Werner, C., Freund, H.J., Zilles, K., 2001. Probabilistic mapping and volume measurement of human primary auditory cortex. NeuroImage 13, 669 – 683.

Rivier, F., Clarke, S., 1997. Cytochrome oxidase, acetylcholinesterase, and NADPH-diaphorase staining in human supratemporal and insular cortex: evidence for multiple

auditory areas. NeuroImage 6, 288 – 304.

Saenz, M., Langers, D.R.M., 2013. Tonotopic mapping of human auditory cortex. Hear. Res. Epub.
Schönwiesner, M., von Cramon, D.Y., Rübsamen, R., 2002. Is it tonotopy after all? NeuroImage 17, 1144 – 1161.

Seifritz, E., Di Salle, F., Esposito, F., Herdener, M., Neuhoff, J.G., Scheffler, K., 2006. Enhancing BOLD response in the auditory system by neurophysiologically tuned fMRI sequence. NeuroImage 29, 1013 – 1022.

Striem-Amit, E., Hertz, U., Amedi, A., 2011. Extensive cochleotopic mapping of human auditory cortical fields obtained with phase-encoding FMRI. PloS One 6, e17832.

Talavage, T.M., Ledden, P.J., Benson, R.R., Rosen, B.R., Melcher, J.R., 2000. Frequency-dependent responses exhibited by multiple regions in human auditory cortex. Hear. Res. 150, 225 – 244.

Talavage, T.M., Sereno, M.I., Melcher, J.R., Ledden, P.J., Rosen, B.R., Dale, A.M., 2004. Tonotopic organization in human auditory cortex revealed by progressions of frequency sensitivity. J. Neurophysiol. 91, 1282 – 1296.

Talavage, T.M., Gonzalez-Castillo, J., Scott, S.K., 2013. Auditory neuroimaging with fMRI and PET. Hear. Res.

Ugurbil, K., 2012. The road to functional imaging and ultrahigh fields. NeuroImage 62, 726 – 735.

Upadhyay, J., Ducros, M., Knaus, T.A., Lindgren, K.A., Silver, A., Tager-Flusberg, H., Kim, D.-S., 2007. Function and connectivity in human primary auditory cortex: a combined fMRI and DTI study at 3 Tesla. Cereb. Cortex 17, 2420 – 2432.

Van der Zwaag, W., Francis, S., Head, K., Peters, A., Gowland, P., Morris, P., Bowtell, R., 2009. fMRI at 1.5, 3 and 7 T: Characterising BOLD signal changes. NeuroImage 47, 1425 – 1434.

Von Economo, C., Horn, L., 1930. ber Winddungsrelief, Masse und Rindenarchitektonik der SupratemporalflŁche, ihre individuellen und ihre Seitenunterschiede. Z. Ges. Neurol. Psychiatr. 130, 678 – 757.

Von Economo, C., Koskinas, G.N., 1925. Die Cytoarchitektonik der Grosshirnrinde des erwachsenen Menschen., Berlin: Springer. ed.

Woods, D.L., Stecker, G.C., Rinne, T., Herron, T.J., Cate, A.D., Yund, E.W., Liao, I., Kang, X., 2009. Functional Maps of Human Auditory Cortex: Effects of Acoustic Features and Attention. PloS One 4, e5183.

Woods, D.L., Herron, T.J., Cate, A.D., Yund, E.W., Stecker, G.C., Rinne, T., Kang, X., 2010. Functional properties of human auditory cortical fields. Front. Syst. Neurosci. 4, 155.

Yacoub, E., Shmuel, A., Logothetis, N., Ugurbil, K., 2007. Robust detection of ocular dominance columns in humans using Hahn Spin Echo BOLD functional MRI at 7 Tesla. NeuroImage 37, 1161 – 1177.

Yang, Y., Engelien, A., Engelien, W., Xu, S., Stern, E., Silbersweig, D.A., 2000. A silent event-related functional MRI technique for brain activation studies without interference of scanner acoustic noise. Magn. Reson. Med. 43, 185 – 190.

3.5 Modulation of Tonotopic Maps by Focal Brain Lesions: case studies

Sandra Da Costa, Lea Zahnd, Wietske van der Zwaag, Reto Meuli, Melissa Saenz, Stephanie Clarke

This article is currently in preparation for submission.

Acknowledgements

This work was supported by a Swiss National Science Foundation Grant 3200030-124897 to S.C. and was done in collaboration with the Centre d'Imagerie BioMédicale of the Université de Lausanne, Université de Genève, Hôpitaux Universitaires de Genève et de Lausanne, Ecole Polytechnique Fédérale de Lausanne, and the Leenaards and Louis-Jeantet Foundations. We also thank Eleonora Fornari and Giovanni Batistella for their help during MR acquisitions and Jean-François Knebel and Laurence Liuzzi from the Neuropsychology and Neurorehabilitation Service for their advice on statistical and neuropsychological tests analysis.

Abstract

The human primary auditory cortex comprises two mirror-symmetric tonotopic representations, which are modulated by attention in normal subjects, suggesting a top-down influence on the processing within primary auditory cortex. Here, we investigated whether focal brain lesions alter tonotopic representations in the intact ipsi- and contralesional primary auditory cortex. We acquired tonotopic maps in three patients with hemispheric or cerebellar lesions, without or with auditory complaints, and compared them to a group of five healthy subjects. We found evidence for tonotopic reorganisations at the level of the primary auditory cortex in cases of brain lesions independently of auditory complaints.

Introduction

Auditory information is a key element of daily social interactions, which is processed along a complex hierarchical pathway involving the cochlear nucleus, inferior colliculus (IC), medial geniculate body of the thalamus (MGB), primary and secondary auditory areas and auditory-related high order regions (reviewed in Saenz and Langers, 2013). Thalamic-cortico and cortico-thalamic connections between the thalamus and the auditory cortex represent the shortest feedback loop of the auditory system (Suga and Ma, 2003). Brainstem nuclei are key interactions sites with other non-auditory regions such as the cerebellum or visual areas (Petacchi et al., 2011; Ramnani, 2006). Low level nuclei, primary and secondary auditory areas are organised according to frequency preferences (cochleotopy or tonotopy), reflecting, thus, a conservative relay of the auditory information from the cochlea till the auditory cortex.

The primary auditory cortex (PAC) itself is functionally defined according to frequency preferences – tonotopic representations – within the medial two-thirds of the Heschl's gyrus (HG), and has been mapped in vivo at ultra-high (Da Costa et al., 2011; De Martino et al., 2013; Formisano et al., 2003) and lower ($<$ 7 T) fields (Da Costa et al., in prep; Humphries et al., 2010; Langers and Dijk, 2012; Moerel et al., 2012; Schönwiesner et al., 2002; Seifritz et al., 2006; Striem-Amit et al., 2011; Talavage et al., 2000, 2004; Woods et al., 2010). The primary mirror-symmetric gradients are robustly mapped despite differences in scanner field strength (Da Costa et al., in prep) and HG configurations (Da Costa et al., 2011).

The tonotopic organisation of PAC can change during lifetime, both through ascending and descending plasticity. Ascending plasticity is related, for example, to auditory experience (Kilgard and Merzenich, 2002; Kilgard et al., 2001; Moore and Gockel, 2011; Pandya et al., 2005; Recanzone et al., 1993; Suga and Ma, 2003; Weinberger, 2004), cochlear lesions (Gu et al., 2012; Irvine, 2007; Moore and Shannon, 2009), tinnitus or hyperacusis (Gu et al., 2010; Langers and Dijk, 2012; Langers et al., 2012; Langers, 2013). Deactivation of primary auditory cortex showed descending-related response modulations in the MGB (Antunes and Malmierca, 2011; Suga and Ma, 2003; Tang et al., 2012), IC (Nakamoto et al., 2008, 2010; Salvi et al., 2000), secondary regions (Carrasco and

Lomber, 2013; Carrasco et al., 2013), and contralateral primary areas (Carrasco et al., 2013).

A general model for cortical plasticity implied that map reorganisations depend on the balance between excitatory and inhibitory inputs at a synaptic level (Buonomano and Merzenich, 1998; Irvine, 2007; Weinberger, 1995, 2004). Thus, a deprived area can become sensitive to sensory inputs from surrounding areas, to which it was irresponsive before the lesion. Human lesions studies showed some evidences for plasticity of auditory networks, such as loss of parallel processing (Adriani et al., 2003a, 2003b) or ipsi- and contralateral reorganisations of specialized networks (Alain et al., 2005; Lazard et al., 2013; Saur et al., 2006; Scheffler et al., 1998; Schofield et al., 2012). Thus, tonotopic plasticity is probably also influenced by postlesional reorganisation occurring after focal ischemic lesions, although this has never been considered in human.

Here, we investigated whether focal brain lesions alter tonotopic representations in the intact primary auditory cortices. We acquired tonotopic maps in three patients with brain or cerebellar lesions with or without auditory complaints and compared them to a group of five healthy subjects. We hypothesised that tonotopic maps are influenced by plastic reorganisation due to brain lesions, but not necessarily correlated with auditory deficits.

Materials and Methods

Patients and control subjects

Five healthy volunteers (3 women, 2 men; age 24 – 39) with no history of neurological or auditory problems and three patients (2 women, 1 man; age 19 – 52) from the Service of neuropsychology and neurorehabilitation of the CHUV participated in the experiment after oral explanation and provision of written informed consent as approved by the Ethics Committee of the Faculty of Biology and Medicine of the University of Lausanne.

Patient 1

Patient 1, student, suffered a cerebellar haemorrhage in the right superior vermis (Table 3.4 and Figure 3.21, P1) from an arteriovenous malformation. Detailed neuropsychological examination revealed mild difficulties in executive attentional functions and mnesic fatigue. The patient reported changes in behaviour after injury, predominantly difficulties in playing piano or listening to music. She complained about sound perception deficits such as different perception between left and right ears. These complaints were certified later during the audiometry test (Figure 3.22, done one year after injury) where low frequencies (125, 250, and 1000 Hz) were louder in the right ear and high frequencies (4000 Hz) were louder in the left ear. She also showed location deficits for the 1000 Hz. In overall, she showed incoherence between sounds presented to the right ear. Tonotopic data was acquired 13 months after injury.

Patient 2

Patient 2, specialized teacher, suffered a traumatic brain injury (TBI) after falling from a ladder. A CT-scan after injury revealed a subdural hematoma in right frontoparietal cortex and in left temporal cortex (Table 3.4). Only the latter was apparent on the anatomical data acquired on her (Figure 3.22, P2). A detailed neuropsychological examination after injury revealed difficulties in attentional functions. Four months after injury, her performances were retested and returned to norm but with some tiredness (Table 3.4). However, she complained about difficulties during social interactions and sound localization, but also sounds intolerance and sensation of blocked ears. An audiometry test revealed normal hearing. Tonotopic data was acquired 6 months after injury.

Patient 3

Patient 3, salesman, suffered a stroke in the right fronto-operculum (Table 3.4 and Figure 3.21, P3) with left facio-brachio-crural hemisyndrome and right hemineglect. A detailed neuropsychological examination revealed a mild impairment in executive attentional functions and working memory as well as fatigue. The audiometry test in this patient was normal (Figure 3.22). Tonotopic data was acquired 19 months after injury.

	Patient 1	**Patient 2**	**Patient 3**
Sex	female	female	male
Age	19 years	42 years	52 years
Etiology	haemorrhage	traumatic brain injury	stroke
Delay since injury	13 months	6 months	19 months
Lesion Site	right cerebellum (sup. vermis)	left STG	right fronto-operculum
HG variants (RH/LH)	CD / CD	CD / CD	PD / CD
Auditory complaints	yes	yes	–
Musical experience	14 years (piano)	–	–
Neuropsychological assessments			
Language	N	N	N
Praxias	N	N	N
Gnosias	N	N	N
Memory	sD (anterograde memory)	N	sD
Executive functions	sD (verbal fluency)	N	sD
Attention	sD	mD (auditory)	mD

Table 3.3: Patients carachetistics. STG: superior temporal gyrus; HG: Heschl's gyrus; CD: complete duplication; PD: partial duplication ; N: with normal limits; mD: mild deficits ; sD : severe deficits. We reported here only brain damages noticed on anatomical scans.

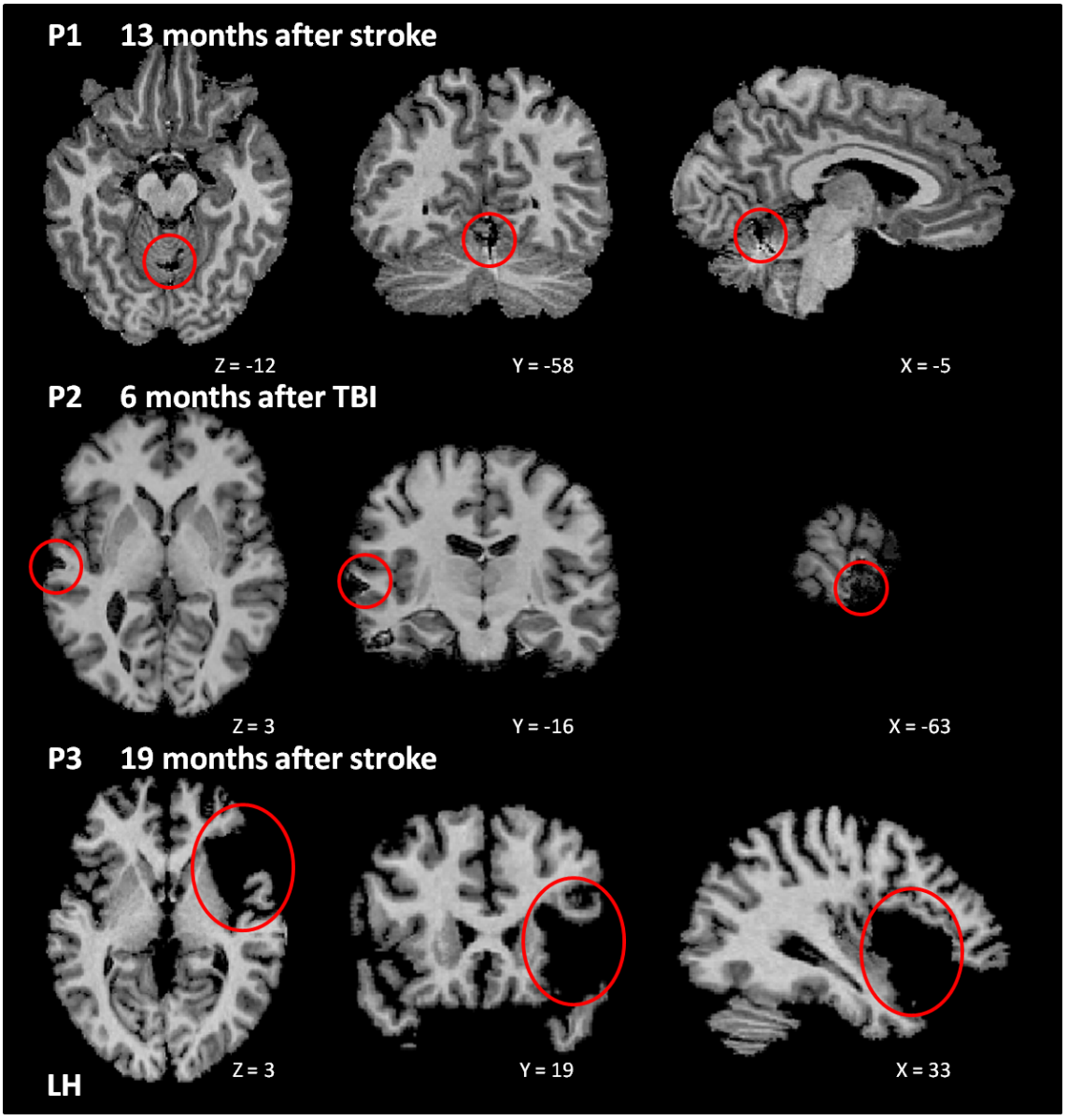

Figure 3.21: Lesions shown at the site of their greatest extent. Anatomical images were transformed into Talairach space.

MRI data acquisition

Imaging sessions of 30 minutes were performed with an actively shielded 3 Tesla Siemens MAGNETOM TRIO whole-body scanners (Siemens Medical Solutions) located

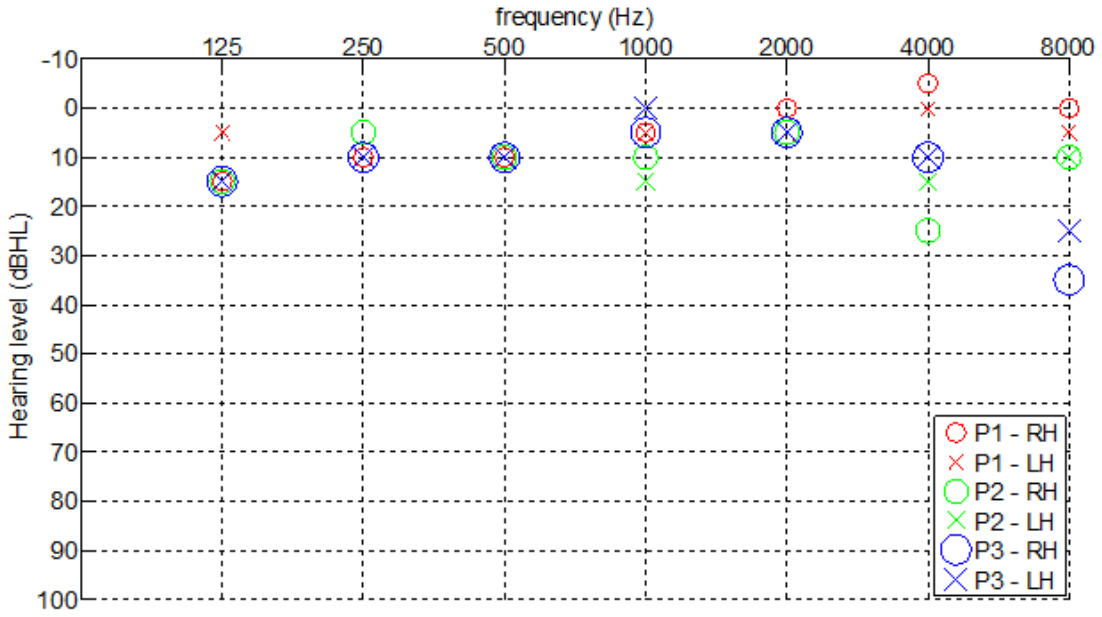

Figure 3.22: Pure tone audiometry. Results of Patient 1 (P1), Patient 2 (P2) and Patient 3 (P3) are represented in red, green and blue, respectively.

at the Centre d'Imagerie BioMédicale (CIBM) in the Centre Hospitalier Universitaire Vaudois (CHUV) in Lausanne, Switzerland.

Two functional datasets were acquired using a 12-channel head volume rf-coil (RAPID Biomedical, Germany) and an EPI pulse sequence (1.8 x 1.8 mm in-plane resolution, slice thickness = 1.8 mm, TR = 2000 ms, TE = 39 ms, flip angle = 80°, slice gap of 10%, matrix size 108 x 108, field of view 194 x 194 mm, bandwidth of 759 Hz/PX, 25 slices parallel to the Sylvian fissure). Anatomical T1-weighted high-resolution images were acquired for each subject using the MP2RAGE pulse sequence (resolution = 1 x 1 x 1 mm, TR = 5000 ms, TE = 2.89 ms, TI1 = 1800 ms, TI2 = 0 ms, slice gap = 1 mm, matrix size = 256 x 240, field of view = 256 x 240; Marques et al., 2010).

Auditory stimuli

MATLAB (The Mathworks, R2008b) and the Psychophysics Toolbox (www.psych-

toolbox.org) were used to generate sounds stimuli (44.1 kHz, 16 bits), which were delivered via MRI-compatible headphones (AudioSystem, NordicNeuroLab) featuring flat frequency transmission from 8 Hz to 35 kHz. Subjects had eyes closed during the entire scan session.

Our tonotopy fMRI paradigm was set up so as to create a travelling wave of BOLD responses through primary auditory cortex (Engel, 2012). For that, we used progressions of pure tones (88 to 8000 Hz, in half-octave steps), presented as described previously (Da Costa et al., 2011, Da Costa et al. in prep). Progressions lasted 28 s and started with a 2 s block of pure tone bursts of the lowest (or highest) frequency and consecutively stepped forward until the last, highest, (or lowest) frequency. In between progressions, a 4 s silent pause was presented and this 32 s cycle was presented 15 times per scan session (8 min each). Both healthy subjects and patients performed two scan sessions (one crescendo and decrescendo progression). Resulting individual maps of the two runs were averaged across high-to-low and low-to-high runs.

The sound intensities were adjusted to equal perceived loudness across all frequencies (ISO 226, phon 65) and matched the perceived volume of a 1000 Hz reference frequency at 65 dB. The scanner noise was attenuated by approximately 30 dB by the headphones, earplugs and foam padding around subjects head. All healthy subjects and patients reported clear and comfortable perception of all tones despite background scanner noise.

Analysis

Data display and analysis were performed with Brain Voyager QX software v2.3 (Brain Innovation) and MATLAB. Linear tread removal, temporal high-pass filtering, and motion correction was applied during the preprocessing. We did not use spatial smoothing. Time-series of the functional data were registered to individual anatomical data in the Talairach space and interpolated to a 1 x 1 x 1 mm^3 volumetric space. Verification of functional-to-anatomical registrations was done visually. Anatomical images were used to generate cortical surface meshes (one for each hemisphere) with automated segmentation tools in BrainVoyager QX. Resulting meshes were slightly inflated (100 steps, with

minimal amount of spatial distortions) in order to improve visibility of the temporal plane.

Linear cross-correlation analyses were performed for each subject in the volumetric space. A cyclical model function was designed based on the first 2 s frequency onset of each cycle and convolved with a canonical hemodynamic function. This model function was shifted every TR (2 s) in order to generate consecutive 14 time-lagged functions. Voxel-by-voxel linear cross-correlations were computed between the 14 cyclical model functions and the measured time-courses of 240 volumes. Using a winner-take-all approach, each voxel was colour-coded according to its highest correlation value (best-fitting lag value). Individual resulting correlations maps were projected onto individual partially-inflated surface meshes without any spatial smoothing. Individual correlation maps of an exemplar healthy subject and the patients are displayed in Figure 3.23 with a statistical threshold $p \leq 0.05$.

Primary regions definition

In each healthy subject and patient hemisphere, we manually defined a contiguous cortical surface including primary regions, A1 and R, using BrainVoyager QX drawing tools (dashed lines in Figure 3.23). The exact borders were independent of the statistical threshold. Anterior and posterior borders were delimited by the middle of high-frequency representations, and lateral and medial borders by the medial two-thirds of HG (in agreement with human architectonics: Hackett et al., 2011; Rivier and Clarke, 1997). The union border between A1 and R was delimited across the low-frequency representation. Tonotopic regions surrounding the patch of interest probably include non-primary belt regions.

Our goal was to compare ipsi- and contralateral tonotopic maps in patients and in healthy subjects. To this end, we manually selected patches of cortical surfaces containing the two primary gradients in each preserved and damaged hemisphere (n = 6), and plotted them with gyral borders overlaid (Figures 3.24, for borders definition see Da Costa et al., 2011).

Tonotopic spatial layouts

Data from the cortical patches was exported into Matlab with coordinates (x, y, z), a best-fitting lag value (1 to 14), and a curvature value for each vertex. Open circles in Figure 3.24 show overlapped voxels collapsed in the z-dimension and plotted onto the x-y plane without any statistical threshold. Each voxel was colour-coded according its best-fitting lag value.

Frequency distributions

Primary auditory cortical surfaces were projected into individual 1 x 1 x 1 mm Talairach space in order to generate 3D regions of interest (ROIs) and a best-frequency value was ascribed to each voxel. Number of voxels attributed to a given frequency band was plotted as red, green and blue lines for each patient and in black for the control group average. Then, we computed the difference between the frequency distributions for each patient and the controls average (Patient - Controls) and plotted the resulting ratio in bar graphs with the same colour-code as used the in spatial layouts in Figure 3.24.

Percent signal change variations

Time courses within the individual ROIs were extracted into Matlab, normalized, and grouped according the best-frequency values. Resulting BOLD signal changes were then averaged across blocks. Amplitude ratios between the maximum and the minimum values were computed and plotted as red, green and blue lines for each patient and in black for the control group average. As for the frequency distributions, we computed the difference between the PSC variations for each patient and the controls average (Patient - Controls) and plotted the resulting ratio in bar graphs with again the same colour coding as in Figure 3.24 and 3.25.

Results

Tonotopic subfields

On visual inspection, all patients had orderly tonotopic representations within both primary auditory cortices, including mirror-symmetric "high-low-low-high" gradients (Figures 3.23 and 3.24, in an exemplar subject and the three patients). Tonotopic maps were not comparable at identical statistical threshold as Patient 2 and 3 maps included only low-frequency representations at p = 0.05 ($r > 0.13$). Thus, statistical thresholds were set a p = 0.05 ($r > 0.13$) for Patient 1 and $p < 0.05$ ($r > 0.11$) for Patient 2 and 3 to obtain patches of approximately equal spatial extent, including the high-frequency representations. For Patient 1 and 2, the tonotopic organisation was less clear in the left than in the right hemisphere, whereas for Patient 3, tonotopic organisation was clearer in the left hemisphere. Thus, frequency representations contralateral to the cerebellar lesion and ipsilateral to brain lesions were less frequency-specific than those found in the opposite hemisphere.

Relative representations of frequencies within primary auditory cortices

Frequency distributions of the control group (n = 5) followed normal distribution with a peak around 500 Hz in both hemispheres (Figure 3.25.A). Individual distributions in patients tended to be flatter and to peak at different frequencies than control subjects. The frequency distributions from all patients peaked at 707 Hz, with a second peak for Patient 2 at 250 Hz. Paired t-tests revealed no significant left-right difference in any of the controls subjects and patients frequency distributions. Paired t-tests between control group and individual patients frequency distributions showed differences in frequency representations for all patients (* in Figure 3.25.B; paired t-tests, $p < 0.05$ Bonferroni corrected; Patient 1 LH: no significant differences; Patient 1 RH: 8000 Hz; Patient 2 LH: 177 and 250 Hz; Patient 2 RH: 250 Hz; Patient 3 LH: 177, 250 and 8000 Hz; Patient 3 RH: 250, 500 and 8000 Hz).

Relative signal variations within primary auditory cortices

Group averaged percent signal changes variations of the controls showed a pseudo-flat distribution across frequency bins with no differences from the mean (mean signal variation in primary auditory cortex across time and frequency, p = 1; Table 3.4 and Figure 3.26.A). PSC variations in Patient 1 peaked at 1414 Hz contralateral to the lesion. Mean PSC across frequencies were comparable between hemispheres, but different between controls and patients (Table 3.4). Paired t-tests between patients and controls PSC variations showed significant differences in frequency signals in Patient 1 and Patient 2 (* in Figure 3.26.B; paired t-tests, $p < 0.05$ Bonferroni corrected; Patient 1 LH: 88, 1000, 1414 and 8000 Hz; Patient 1 RH: 2828 and 4000 Hz; Patient 2 LH: 250 and 2828 Hz; Patient 2 RH: 88 and 8000 Hz), but not in Patient 3. Only signals for 1000 and 1414 Hz were significantly higher in patients compared to controls ($p < 0.05$, Bonferroni corrected), other significant PSC variations were in favour of the controls (Figure 3.26).

	Average controls	**Patient 1**	**Patient 2**	**Patient 3**
Right hemisphere	$1.68\% \pm 0.17$	$1.22\% \pm 0.40$	$1.09\% \pm 0.51$	$1.29\% \pm 0.35$
Left hemisphere	$1.55\% \pm 0.28$	$1.29\% \pm 0.77$	$1.13\% \pm 0.40$	$1.22\% \pm 0.33$

Table 3.4: Mean percent signal variation across time and frequencies in controls and patients. Mean % $\pm$ std.

Discussion

Our goal was to investigate tonotopic gradients within primary auditory cortex in brain damaged patients with/without auditory complaints. Our results revealed maintained tonotopic gradients in ipsi- and contralesional hemispheres, despite partial alteration of the relative frequency representations. Low frequencies tended to be more represented in primary auditory cortices both ipsi- and contralateral to the lesion. Percent BOLD signal changes for frequencies around 1000 Hz were enhanced contralaterally to cerebellar lesion and decreased ipsilaterally to hemispheric lesions.

Tonotopic gradients are maintained by neural wiring

Acoustic information is initially decomposed and mapped at lower auditory nuclei, such as medial geniculate body of the thalamus (MGB), inferior colliculus, superior olivary complex and cochlear nuclei, according to temporal and spectral features before reaching primary and secondary auditory areas. Feature-selective hierarchical coding is preserved by vertical ascending thalamo-cortical and horizontal cortico-cortical connections all along the auditory pathway in healthy subjects. Neurons of ventral and dorsolateral MGB project to relays in layers IV/IIIb, and I/III/IV of primary and secondary auditory areas, respectively (for review, see Brugge, 2013). From primary and secondary areas, the acoustic information flow is spread to auditory-related regions via horizontal connections (Brugge et al., 2003; Liegeois-Chauvel et al., 1991). In this study, patients had no injury in areas implicated in the auditory pathway. Our results gave evidence that, despite plastic changes in the remaining cortex due to local brain injury (see below), frequency representations in patient primary auditory cortex are maintained by strong intact hierarchical connections. Although, there is also evidence for adult auditory plasticity in human and animal models (Buonomano and Merzenich, 1998; Irvine, 2007; Weinberger, 1995, 2004) that may account for more specific representation modifications.

Tonotopic maps are modulated by diaschisis-like neural plasticity

After a stroke event, imaging techniques, such as PET of MRI, measured a reduced metabolism or cerebral blood flow in a region connected to the injured area, due to loss of

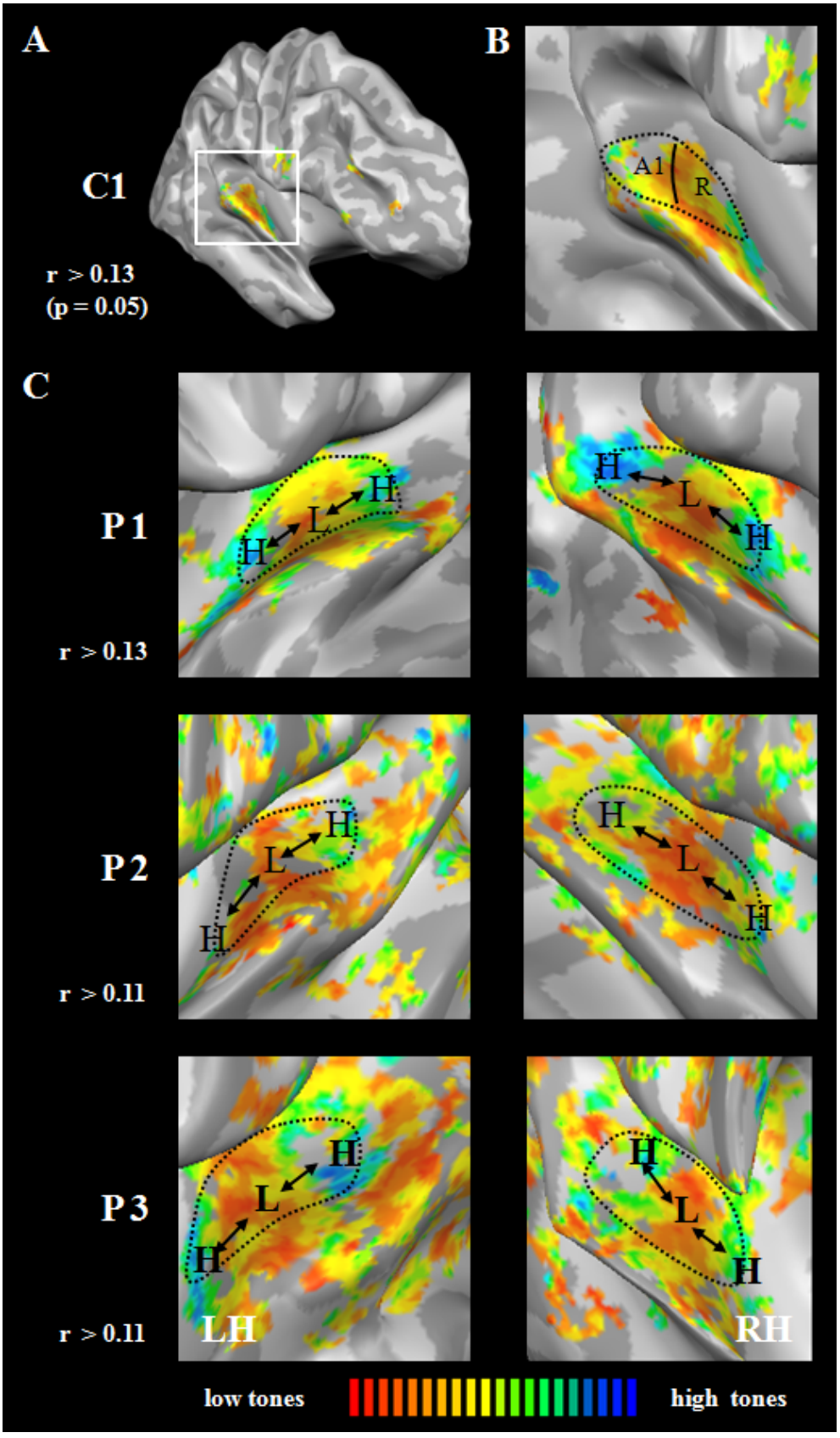
A
B
C1
r > 0.13
(p = 0.05)
A1
R
C
P1
r > 0.13
P2
r > 0.11
P3
r > 0.11
H
L
LH
RH
low tones
high tones

Figure 3.23: Tonotopic maps within the primary auditory cortex. A. Inflated right hemisphere with typical mirror-symmetric gradients "high-low-low-high" of a healthy subject (C1) at 3 Tesla. **B.** Enlargement of the region within the white box. **C – E.** Patients tonotopic maps in both hemispheres. Statistical thresholds were set at $p \leq 0.05$ in order to cover progression gradients in all subjects. Dashed lines delimited the primary areas A1 and R. C1: healthy control; P1: Patient 1; P2: Patient 2; P3: Patient 3; H: clusters preferring high frequencies; L: clusters preferring low frequencies; LH: left hemisphere; RH: right hemisphere.

excitatory inputs in the latter and increased inhibition in the former region. This phenomenon is called diaschisis and is related to changes in cortico-cerebellar, thalamocortical intra- and interhemispheric connectivity (Engelhardt and Gomes, 2013) and regulation mechanisms of inhibitory and excitatory receptors, $GABA_A$ and NMDA, respectively. Neurons surrounding focal lesions became more excitable because of an imbalance between NMDA upregulation and $GABA_A$ downregution (Gaucher et al., 2013; Sacco et al., 2009; Schiene et al., 1996). These inhibition downregulation effects could explain a general signal changes reduction in both hemispheres for all patients.

BOLD signal intensities within primary auditory areas were generally higher in patients than in controls, which is in agreement with findings on hyperacusis patients with higher activation in primary auditory cortex than subjects with normal hearing. Sound-related activations increases with decreasing sound-level tolerance (Gu et al., 2010). However, another auditory paradigm (such as environmental sounds against scanner noise) should be used to test whether BOLD signal increase is related to the frequency preferences per se or to general higher BOLD responses independent of the stimuli used. Moreover, sound-level tolerance was correlated to activation in the inferior colliculus and medial geniculate body of the thalamus. But theses signal increases could also be related to attentional effects as demonstrated in selective auditory experiments (Da Costa et al., 2013; Paltoglou et al., 2011; Rinne et al., 2007, 2008). Thus, hyperactivity in primary auditory cortex might be due to auditory aversive conditioning, which reinforces aberrant auditory activity (Gu et al., 2010). Gu et al. (2010) also found correlations between anterolateral areas (anterolateral HG and ALA) and sound-level tolerance. This would explain auditory complaints for Patient 2 but not necessarily for Patient 1. Animal and patient studies (Gu et al., 2010; Salvi et al., 2000) proposed that the response elevation might be related to an

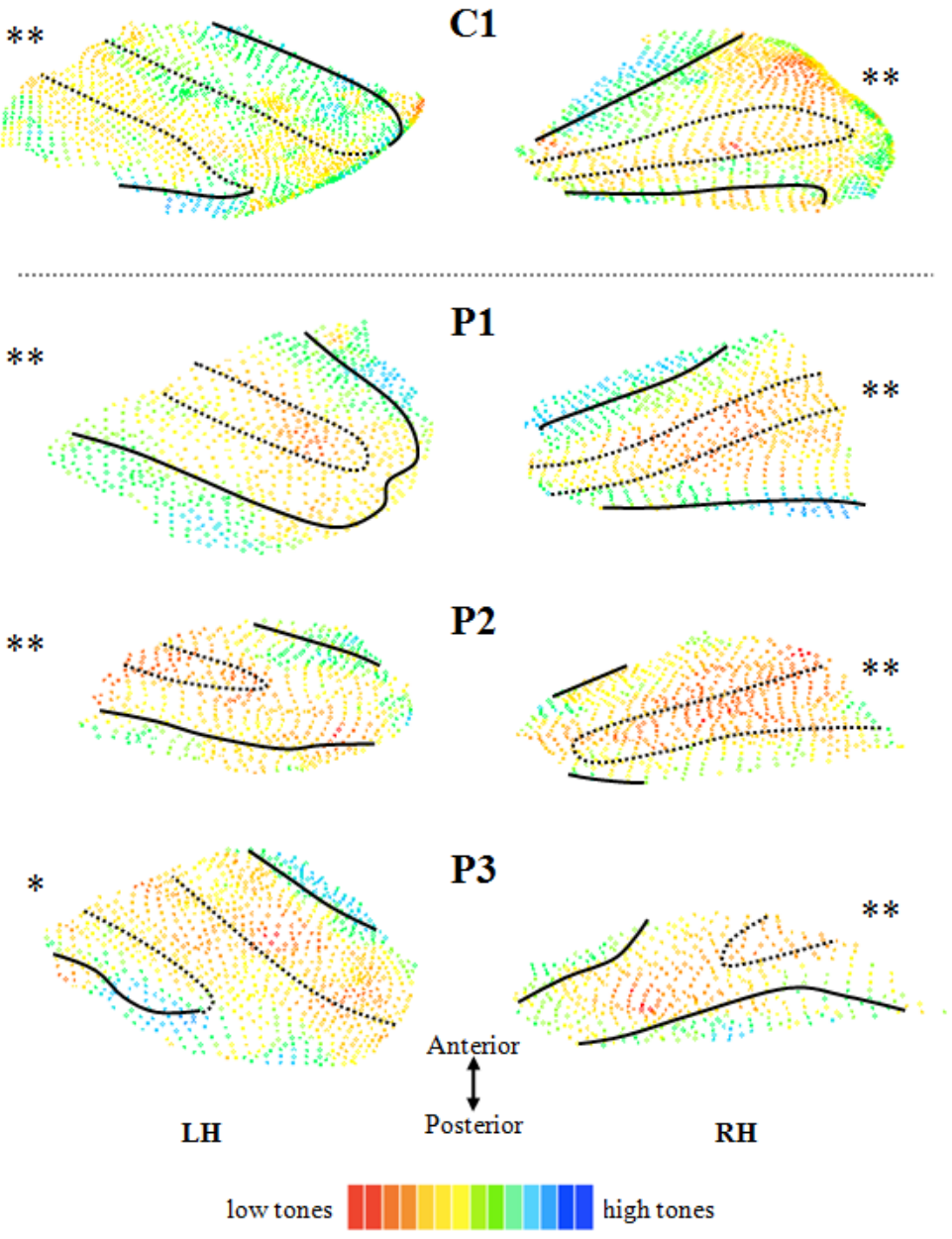

Figure 3.24: Primary auditory areas spatial layouts relative to HG. Cortical surface meshes were used to extract primary surface patches which were plotted then with HG borders. Overlapping voxels collapsed z-dimension are shown with open circles. Colour scale represents frequency preferences (low frequencies in red and high frequencies in blue). First row: spatial layout of an exemplar control subject, C1. Other rows: spatial layouts from Patient 1 (P1), Patient 2 (P2), and Patient 3 (P3). Solid lines: Heschl's sulcus and first temporal sulcus. Dashed-lines: intermediate sulcus. *: HG partial duplication; **: HG complete duplication.

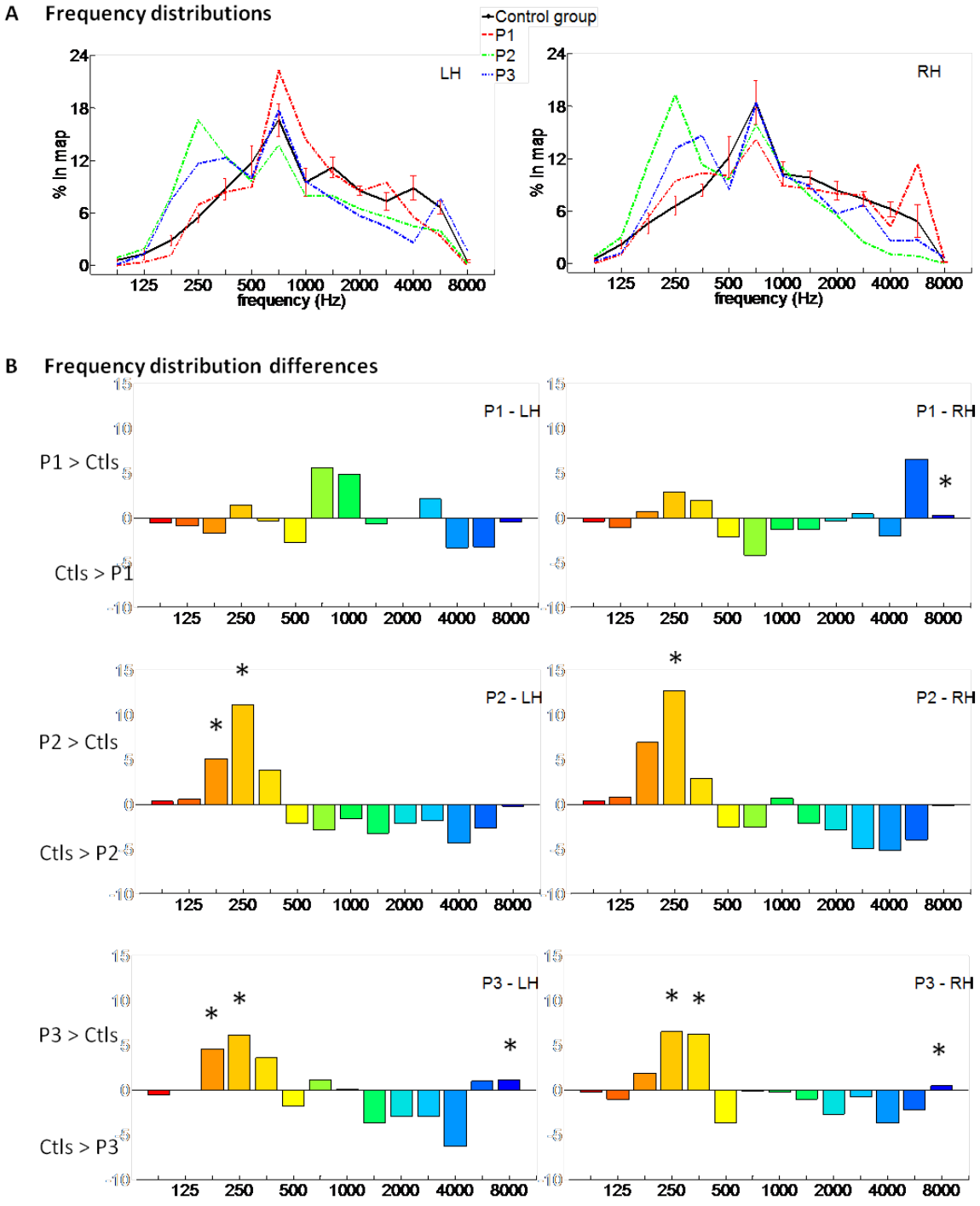
A Frequency distributions
Control group
P1
P2
P3
LH
RH
% In map
frequency (Hz)
B Frequency distribution differences
P1 - LH
P1 - RH
P2 - LH
P2 - RH
P3 - LH
P3 - RH
P1 > Ctls
Ctls > P1
P2 > Ctls
Ctls > P2
P3 > Ctls
Ctls > P3

Figure 3.25: Frequency distributions. Tonotopic average maps were quantified in percentages of best-fitted frequency per total number of voxels. Each bar represents the percentage of voxels dedicated to a specific frequency and error bars the standard errors across subjects and runs. **A.** Mean frequency distribution of a control group (n = 5, black line; error bars represent standard errors across subjects) and for each patient (red, green and blue lines). All curves peaked at 707 Hz, with a double peak for P2 (green line). Paired t-tests of the frequency distributions showed no differences between left and right hemispheres ($p > 0.01$, uncorrected). **B.** In order to visualize differences in frequency distributions, we computed the difference between frequency distributions of each patient and the control group. Positive values corresponded to distributions higher in patients compared to controls and negative values the opposite. Significant differences between patients and controls are marked by asterisks (paired t-tests, $p < 0.05$, Bonferroni corrected). P1: Patient 1; P2: Patient 2; P3: Patient 3; Ctls: controls; LH: left hemisphere; RH: right hemisphere.

Figure 3.26: Percent signal changes (PSC) variations. A. Amplitude ratios from frequency-related time courses are displayed in PSC variations per frequency bin. In black, average PSC for control group (n = 5) for right and left hemisphere. Error bars represent standard errors across subjects. Other colors, PSCs for each patient in right and left hemispheres. **B.** PSC variation differences between patients and controls. As for frequency distributions differences, we computed the difference between controls group and individual PSC variations. Positive values corresponded to PSC variations higher in the control group compared to the patient and negative values the opposite. Significant differences between patients and controls are marked by asterisks (paired t-tests, $p < 0.05$, Bonferroni corrected). P1: Patient 1; P2: Patient 2; P3: Patient 3; Ctls: controls; LH: left hemisphere; RH: right hemisphere.

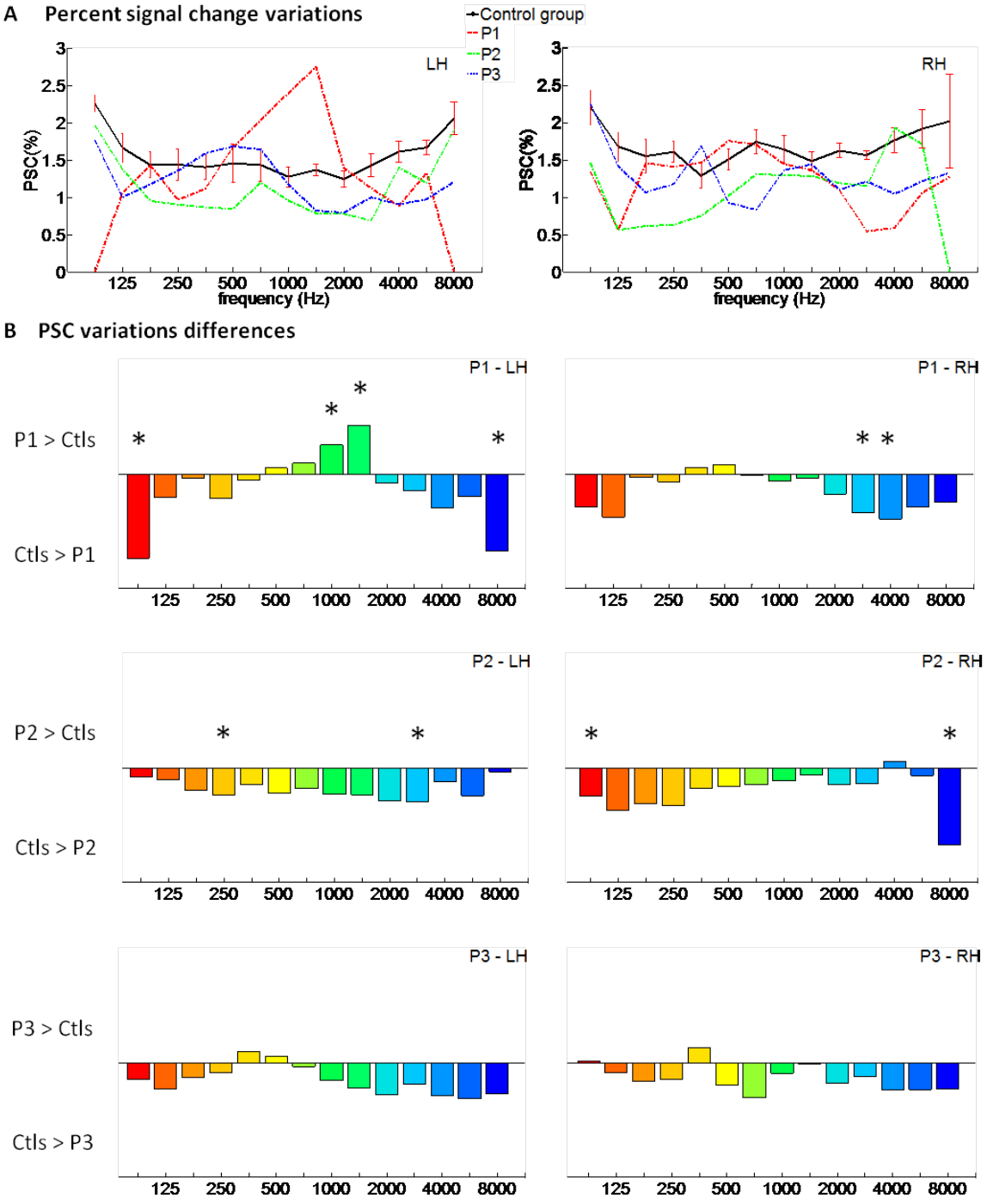
A Percent signal change variations
Control group
P1
P2
P3
LH
RH
PSC(%)
frequency (Hz)
125 250 500 1000 2000 4000 8000
B PSC variations differences
P1 - LH
P1 - RH
P1 > Ctls
Ctls > P1
P2 - LH
P2 - RH
P2 > Ctls
Ctls > P2
P3 - LH
P3 - RH
P3 > Ctls
Ctls > P3

abnormal gain within the auditory pathways linked to a GABA-mediated inhibition. This phenomenon could be similar to a phantom sensation in amputees (Cook et al., 2004).

Tonotopic maps are influenced by diaschisis-like cerebellar-cortical effects

Patient 1 had a cerebellar lesion within the right superior vermis. According to various connectivity atlases, this region may be part of the cerebellar lobule V in the SUIT atlas, which is involved in motor control (Diedrichsen et al., 2009; O'Reilly et al., 2010). Indeed, during the acute phase, the patient presented a dysdiadococinesia, which is typically related to cerebellar lesion and rescued by physiotherapy treatments. This region is also functionally connected to the STG and other regions of the attention network (Bernard et al., 2012; Buckner et al., 2011; Pastor et al., 2008; Sang et al., 2012). The cerebellum was considered mainly as a motor coordinator (Manni and Petrosini, 2004; Stoodley et al., 2012), however recent studies showed its involvement in more elaborate cognitive processes (for review, D'Angelo and Casali, 2013). The cerebellum is not directly linked to the cerebrum. The descending cerebro-cerebellar pathway has one intermediate relay in the olivary complex at the level of the pons, whereas the ascending connections go through two relays, one in the deep cerebellar nuclei and the second in the thalamus (Ramnani, 2006). Cerebro-pontine-cerebellar connections with the temporal lobes are relevant in timing judgement, working memory, attention switching and language processing (D'Angelo and Casali, 2013; Filippi et al., 2011; Lockwood et al., 1999; Petacchi et al., 2011, 2005; Rao et al., 1997). More specifically, human case studies reported pitch discrimination and hearing deficits after a right superior cerebellar artery infarction (Baillieux et al., 2010; Lee et al., 2008; Parsons et al., 2009). Thus, cerebellar lesions could induce diaschisis effects in the contralateral pontine nuclei which relay the disturbance to high order areas such as primary auditory cortex. The inferior colliculus nucleus hyperactivity could be related to hyperactive responses in the auditory cortex, as shown in the animal model (Salvi et al., 2000).

Tonotopic maps reorganisation affect auditory scene analysis pathways

Auditory complaints from Patient 1 and 2 may be related to auditory scene analysis problems. The auditory system is permanently playing with the decomposition of a com-

plex mixture of auditory information (Bregman et al., 1990). This auditory scene streaming involves fast top-down (attention) and bottom-up (salience) processes (Gutschalk and Dykstra, 2013) within lower and higher order regions. These cortico-cortico, thalamic-cortical and cortico-thalamic connections are also important in auditory plasticity and learning.

At the brainstem level, descending connections adjust grouping or dissociating of auditory representations in the IC (Nakamoto et al., 2010; Salvi et al., 2000; Suga and Ma, 2003), and enhance representations of incoming auditory information in the MGB (Scharinger et al., 2013; Suga and Ma, 2003; von Kriegstein et al., 2008). The MGB is considered as a cognitive hub dealing with short-term auditory learning (Scharinger et al., 2013), fast time-varying auditory features at phoneme level (Alain et al., 2005; Suga and Ma, 2003; von Kriegstein et al., 2008), and connecting primary as well as secondary auditory areas (Hackett et al., 2011). MGB dysfunction leads to deficits in dyslexia or imperceptions of environmental sounds (such as speech, music, etc; Daz et al., 2012; Kaga et al., 2000), and hyperactivity of the MGB medial neurons make primary auditory neurons less sensitive to fine auditory signals. Moreover, left MGB, auditory cortex and planum temporal are involved in speech separation and identification (Alain et al., 2005). Disregulation of this thalamic-cortical auditory network could explain partially auditory complaints in Patient 2, but not necessary in Patient 1.

At the cortical level, regions from the auditory selective attention network may be affected by diaschisis effects related to the lesion site or other regions sharing the same pathways. The left inferior parietal lobule (IPL) is important for several attentional aspects such as short-term memory comparison during figure-ground segregation and phoneme categorization (Cohen, 2009; Guenther et al., 2004; Husain et al., 2006; Leff et al., 2009; Scharinger et al., 2013; Teki et al., 2011; Turkeltaub and Branch Coslett, 2010). Disturbance of the left IPL would explain auditory complaints in Patient 2 but not in Patient 1. However, auditory short-term memory is important in determining sentence-level speech comprehension ability, thus we can hypothesise that Patient 1 has also impairments in this network maybe due to hyperactivation of the auditory cortex, but our results do not allow such straightforward conclusions.

Overall, results from Patient 2 are clearly interpretable in relation to her auditory complaints and lesion site in the lateral portion of HG. Several evidences from the literature showed implication of this region in pitch extraction and processing, and complex sounds perception and categorisation (Bermudez et al., 2009; Griffiths and Warren, 2002; Johnsrude et al., 2000; Liegeois-Chauvel et al., 1991; Patterson et al., 2002; Schnwiesner et al., 2005; Zatorre and Belin, 2001). Thus, her auditory complaints are directly due to the lesion itself rather tonotopic maps reorganisation. Signal increases are due to diaschisis-like cerebral effects as well for Patient 3. The same for Patient 1, her cerebellar lesion colocalised with regions communicating with nuclear relays involved in pitch discrimination (Baillieux et al., 2010; Lee et al., 2008; Parsons et al., 2009), which, if impaired by diaschisis-like cerebellar effects induced higher signal intensities in primary auditory areas.

Limitations

Our patient results showed a tendency to increase/decrease signal intensities of frequencies within the speech spectral range (from 500 to 2000 Hz) depending on lesion site. Disturbances in speech spectra representations could explain difficulties and complaints related to the impaired social interactions in Patient 1 and 2. However, tonotopic mapping functionally measures low level pure tone discrimination by both ears. More complex sounds, such as environmental sounds (animals, human vocalizations, instruments, tools, etc), or tasks (compared to passive listening) might be more appropriate to test (non-)primary auditory cortex modulations, and to link these effects to auditory complaints and an eventual laterality effect.

Moreover, we should acknowledge that our control group had a mean age (32.2 years) younger than Patient 2 and 3, and older than Patient 1. Frequency distributions in Patients 2 and 3 might be also affected by age-related plasticity. To certify this hypothesis we should acquire more age-matched control subjects and retest frequency distributions.

In order to disentangle the implication of higher-order attention from top-down effects, we should test attention modulation of primary auditory areas for pitch and speech processing in the same patient subset or in a larger patient population. Moreover, differences

in grey matter volume in the auditory cortex, as a result of the lesion, could be correlated to auditory complaints. A recent study showed that increased grey matter volume in temporal cortex is associated with difficulties in auditory processing (Erb et al., 2012). Thus, in a future experiment, we could investigate the correlation between grey matter and thickness in stroke patients with or without auditory complaints and correlate these to different neuropsychological auditory scores or frequency/signal variations.

Conclusion

The passive tonotopic paradigm was only 16min long and was used easily as an initial localizer of the primary auditory cortex. Patients with brain lesions were able to perform it without significant effort, which offered the possibility to study auditory plasticity in stroke patients without or with auditory complaints. Our preliminary results demonstrated tonotopic reorganisation in stroke patients in cases of brain lesions independently of auditory complaints which could potentially linked to diaschisis-like neural plasticity.

References

Adriani, M., Bellmann, A., Meuli, R., Fornari, E., Frischknecht, R., Bindschaedler, C., Rivier, F., Thiran, J.-P., Maeder, P., Clarke, S., 2003a. Unilateral hemispheric lesions disrupt parallel processing within the contralateral intact hemisphere: an auditory fMRI study. NeuroImage 20 Suppl 1, S66 – 74.

Adriani, M., Maeder, P., Meuli, R., Thiran, A.B., Frischknecht, R., Villemure, J.-G., Mayer, J., Annoni, J.-M., Bogousslavsky, J., Fornari, E., Thiran, J.-P., Clarke, S., 2003b. Sound recognition and localization in man: specialized cortical networks and effects of acute circumscribed lesions. Exp. Brain Res. Exp. Hirnforsch. Expérimentation Cérébrale 153, 591 – 604.

Alain, C., Reinke, K., McDonald, K.L., Chau, W., Tam, F., Pacurar, A., Graham, S., 2005. Left thalamo-cortical network implicated in successful speech separation and identification. NeuroImage 26, 592 – 599.

Antunes, F.M., Malmierca, M.S., 2011. Effect of Auditory Cortex Deactivation on Stimulus-Specific Adaptation in the Medial Geniculate Body. J. Neurosci. 31, 17306 – 17316.

Baillieux, H., De Smet, H.J., Dobbeleir, A., Paquier, P.F., De Deyn, P.P., Marin, P., 2010. Cognitive and affective disturbances following focal cerebellar damage in adults: a neuropsychological and SPECT study. Cortex J. Devoted Study Nerv. Syst. Behav. 46, 869 – 879.

Bermudez, P., Lerch, J.P., Evans, A.C., Zatorre, R.J., 2009. Neuroanatomical Correlates of Musicianship as Revealed by Cortical Thickness and Voxel-Based Morphometry. Cereb. Cortex 19, 1583 – 1596.

Bernard, J.A., Seidler, R.D., Hassevoort, K.M., Benson, B.L., Welsh, R.C., Wiggins, J.L., Jaeggi, S.M., Buschkuehl, M., Monk, C.S., Jonides, J., Peltier, S.J., 2012. Resting state cortico-cerebellar functional connectivity networks: a comparison of anatomical and self-organizing map approaches. Front. Neuroanat. 6, 31.

Bregman, A.S., Liao, C., Levitan, R., 1990. Auditory grouping based on fundamental frequency and formant peak frequency. Can. J. Psychol. 44, 400 – 413.

Brugge, J.F., 2013. Chapter 2 - Anatomy and physiology of auditory pathways and cortex, in: Gastone G. Celesia (Ed.), Handbook of Clinical Neurophysiology, Disorders of Peripheral and Central Auditory Processing. Elsevier, pp. 25 – 59.

Brugge, J.F., Volkov, I.O., Garell, P.C., Reale, R.A., Howard, M.A., 2003. Functional Connections Between Auditory Cortex on Heschl's Gyrus and on the Lateral Superior Temporal Gyrus in Humans. J. Neurophysiol. 90, 3750 – 3763.

Buckner, R.L., Krienen, F.M., Castellanos, A., Diaz, J.C., Yeo, B.T.T., 2011. The organization of the human cerebellum estimated by intrinsic functional connectivity. J. Neurophysiol. 106, 2322 – 2345.

Buonomano, D.V., Merzenich, M.M., 1998. CORTICAL PLASTICITY: From Synapses to Maps. Annu. Rev. Neurosci. 21, 149 – 186.

Carrasco, A., Kok, M.A., Lomber, S.G., 2013. Effects of Core Auditory Cortex Deactivation on Neuronal Response to Simple and Complex Acoustic Signals in the Contralateral Anterior Auditory Field. Cereb. Cortex. Epub.

Carrasco, A., Lomber, S.G., 2013. Influence of inter-field communication on neuronal response synchrony across auditory cortex. Hear. Res. 304, 57 – 69.

Cohen, Y.E., 2009. Multimodal activity in the parietal cortex. Hear. Res. 258, 100 – 105.

Cook, D.B., Lange, G., Ciccone, D.S., Liu, W.-C., Steffener, J., Natelson, B.H., 2004. Functional imaging of pain in patients with primary fibromyalgia. J. Rheumatol. 31, 364 – 378.

D'Angelo, E., Casali, S., 2013. Seeking a unified framework for cerebellar function and dysfunction: from circuit operations to cognition. Front. Neural Circuits 6, 116.

Da Costa, S., van der Zwaag, W., Marques, J.P., Frackowiak, R.S.J., Clarke, S., Saenz, M., 2011. Human Primary Auditory Cortex Follows the Shape of Heschl's Gyrus. J. Neurosci. 31, 14067 – 14075.

Da Costa, S., van der Zwaag, W., Miller, L.M., Clarke, S., Saenz, M., 2013. Tuning In to Sound: Frequency-Selective Attentional Filter in Human Primary Auditory Cortex. J. Neurosci. 33, 1858 – 1863.

De Martino, F., Zimmermann, J., Muckli, L., Ugurbil, K., Yacoub, E., Goebel, R., 2013. Cortical Depth Dependent Functional Responses in Humans at 7T: Improved Specificity with 3D GRASE. PloS One 8, e60514.

Díaz, B., Hintz, F., Kiebel, S.J., Kriegstein, K. von, 2012. Dysfunction of the auditory thalamus in developmental dyslexia. Proc. Natl. Acad. Sci. 109, 13841 – 13846.

Diedrichsen, J., Balsters, J.H., Flavell, J., Cussans, E., Ramnani, N., 2009. A probabilistic MR atlas of the human cerebellum. NeuroImage 46, 39 – 46.

Engel, S.A., 2012. The development and use of phase-encoded functional MRI designs. NeuroImage 62, 1195 – 1200.

Engelhardt, E., Gomes, M. da M., 2013. Shock, diaschisis and von Monakow. Arq. Neuropsiquiatr. 71, 487 – 489.

Erb, J., Henry, M.J., Eisner, F., Obleser, J., 2012. Auditory skills and brain morphology predict individual differences in adaptation to degraded speech. Neuropsychologia 50, 2154 – 2164.

Filippi, R., Richardson, F.M., Dick, F., Leech, R., Green, D.W., Thomas, M.S.C., Price, C.J., 2011. The Right Posterior Paravermis and the Control of Language Interference. J. Neurosci. 31, 10732 – 10740.

Formisano, E., Kim, D.S., Di Salle, F., van de Moortele, P.F., Ugurbil, K., Goebel, R., 2003. Mirror-symmetric tonotopic maps in human primary auditory cortex. Neuron 40, 859 – 869.

Gaucher, Q., Huetz, C., Gourvitch, B., Edeline, J.-M., 2013. Cortical Inhibition Reduces Information Redundancy at Presentation of Communication Sounds in the Primary Auditory Cortex. J. Neurosci. 33, 10713 – 10728.

Griffiths, T.D., Warren, J.D., 2002. The planum temporale as a computational hub. Trends Neurosci. 25, 348 – 353.

Gu, J.W., Halpin, C.F., Nam, E.-C., Levine, R.A., Melcher, J.R., 2010. Tinnitus, diminished sound-level tolerance, and elevated auditory activity in humans with clinically normal hearing sensitivity. J. Neurophysiol. 104, 3361 – 3370.

Gu, J.W., Herrmann, B.S., Levine, R.A., Melcher, J.R., 2012. Brainstem auditory evoked potentials suggest a role for the ventral cochlear nucleus in tinnitus. J. Assoc. Res. Otolaryngol. JARO 13, 819 – 833.

Guenther, F.H., Nieto-Castanon, A., Ghosh, S.S., Tourville, J.A., 2004. Representation of Sound Categories in Auditory Cortical Maps. J. Speech Lang. Hear. Res. 47, 46.

Gutschalk, A., Dykstra, A.R., 2013. Functional imaging of auditory scene analysis. Hear. Res. Epub.

Hackett, T.A., Barkat, T.R., O'Brien, B.M.J., Hensch, T.K., Polley, D.B., 2011. Linking topography to tonotopy in the mouse auditory thalamocortical circuit. J. Neurosci. Off. J. Soc. Neurosci. 31, 2983 – 2995.

Humphries, C., Liebenthal, E., Binder, J.R., 2010. Tonotopic organization of human auditory cortex. NeuroImage 50, 1202 – 1211.

Husain, F.T., Fromm, S.J., Pursley, R.H., Hosey, L.A., Braun, A.R., Horwitz, B., 2006. Neural bases of categorization of simple speech and nonspeech sounds. Hum. Brain Mapp. 27, 636 – 651.

Irvine, D.R.F., 2007. Auditory cortical plasticity: Does it provide evidence for cognitive processing in the auditory cortex? Hear. Res. 229, 158 – 170.

Johnsrude, I.S., Penhune, V.B., Zatorre, R.J., 2000. Functional specificity in the right hu-

man auditory cortex for perceiving pitch direction. Brain J. Neurol. 123 (Pt 1), 155 – 163.

Kaga, K., Shindo, M., Tanaka, Y., Haebara, H., 2000. Neuropathology of auditory agnosia following bilateral temporal lobe lesions: a case study. Acta Otolaryngol. (Stockh.) 120, 259 – 262.

Kilgard, M.P., Merzenich, M.M., 2002. Order-sensitive plasticity in adult primary auditory cortex. Proc. Natl. Acad. Sci. 99, 3205 – 3209.

Kilgard, M.P., Pandya, P.K., Vazquez, J., Gehi, A., Schreiner, C.E., Merzenich, M.M., 2001. Sensory input directs spatial and temporal plasticity in primary auditory cortex. J. Neurophysiol. 86, 326 – 338.

Langers, D.R.M., de Kleine, E., van Dijk, P., 2012. Tinnitus does not require macroscopic tonotopic map reorganization. Front. Syst. Neurosci. 6, 2.

Langers, D.R.M., Dijk, P. van, 2012. Mapping the Tonotopic Organization in Human Auditory Cortex with Minimally Salient Acoustic Stimulation. Cereb. Cortex 22, 2024 – 2038.

Langers, D.R.M., 2013. Assessment of tonotopically organised subdivisions in human auditory cortex using volumetric and surface-based cortical alignments. Hum. Brain Mapp. Epub.

Lazard, D.S., Innes-Brown, H., Barone, P., 2013. Adaptation of the communicative brain to post-lingual deafness. Evidence from functional imaging. Hear. Res. Epub.

Lee, E., Sohn, H.-Y., Kwon, M., Kim, J.S., 2008. Contralateral hyperacusis in unilateral pontine hemorrhage. Neurology 70, 2413 – 2415.

Leff, A.P., Schofield, T.M., Crinion, J.T., Seghier, M.L., Grogan, A., Green, D.W., Price, C.J., 2009. The left superior temporal gyrus is a shared substrate for auditory short-term memory and speech comprehension: evidence from 210 patients with stroke. Brain J. Neurol. 132, 3401–3410.

Liegeois-Chauvel, C., Musolino, A., Chauvel, P., 1991. Localization of the primary auditory area in man. Brain J. Neurol. 114 (Pt 1A), 139 – 151.

Lockwood, A.H., Salvi, R.J., Coad, M.L., Arnold, S.A., Wack, D.S., Murphy, B.W., Burkard, R.F., 1999. The Functional Anatomy of the Normal Human Auditory System:

Responses to 0.5 and 4.0 kHz Tones at Varied Intensities. Cereb. Cortex 9, 65 – 76.

Manni, E., Petrosini, L., 2004. A century of cerebellar somatotopy: a debated representation. Nat. Rev. Neurosci. 5, 241 – 249.

Marques, J.P., Kober, T., Krueger, G., van der Zwaag, W., Van de Moortele, P.-F., Gruetter, R., 2010. MP2RAGE, a self bias-field corrected sequence for improved segmentation and T1-mapping at high field. NeuroImage 49, 1271 – 1281.

Moerel, M., De Martino, F., Formisano, E., 2012. Processing of natural sounds in human auditory cortex: tonotopy, spectral tuning, and relation to voice sensitivity. J. Neurosci. Off. J. Soc. Neurosci. 32, 14205 – 14216.

Moore, D.R., Shannon, R.V., 2009. Beyond cochlear implants: awakening the deafened brain. Nat. Neurosci. 12, 686 – 691.

Moore, B.C.J., Gockel, H.E., 2011. Resolvability of components in complex tones and implications for theories of pitch perception. Hear. Res. 276, 88 – 97.

Nakamoto, K.T., Jones, S.J., Palmer, A.R., 2008. Descending projections from auditory cortex modulate sensitivity in the midbrain to cues for spatial position. J. Neurophysiol. 99, 2347 – 2356.

Nakamoto, K.T., Shackleton, T.M., Palmer, A.R., 2010. Responses in the Inferior Colliculus of the Guinea Pig to Concurrent Harmonic Series and the Effect of Inactivation of Descending Controls. J. Neurophysiol. 103, 2050 – 2061.

O'Reilly, J.X., Beckmann, C.F., Tomassini, V., Ramnani, N., Johansen-Berg, H., 2010. Distinct and overlapping functional zones in the cerebellum defined by resting state functional connectivity. Cereb. Cortex N. Y. N 1991 20, 953 – 965.

Paltoglou, A.E., Sumner, C.J., Hall, D.A., 2011. Mapping feature–sensitivity and attentional modulation in human auditory cortex with functional magnetic resonance imaging. Eur. J. Neurosci. 33, 1733 – 1741.

Pandya, P.K., Moucha, R., Engineer, N.D., Rathbun, D.L., Vazquez, J., Kilgard, M.P., 2005. Asynchronous inputs alter excitability, spike timing, and topography in primary auditory cortex. Hear. Res. 203, 10 – 20.

Parsons, L.M., Petacchi, A., Schmahmann, J.D., Bower, J.M., 2009. Pitch discrimination

in cerebellar patients: evidence for a sensory deficit. Brain Res. 1303, 84 – 96.

Pastor, M.A., Vidaurre, C., Fernndez-Seara, M.A., Villanueva, A., Friston, K.J., 2008. Frequency-Specific Coupling in the Cortico-Cerebellar Auditory System. J. Neurophysiol. 100, 1699 – 1705.

Patterson, R.D., Uppenkamp, S., Johnsrude, I.S., Griffiths, T.D., 2002. The processing of temporal pitch and melody information in auditory cortex. Neuron 36, 767 – 776.

Petacchi, A., Kaernbach, C., Ratnam, R., Bower, J.M., 2011. Increased activation of the human cerebellum during pitch discrimination: a positron emission tomography (PET) study. Hear. Res. 282, 35 – 48.

Petacchi, A., Laird, A.R., Fox, P.T., Bower, J.M., 2005. Cerebellum and auditory function: an ALE meta-analysis of functional neuroimaging studies. Hum. Brain Mapp. 25, 118 – 128.

Ramnani, N., 2006. The primate cortico-cerebellar system: anatomy and function. Nat. Rev. Neurosci. 7, 511 – 522.

Rao, S.M., Harrington, D.L., Haaland, K.Y., Bobholz, J.A., Cox, R.W., Binder, J.R., 1997. Distributed neural systems underlying the timing of movements. J. Neurosci. Off. J. Soc. Neurosci. 17, 5528 – 5535.

Recanzone, G.H., Schreiner, C.E., Merzenich, M.M., 1993. Plasticity in the frequency representation of primary auditory cortex following discrimination training in adult owl monkeys. J. Neurosci. Off. J. Soc. Neurosci. 13, 87 – 103.

Rinne, T., Kirjavainen, S., Salonen, O., Degerman, A., Kang, X., Woods, D.L., Alho, K., 2007. Distributed cortical networks for focused auditory attention and distraction. Neurosci. Lett. 416, 247 – 251.

Rinne, T., Balk, M.H., Koistinen, S., Autti, T., Alho, K., Sams, M., 2008. Auditory selective attention modulates activation of human inferior colliculus. J. Neurophysiol. 100, 3323 – 3327.

Rivier, F., Clarke, S., 1997. Cytochrome oxidase, acetylcholinesterase, and NADPH-diaphorase staining in human supratemporal and insular cortex: evidence for multiple auditory areas. NeuroImage 6, 288 – 304.

Sacco, C.B., Tardif, E., Genoud, C., Probst, A., Tolnay, M., Janzer, R.-C., Verney, C., Kraftsik, R., Clarke, S., 2009. GABA receptor subunits in human auditory cortex in normal and stroke cases. Acta Neurobiol. Exp. (Warsz.) 69, 469 – 493.

Saenz, M., Langers, D.R.M., 2013. Tonotopic mapping of human auditory cortex. Hear. Res. Epub.

Salvi, R.J., Wang, J., Ding, D., 2000. Auditory plasticity and hyperactivity following cochlear damage. Hear. Res. 147, 261 – 274.

Sang, L., Qin, W., Liu, Y., Han, W., Zhang, Y., Jiang, T., Yu, C., 2012. Resting-state functional connectivity of the vermal and hemispheric subregions of the cerebellum with both the cerebral cortical networks and subcortical structures. NeuroImage 61, 1213 – 1225.

Saur, D., Lange, R., Baumgaertner, A., Schraknepper, V., Willmes, K., Rijntjes, M., Weiller, C., 2006. Dynamics of language reorganization after stroke. Brain J. Neurol. 129, 1371 – 1384.

Scharinger, M., Henry, M.J., Erb, J., Meyer, L., Obleser, J., 2013. Thalamic and parietal brain morphology predicts auditory category learning. Neuropsychologia. Epub.

Scheffler, K., Bilecen, D., Schmid, N., Tschopp, K., Seelig, J., 1998. Auditory cortical responses in hearing subjects and unilateral deaf patients as detected by functional magnetic resonance imaging. Cereb. Cortex N. Y. N 1991 8, 156 – 163.

Schiene, K., Bruehl, C., Zilles, K., Qü, M., Hagemann, G., Kraemer, M., Witte, O.W., 1996. Neuronal hyperexcitability and reduction of GABAA-receptor expression in the surround of cerebral photothrombosis. J. Cereb. Blood Flow Metab. Off. J. Int. Soc. Cereb. Blood Flow Metab. 16, 906 – 914.

Schofield, T.M., Penny, W.D., Stephan, K.E., Crinion, J.T., Thompson, A.J., Price, C.J., Leff, A.P., 2012. Changes in Auditory Feedback Connections Determine the Severity of Speech Processing Deficits after Stroke. J. Neurosci. 32, 4260 – 4270.

Schönwiesner, M., von Cramon, D.Y., Rübsamen, R., 2002. Is it tonotopy after all? NeuroImage 17, 1144 – 1161.

Schönwiesner, M., Rübsamen, R., von Cramon, D.Y., 2005. Hemispheric asymmetry for spectral and temporal processing in the human antero-lateral auditory belt cortex. Eur. J.

Neurosci. 22, 1521 – 1528.

Seifritz, E., Di Salle, F., Esposito, F., Herdener, M., Neuhoff, J.G., Scheffler, K., 2006. Enhancing BOLD response in the auditory system by neurophysiologically tuned fMRI sequence. NeuroImage 29, 1013 – 1022.

Stoodley, C.J., Valera, E.M., Schmahmann, J.D., 2012. Functional topography of the cerebellum for motor and cognitive tasks: an fMRI study. NeuroImage 59, 1560 – 1570.

Striem-Amit, E., Hertz, U., Amedi, A., 2011. Extensive cochleotopic mapping of human auditory cortical fields obtained with phase-encoding FMRI. PloS One 6, e17832.

Suga, N., Ma, X., 2003. Multiparametric corticofugal modulation and plasticity in the auditory system. Nat. Rev. Neurosci. 4, 783 – 794.

Talavage, T.M., Ledden, P.J., Benson, R.R., Rosen, B.R., Melcher, J.R., 2000. Frequency-dependent responses exhibited by multiple regions in human auditory cortex. Hear. Res. 150, 225 – 244.

Talavage, T.M., Sereno, M.I., Melcher, J.R., Ledden, P.J., Rosen, B.R., Dale, A.M., 2004. Tonotopic organization in human auditory cortex revealed by progressions of frequency sensitivity. J. Neurophysiol. 91, 1282 – 1296.

Tang, J., Yang, W., Suga, N., 2012. Modulation of thalamic auditory neurons by the primary auditory cortex. J. Neurophysiol. 108, 935 – 942.

Teki, S., Grube, M., Kumar, S., Griffiths, T.D., 2011. Distinct Neural Substrates of Duration-Based and Beat-Based Auditory Timing. J. Neurosci. 31, 3805 – 3812.

Turkeltaub, P.E., Branch Coslett, H., 2010. Localization of sublexical speech perception components. Brain Lang. 114, 1 – 15.

Von Kriegstein, K., Patterson, R.D., Griffiths, T.D., 2008. Task-Dependent Modulation of Medial Geniculate Body Is Behaviorally Relevant for Speech Recognition. Curr. Biol. 18, 1855 – 1859.

Weinberger, N.M., 1995. Dynamic regulation of receptive fields and maps in the adult sensory cortex. Annu. Rev. Neurosci. 18, 129 – 158.

Weinberger, N.M., 2004. Specific long-term memory traces in primary auditory cortex.

Nat. Rev. Neurosci. 5, 279 – 290.

Woods, D.L., Herron, T.J., Cate, A.D., Yund, E.W., Stecker, G.C., Rinne, T., Kang, X., 2010. Functional properties of human auditory cortical fields. Front. Syst. Neurosci. 4, 155.

Zatorre, R.J., Belin, P., 2001. Spectral and Temporal Processing in Human Auditory Cortex. Cereb. Cortex 11, 946 – 953.

Chapter 4

General discussion

In this thesis, I showed that, in healthy young controls, (1) there is a anatomical-functional continuum between Heschl's gyrus variants and the primary auditory cortex, assessed at high and standard imaging resolution (Da Costa et al., 2011; Da Costa et al., in preparation), (2) primary auditory tonotopic areas responses can be modulated by top-down mechanisms such as attention (Da Costa et al., 2013), (3) auditory cortex processes auditory information differently depending on semantic category (Da Costa et al., in preparation), and also that (4) primary auditory frequency maps are modulated by diaschisis-like neuronal plasticity after brain injury (Da Costa et al., in preparation). The relevance and the scope of each study are described in the corresponding sections. Here, I will focus on the possible future studies.

4.1 Going one step beyond tonotopy at high resolution

In the first study, we defined the primary auditory cortex based on functional mapping of frequency preferences. Tonotopic maps were easily measured due to advantages from high resolution imaging and phase-encoding analysis. The combination of both techniques enabled clear and robust measured frequency gradients within and outside primary auditory cortices. Frequency gradients are commonly used to identify anterior and posterior borders of primary areas. However, medial and lateral borders definitions are more experimenter-dependant. These limits can be subjectively set to the medial two-thirds of Heschl's gyrus, based on previous cytoarchitechtonic or probabilistic studies on post-mortem brains (Galaburda and Sanides, 1980; Morosan et al., 2001, 2004; Rademacher et al., 2001; Rivier and Clarke, 1997; Schleicher et al., 2009; Wallace et al., 2002), but they will differ anatomically from subjects one. New protocols, including sequences

mapping tissue properties such as proton densities for R1 contrast imaging, would (1) increase robustness of primary auditory areas definition and (2) be applied individually taking in account all types of Heschl's gyrus variants (see introduction). Recent studies with promising results illustrated this favourable combination at lower fields (Dick et al., 2012; Lutti et al., 2013; Sigalovsky et al., 2006; Wasserthal et al., 2013). Thus, one could speculate that the combination of ultra-high field proton density and fine tonotopic mapping could improve auditory areas subdivisions.

Alternatively, ultra-high field imaging could be used to highlight fine connectivity between primary auditory cortex and other auditory regions. Connectivity is usually investigated at high field strength with resting state functional connectivity analysis, diffusion imaging or task-related functional imaging. However, with the Human Connectome Project, there is some hope for new sequences development at ultra-high fields (Ugurbil et al., 2013). Thus, we could develop and use diffusion spectrum imaging (DSI) sequences to investigate primary auditory cortex connections by (1) using A1 and R areas as seed regions and looking at general connectivity with a whole brain approach or (2) focusing only on the superatemporal plane and investigating local connectivity between primary and belt areas (as in Fan et al., 2013). In the tonotopy studies, we gained in spatial resolution by scanning only a portion of the temporal lobe. Maybe restricting the DSI acquisition to a slab including only the temporal lobe will increase the resolution and power of the connectivity pattern by revealing discreet connections masked by large connectivity fibres in a whole brain approach.

High spatial resolution was deterministic in the tonotopic results where frequency preferences were mainly restricted to primary and secondary auditory areas. Consequently, we used a region of interest approach where only a slice of 45 mm centred on the auditory cortex was acquired. For higher processes such as attention, a whole brain approach with the technical advances in sequence developing could be an alternative. Top-down modulations are apparent in primary auditory regions, however, they could also be correlated to others regions of the attention network. Whole brain functional imaging (De Martino et al., 2011) will give the global view of the network and open possibilities for more elaborate analysis, such as dynamic causal modelling (DCM), highlighting attentional modulations at different levels of the network (as in Walz et al., 2013). In counterpart,

scan sessions will last longer and resolution benefits will not be sufficient enough to justify such approach at 7T compared to standard 3T acquisitions.

In this thesis, the main auditory region studied was the supratemporal plane. However, one could investigate the entire auditory pathway simultaneously with the same paradigm by orienting the acquisition slice perpendicular to the AC-PC plane or slightly tilted by few degrees in order to cover auditory cortices and lower level nuclei such as the inferior colliculus and medial geniculate body. Time-course amplitudes are smaller in brainstem relays than in cortical auditory areas (Sigalovsky and Melcher, 2006), thus we should perform this study at ultra-high field. For the moment, only separate tonotopic mapping of these regions was performed at ultra-high field (Da Costa et al., 2011; De Martino et al., 2013; Formisano et al., 2003). Thus, there is already some evidence that tonotopic mapping could be achieved in multiple locations along the auditory pathways within the same subject and acquisition, with, of course, some technical challenges such as field inhomogeneities, heart beat and motion artefacts. These latter could be attenuated if we monitor them in parallel during MR acquisitions.

4.2 Attention modulation in patients

In the patient study, diaschisis-like neuronal plasticity induced tonotopic maps reorganisation. However, these maps rearrangements could be also modulated by top-down modulations. In order to test this hypothesis, whole brain acquisitions are necessary. Despite a loss in spatial resolution, a whole brain approach, more elaborated analysis such as DCM, event-related designs or diffusion tensor imaging (DTI) could highlight eventual changes in higher order auditory-related areas (as in Han et al., 2013). Thus, regions correlated with high signal variations in the primary auditory cortex should be functionally connected together.

These maps rearrangements could be also due to auditory attentional deficits, which could perhaps be overridden by attentional training on pure tones. In parallel, auditory attentional plasticity could also be another aspect (Ahveninen et al., 2011; Bidet-Caulet et al.,

2007; Fujiwara et al., 1998; Hillyard et al., 1973; Jäncke et al., 1999; Oh et al., 2013; Paltoglou et al., 2009, 20011; Petkov et al., 2004; Rinne et al., 2008; Woldorff et al., 1993; Woods et al., 1984, 2009). In my second study, primary auditory responses are nicely modulated by attention effects. Do these effects last long enough to induce plasticity after long sessions of training? In order to test this hypothesis, we could design a protocol with several-days training sessions where healthy young and old subjects would be trained for 1 hour per day always with the attention paradigm (2-IFC task) including a wide battery of tones. Functional and structural MRI data could be acquired prior and after the training period. This protocol could be part of a short project such as a master project. Behavioural results such as short response times and high percentage of correct responses should reflect good learning and attention modulation in both groups, as we should not expect any differences between young and old healthy subjects (Lawo and Koch, 2012). The contrast between functional sessions (pre-post training) should highlight attention-related areas such as the inferior parietal lobule (Huang et al., 2013; Larson and Lee, 2014) or attention modulation effect of primary auditory areas could be increased with training. Once behavioural and imaging hypothesis are verified, a further step will be to test the same learning plasticity in elderly and/or in patients with mild or severe impairments, with maybe some design adjustments depending on patients attentional load. We should keep in mind that stroke or traumatic brain injured patients are easily prone to fatigue, which could reduce or even completely wash-out the expected attentional effects. Thus, we should scan a large heterogeneous patient population before stating final conclusions. But, we could nevertheless speculate that patients will have longer response times, worse percentage of correct responses prior to training (Keller et al., 1995; Swick et al., 2004), and intermediate response times, above chance lever in the last session. Auditory attention paradigms could be a new set of tools for rehabilitation in stroke patients with auditory complaints or major hyperacusis.

Functional imaging lacks in temporal resolution. However, combining whole brain and EEG imaging on patients in the same protocol with the same experimental task and paradigm could also give insights on attentional deficits within early-stage processing time windows corresponding to bottom-up processes, but also within later higher-order processing time windows (Walz et al., 2013). Furthermore, difficulties in patients with auditory complaints could be related to a slowing down of the same processes. Thus, this

would be another important aspect to investigate in elderly auditory processing.

4.3 Repetition suppression effects related to position

In the third experiment, we showed that the repetition of static environmental sounds, appearing at the same position (in the middle or in front of subjects head, induced repetition suppression in right posterior and medial early-stage auditory areas, but also in right superior and middle temporal gyri. We could use the repetition suppression paradigm as control for a new experiment where repetitions will be position-liked. Repetition blocks made of different sounds of the same source positioned at different angles in the azimuth plane vs. control blocks of different sounds of different sources will give the dynamic semantic repetition effect. This should highlight the same regions than our previous experiment (right posterior and medial early-stage auditory areas). Repetition blocks made of different sounds of the same source positioned at different angles in the azimuth plane vs. control blocks of different sounds of the same source at the 0○ of the azimuth will give the position repetition effect. We speculate that this contrast should highlight clearly regions of the "where" pathway posterior to those from dynamic and static semantic repetition effects, such as posterior planum temporal. This would be in accordance with previous findings from sound localization studies (for review, Ahveninen et al., 2014). A whole brain acquisition with this complex paradigm could identify other regions also involved in semantic repetition suppression effects, such as the inferior parietal lobule. This global view could confirm the "what" and "where" pathways, but also maybe emphasize more subtle differences within the "where" pathways. Interestingly, functional connectivity analysis with seed regions from the dynamic and static semantic repetition effects could reinforce distinction between early subdivision of the where pathway.

Repetition suppression effects were measured in early-stage auditory areas which are connected to lower auditory relays. Evidences from patient studies showed that the inferior colliculus is important for sound source localization and lateralization (Aharonson et al., 1998; Brugge, 2013; Furst and Algom, 1995; Furst et al., 2000; Litovsky et al., 2002). So, are repetition suppression effects specific to early-stage processing or low level decom-

position? To answer this question, we could repeat the repetition suppression experiment or a more complex version with focal fMRI acquisition centred on the midbrain. Due to relatively high distortions around this region, we should record in parallel heart beat and respiratory movements and include them as covariates during the analysis.

4.4 How to overcome current limitations ?

In all studies from this thesis, the acquisition slab was limited to the regions within or parallel to the Sylvian fissure. This poses no problem as long as we focus on primary and secondary auditory areas within the supratemporal plane. Even more, this was necessary and useful to demonstrate tonotopic preferences and fine repetition suppression effects within early-stage auditory areas. Whole brain acquisitions will draw attention to regions correlated with early-stage auditory areas and broader networks. In the attention study, we deliberately focused on primary and non-primary areas. Thus, we did not cover regions implicated in the attention network such as the temporoparietal junction or the inferior frontal gyrus, neither lower relays such as the medial geniculate body.

Another limitation in this thesis was the number of patients in the last study, which was initiated only a few months before the end of my thesis. Results are based on a small heterogeneous group of three patients. In order to strengthen our conclusions, we should acquire a large number of patients, with a range of lesion types. A large database of tonotopic maps in patients with or without auditory complaints might clarify why certain patients develop specific auditory complaints and others not.

References

Aharonson, V., Furst, M., Levine, R.A., Chaigrecht, M., Korczyn, A.D., 1998. Lateralization and binaural discrimination of patients with pontine lesions. J. Acoust. Soc. Am. 103, 2624 – 2633.

Ahveninen, J., Hämäläinen, M., Jääskeläinen, I.P., Ahlfors, S.P., Huang, S., Lin, F.-H., Raij, T., Sams, M., Vasios, C.E., Belliveau, J.W., 2011. Attention-driven auditory cortex short-term plasticity helps segregate relevant sounds from noise. Proc. Natl. Acad. Sci. 108, 4182 – 4187.

Ahveninen, J., Kopco, N., Jääskeläinen, I.P., 2014. Psychophysics and neuronal bases of sound localization in humans. Hear. Res. 307, 86 – 97.

Bidet-Caulet, A., Fischer, C., Besle, J., Aguera, P.-E., Giard, M.-H., Bertrand, O., 2007. Effects of selective attention on the electrophysiological representation of concurrent sounds in the human auditory cortex. J. Neurosci. Off. J. Soc. Neurosci. 27, 9252 – 9261.

Brugge, J.F., 2013. Chapter 2 - Anatomy and physiology of auditory pathways and cortex, in: Gastone G. Celesia (Ed.), Handbook of Clinical Neurophysiology, Disorders of Peripheral and Central Auditory Processing. Elsevier, pp. 25 – 59.

Da Costa, S., van der Zwaag, W., Marques, J.P., Frackowiak, R.S.J., Clarke, S., Saenz, M., 2011. Human Primary Auditory Cortex Follows the Shape of Heschl's Gyrus. J. Neurosci. 31, 14067 – 14075.

Da Costa, S., van der Zwaag, W., Miller, L.M., Clarke, S., Saenz, M., 2013. Tuning In to Sound: Frequency-Selective Attentional Filter in Human Primary Auditory Cortex. J. Neurosci. 33, 1858 – 1863.

De Martino, F., Esposito, F., van de Moortele, P.-F., Harel, N., Formisano, E., Goebel, R., Ugurbil, K., Yacoub, E., 2011. Whole brain high-resolution functional imaging at ultra high magnetic fields: an application to the analysis of resting state networks. NeuroImage 57, 1031 – 1044.

De Martino, F., Moerel, M., van de Moortele, P.-F., Ugurbil, K., Goebel, R., Yacoub, E., Formisano, E., 2013. Spatial organization of frequency preference and selectivity in the human inferior colliculus. Nat. Commun. 4, 1386.

Dick, F., Tierney, A.T., Lutti, A., Josephs, O., Sereno, M.I., Weiskopf, N., 2012. In Vivo Functional and Myeloarchitectonic Mapping of Human Primary Auditory Areas. J. Neurosci. 32, 16095 – 16105.

Fan, L., Wang, J., Zhang, Y., Han, W., Yu, C., Jiang, T., 2013. Connectivity-Based Parcellation of the Human Temporal Pole Using Diffusion Tensor Imaging. Cereb. Cortex. Epub.

Formisano, E., Kim, D.S., Di Salle, F., van de Moortele, P.F., Ugurbil, K., Goebel, R., 2003. Mirror-symmetric tonotopic maps in human primary auditory cortex. Neuron 40, 859 – 869.

Fujiwara, N., Nagamine, T., Imai, M., Tanaka, T., Shibasaki, H., 1998. Role of the primary auditory cortex in auditory selective attention studied by whole-head neuromagnetometer. Brain Res. Cogn. Brain Res. 7, 99 – 109.

Furst, M., Algom, D., 1995. Lateralization and discrimination of dichotic clicks: evidence from patients with brainstem lesions and normal cohorts. J. Basic Clin. Physiol. Pharmacol. 6, 149 – 171.

Furst, M., Aharonson, V., Levine, R.A., Fullerton, B.C., Tadmor, R., Pratt, H., Polyakov, A., Korczyn, A.D., 2000. Sound lateralization and interaural discrimination. Effects of brainstem infarcts and multiple sclerosis lesions. Hear. Res. 143, 29 – 42.

Galaburda, A., Sanides, F., 1980. Cytoarchitectonic organization of the human auditory cortex. J. Comp. Neurol. 190, 597 – 610.

Han, Z., Ma, Y., Gong, G., He, Y., Caramazza, A., Bi, Y., 2013. White matter structural connectivity underlying semantic processing: evidence from brain damaged patients. Brain 136, 2952 – 2965.

Hillyard, S.A., Hink, R.F., Schwent, V.L., Picton, T.W., 1973. Electrical signs of selective attention in the human brain. Science 182, 177 – 180.

Huang, S., Seidman, L.J., Rossi, S., Ahveninen, J., 2013. Distinct cortical networks activated by auditory attention and working memory load. NeuroImage 83, 1098 – 1108.

Jäncke, L., Mirzazade, S., Shah, N.J., 1999. Attention modulates activity in the primary and the secondary auditory cortex: a functional magnetic resonance imaging study in human subjects. Neurosci. Lett. 266, 125 – 128.

Keller, I., Schlenker, A., Pigache, R.M., 1995. Selective impairment of auditory attention following closed head injuries or right cerebrovascular accidents. Brain Res. Cogn. Brain Res. 3, 9 – 15.

Larson, E., Lee, A.K.C., 2014. Switching auditory attention using spatial and non-spatial features recruits different cortical networks. NeuroImage 84, 681 – 687.

Lawo, V., Koch, I., 2012. Examining Age-Related Differences in Auditory Attention Control Using a Task-Switching Procedure. J. Gerontol. B. Psychol. Sci. Soc. Sci. Epub.

Litovsky, R.Y., Fligor, B.J., Tramo, M.J., 2002. Functional role of the human inferior colliculus in binaural hearing. Hear. Res. 165, 177 – 188.

Lutti, A., Dick, F., Sereno, M.I., Weiskopf, N., 2013. Using high-resolution quantitative mapping of R1 as an index of cortical myelination. NeuroImage. Epub.

Morosan, P., Rademacher, J., Schleicher, A., Amunts, K., Schormann, T., Zilles, K., 2001. Human Primary Auditory Cortex: Cytoarchitectonic Subdivisions and Mapping into a Spatial Reference System. NeuroImage 13, 684 – 701.

Morosan, P., Rademacher, J., Palomero-Gallagher, N., Zilles, K., 2004. Anatomical organization of the human auditory cortex: Cytoarchitecture and transmitter receptors., in: The Auditory Cortex - A Synthesis of Human And Animal Research.

Oh, J., Kwon, J.H., Yang, P.S., Jeong, J., 2013. Auditory imagery modulates frequency-specific areas in the human auditory cortex. J. Cogn. Neurosci. 25, 175 – 187.

Paltoglou, A.E., Sumner, C.J., Hall, D.A., 2009. Examining the role of frequency specificity in the enhancement and suppression of human cortical activity by auditory selective attention. Hear. Res. 257, 106 – 118.

Paltoglou, A.E., Sumner, C.J., Hall, D.A., 2011. Mapping feature?sensitivity and attentional modulation in human auditory cortex with functional magnetic resonance imaging. Eur. J. Neurosci. 33, 1733 – 1741.

Petkov, C.I., Kang, X., Alho, K., Bertrand, O., Yund, E.W., Woods, D.L., 2004. Attentional modulation of human auditory cortex. Nat. Neurosci. 7, 658 – 663.

Rademacher, J., Morosan, P., Schormann, T., Schleicher, A., Werner, C., Freund, H.J., Zilles, K., 2001. Probabilistic mapping and volume measurement of human primary auditory cortex. NeuroImage 13, 669 – 683.

Rinne, T., Balk, M.H., Koistinen, S., Autti, T., Alho, K., Sams, M., 2008. Auditory selective attention modulates activation of human inferior colliculus. J. Neurophysiol. 100, 3323 – 3327.

Rivier, F., Clarke, S., 1997. Cytochrome oxidase, acetylcholinesterase, and NADPH-diaphorase staining in human supratemporal and insular cortex: evidence for multiple auditory areas. NeuroImage 6, 288 – 304.

Schleicher, A., Morosan, P., Amunts, K., Zilles, K., 2009. Quantitative architectural analysis: a new approach to cortical mapping. J. Autism Dev. Disord. 39, 1568 – 1581.

Sigalovsky, I.S., Fischl, B., Melcher, J.R., 2006. Mapping an intrinsic MR property of gray matter in auditory cortex of living humans: a possible marker for primary cortex and hemispheric differences. NeuroImage 32, 1524 – 1537.

Sigalovsky, I.S., Melcher, J.R., 2006. Effects of sound level on fMRI activation in human brainstem, thalamic and cortical centers. Hear. Res. 215, 67 – 76.

Swick, D., Miller, K.M., Larsen, J., 2004. Auditory repetition priming is impaired in pure alexic patients. Brain Lang. 89, 543 – 553.

Ugurbil, K., Xu, J., Auerbach, E.J., Moeller, S., Vu, A.T., Duarte-Carvajalino, J.M., Lenglet, C., Wu, X., Schmitter, S., Van de Moortele, P.F., Strupp, J., Sapiro, G., De Martino, F., Wang, D., Harel, N., Garwood, M., Chen, L., Feinberg, D.A., Smith, S.M., Miller, K.L., Sotiropoulos, S.N., Jbabdi, S., Andersson, J.L.R., Behrens, T.E.J., Glasser, M.F., Van Essen, D.C., Yacoub, E., 2013. Pushing spatial and temporal resolution for functional and diffusion MRI in the Human Connectome Project. NeuroImage 80, 80 – 104.

Wallace, M.N., Johnston, P.W., Palmer, A.R., 2002. Histochemical identification of cortical areas in the auditory region of the human brain. Exp. Brain Res. Exp. Hirnforsch. Expérimentation Cérébrale 143, 499 – 508.

Walz, J.M., Goldman, R.I., Carapezza, M., Muraskin, J., Brown, T.R., Sajda, P., 2013. Simultaneous EEG-fMRI Reveals Temporal Evolution of Coupling between Supramodal Cortical Attention Networks and the Brainstem. J. Neurosci. 33, 19212 – 19222.

Wasserthal, C., Brechmann, A., Stadler, J., Fischl, B., Engel, K., 2013. Localizing the human primary auditory cortex in vivo using structural MRI. NeuroImage. Epub.

Woldorff, M.G., Gallen, C.C., Hampson, S.A., Hillyard, S.A., Pantev, C., Sobel, D., Bloom, F.E., 1993. Modulation of early sensory processing in human auditory cortex during auditory selective attention. Proc. Natl. Acad. Sci. 90, 8722 – 8726.

Woods, D.L., Hillyard, S.A., Hansen, J.C., 1984. Event-related brain potentials reveal similar attentional mechanisms during selective listening and shadowing. J. Exp. Psychol. Hum. Percept. Perform. 10, 761 – 777.

Woods, D.L., Stecker, G.C., Rinne, T., Herron, T.J., Cate, A.D., Yund, E.W., Liao, I., Kang, X., 2009. Functional Maps of Human Auditory Cortex: Effects of Acoustic Features and Attention. PloS One 4, e5183.

Chapter 5

General conclusion

The data presented in this thesis revealed four organisational principles of the human auditory cortex. First, there is a clear continuous anatomicalfunctional relationship within all range of HG morphological variants. Tonotopic mirror-symmetric primary gradients (A1 and R) are perpendicular to HG and spanned both divisions of HG in cases of duplications. Moreover, the common low frequency union between A1 and R was consistently centred on the gyral crown of single HGs and within the sulcal divide of duplicated HGs. Second, primary auditory neurons, tuned to preferred frequencies, could filter selected sound information based on frequency-content. Neural responses within the low- or high-frequency-tuned voxels were enhanced depending on subjects attention to low- or high-frequency tones, respectively. This pattern was quickly reversed by subjects attentional switch. Third, patients with brain lesions were able to perform the tonotopic paradigm without significant effort. This offered the possibility to study auditory plasticity in stroke patients without or with auditory complaints. Our preliminary results demonstrated that tonotopic maps reorganised independently of auditory complaints potentially via diaschisis-like neural plasticity. Finally, the passive tonotopic paradigm could be used straightforwardly as an initial localizer of primary tonotopic auditory cortex, and hence give access to a better understanding of the surrounding non-primary areas. Therefore, we were able to show that environmental sounds are differentially processed by right posterior and medial early-stage auditory areas. Repetitions of the different sounds of the same source induced repetition suppression effects in the right posterior and medial early-stage auditory areas, right posterior middle temporal gyrus, and repetition enhancement in the anterior medial temporal gyrus. Thus, parts of the planum temporale and medial Heshcl's gyrus are likely to carry semantic representations of static environmental sounds.

“We only hear the questions we are able to find an answer.”

Friedrich Nietzsche